Flocking and Formation as Mission Control Strategies for Multi-Agent Systems:

Comparative Evaluation and Development of a Cooperative Approach

Vom Promotionsausschuss der
Technischen Universität Hamburg

zur Erlangung des akademischen Grades

Doktor-Ingenieur (Dr.-Ing.)

genehmigte Dissertation

von

Avraham Turgeman

aus

Beer-Yaakov, Israel

2021

Vorsitzende des Promotionsverfahrens:	Prof. Dr.-Ing. Volker Gollnick
1. Gutachter:	Prof. Dr. Herbert Werner
2. Gutachter:	Prof. Dr.-Ing. Karl-Heinz Zimmerman
Tag der mündlichen Prüfung:	20. May 2021

Acknowledgments

The present dissertation is the result of four years of work at the Institute of Control Systems at Hamburg University of Technology. I owe a great deal of gratitude to my advisor, Prof. Dr. Herbert Werner. His broad knowledge and experience, along with constant support that translated to hours of teaching and discussion, have paved the way to the presented results. His tremendous confidence and trust have helped me reach heights that I thought were out of my reach. This thesis would not have been possible without his persistent mentorship.

A great thanks is given to the Robotarium project at the Institute for Robotics and Intelligent Machines at Georgia Institute of Technology for giving me the opportunity of examine and verify my algorithms in a realistic environment using their Gritbots wheeled robots.

I would like to thank my colleagues and friends at the Institute of Control Systems for enriching my knowledge and for making my work enjoyable, in particular, Ann-Kathrin Schug, Pablo Gonzales, Christine Kloock, and Patrik Gottsch. A special thanks goes to Furugh Mirali and Antonio Mendez for being close friends who kept me motivated, and for being always available for questions and discussions. A special thanks also goes to Adwait Datar for his important contribution to my work in the field of flocking. His careful attention and brilliant way of thinking helped me provide a robust and stable solution, and is greatly valued. His unique and pleasant personality taught me a great lesson for life, and for that I am very grateful.

Finally, I would like to thank the Jewish community in Hamburg for making the stay of my family and I not only possible, but also full of unforgettable memories. This dissertation is dedicated to my wife, Hadar, and our three children, Daniel, Shira, and Jonathan. They provide me with the greatest lessons and values in life.

Summary

The contribution of this thesis is the development of algorithms to explore and monitor unknown complex fields with different concentration levels. Using distributed control schemes, each agent is equipped with local sensors, such as range and current concentration, where the swarm is required to locate the source while remaining together as a group. For a more realistic approach, we allow noise-corrupted measurements and the presence of obstacles. Moreover, we provide a solution for relaxing several conservative assumptions, such as a single isolated maximum or initial distribution at sensible concentration areas. The suggested approach is applicable to tracking different hazards, such as oil spills or toxic clouds. This enables continued monitoring and intervention abilities to reduce a disaster's impact.

Here, we compare two different, yet equally important approaches: formation and flocking. We wish to understand the differences between the two in terms of performance, stability, and robustness. Complex tasks, such as level-curve tracking and multiple extrema, are used to test the behavior of the proposed methods. The case of multiple sources is unique, where agents are required to have equal distribution among the different extrema, which requires the complex algorithm contributed here.

In addition to investigating cooperative motion, we examine different types of extremum-seeking techniques. While we propose a distributed gradient-estimation process in formation-based mission control, we establish a unified, gradient-free law in flocking. The agents are governed by different model types, such as single/double integrator and non-holonomic unicycles. Stability analyses are provided for the different cases. In addition, we propose a unique and novel approach combining flocking and formation. Using a hierarchy structure, the agents are able to perform explicit formation in small groups while establishing a higher relation between the different groups in flocking behavior. Thus, we benefit from the advantages of both formation rigidity and flocking flexibility.

The proposed methods are tested in various simulations in 2D, as well as in 3D involving spheres, different contours, and numerical representation of an oil spill. In addition, realistic experiments are conducted for different scenarios of time-varying fields to examine and evaluate our algorithms.

Contents

Notation

$\mathbb{R}$	field of real numbers
$\mathbb{R}_+$	field of none-negative real numbers
$\mathcal{N}_i$	set of neighbors with respect to agent i
$\|\mathcal{N}_i\|$	size of neighbors set
$G = (\mathcal{V}, \mathcal{E})$	graph with $\|\mathcal{V}\|$ vertices and $\|\mathcal{E}\|$ edges
$\mathcal{A}$	adjacency matrix
Δ	degree matrix
L	laplacian matrix
I_m	the identity matrix in $\mathbb{R}^{m\times m}$
$\otimes$	the kronecker product
$\hat{L}$	Kronecker product of the laplacian matrix with identity matrix
$\psi(q_i)$	concentration level measured by agents i located at q_i
$\psi_{i,ref}$	field reference concentration level
$\hat{g}_i$	estimated gradient
$\mathcal{E}_i$	even distribution process flag
S_l^p	discrete switching vector at iteration step p
$P_{i,l}$	resulted selected task from discrete consensus protocol
u_i	control law of agent i
e_i	feedback error of agent i
$f_o(\rho_{io})$	obstacle avoidance potential function
$\gamma_{i,o}$	obstacle repulsive element
$\Delta r_{f,i}$	formation signal-to-noise adaptive element
$\sigma_{\psi,i}$	noise level evaluation parameter
r_s	agent's sensing radius
l_i	agent's *luciferin* level
$h_f,\ w_f$	bounded search area height and width
ξ_α	set of agents locating extremum at $\hat{r}_\alpha$
p_{ψ_α}	source density
N_ψ	sum of extrema
$\tilde{N}_\psi$	sum of estimated extrema
e_{ψ_α}	density error
$\mathbf{q}$	position column vector of $[q_1^T, \ldots, q_N^T]$
$\mathbf{q}^*$	swarm center-of-mass equilibrium
$\|\|z\|\|_\sigma$	sigma norm
$\sigma_\epsilon(z)$	sigma norm gradient
ρ_h	*bump* function
$\phi_s(z)$	sigmoid function
ϕ_i^j	flocking repulsive/attractive element
$\varphi_{ix}, \varphi_{iy}, \varphi_{i\theta}$	control input for unicycle model
$\mathcal{Q}$	set of γ-agents (match-making)

$\mathcal{J}_{\mathcal{Q}}$	γ-agents index set
$\hat{\psi}$	estimated field
Λ	number of agents in a subgroup ($= \mathcal{N}_i + 1$)
N_l	sum of virtual leaders
$\mathcal{N}_l^n$	set of agents corresponding to a γ_n-agent
$\mathcal{N}_n$	γ_n neighborhood set
ψ_n	field's average measurement of group Λ
μ_n	γ_n constraint value

Acronyms and Abbreviations

MAS	multi agent system
GSO	glowworm swarm optimization
ACO	ant colony optimization
PSO	particle swarm optimization
SNR	signal to noise ratio
IFF	information flow filter
LTL	linear temporal logic
WFF	well formed formulas
MESA	multiple extrema seeking algorithm
CFFT	cooperative flocking and formation control
AUV	autonomous underwater vehicle
PCA	principal component analysis

Chapter 1

Introduction and Motivation

On March 11, 2011, a tsunami following the Tohoku earthquake caused an accident at the Fukushima Nuclear Power Plant, which led to three nuclear meltdowns and the release of radioactive materials. On April 20, 2010, in the Gulf of Mexico, a wellhead blowout released 4.9 million barrels (794 million liters) of oil into the ocean, causing the largest marine oil spill disaster in history. These, as well as other unfortunate accidents, require fast and accurate response from the authorities so that such disasters can be located and monitored. Here, we represent such problems as a generic mission-control problem, where $\psi : \mathbb{R}^m \to \mathbb{R}^+$ represents the distribution of a relevant quantity (concentration of factors such as radioactivity and pollution) and m (here, $m = 2, 3$) is the dimension of the space to be explored.

Source Seeking

One aspect of the field exploration which has received considerable attention is the *source-seeking* problem where a group of agents are required to locate the extremum of an unknown field. Several researchers have proposed solutions based on a single agent only (e.g., [Cochran and Krstic, 2009], [Liu and Krstic, 2010], [Stanković and Stipanović, 2010]), which possess several advantages, such as reduced communication issues and ease of maneuvering. In [Cochran et al., 2009], two source-seeking methods without a global positioning system are introduced. Using only the constant forward velocity or both constant forward and pitch velocities by actuating the pitch and yaw (according to each implementation) allows a static/moving source to be located in a 3D environment. The constant velocity causes the vehicle to revolve around the source, which leads to an inefficient solution. A way to overcome this is to tune both the forward and angular velocities, as proposed in [Lin et al., 2014]. A different approach presented in [Matveev et al., 2014] is, instead of trying to align the velocity vector with the field gradient (which requires gradient estimation), to employ a hybrid controller with three discrete states corresponding to the hysteresis rules, which drives the robot to the field's maximum. Nevertheless, the disadvantages are broad. From a single malfunction criterion to a sensing limitation, a group of agents offers enhanced robustness, efficiency, and exploration capabilities. Using cooperative control to exchange information between neighbors, a group is able to explore, track, and adjust to time-varying field behavior (e.g., [Fiorelli et al., 2006], [Li et al., 2014], [Paliotta et al., 2015]). For instance, in [Ogren et al., 2004] , the agents are considered to be mobile sensors, where the distributed formation control is based on virtual bodies and artificial potentials, and the agents adapt their sensing resolutions based

on gradient estimation and formation geometry. To coordinate the agents' motion in a plane, in [Sydney and Paley, 2014], a multi-vehicle sampling algorithm is proposed to generate trajectories for coverage of a non-stationary field, and [Sepulchre et al., 2007] proposes a methodology that stabilizes an isolated relative equilibrium for parallel and circular motions in a model of all-to-all coupled identical particles.

Level-Curve Tracking

An advanced task is to track different *level curves* to evaluate a field's shape and boundaries. In [Rahmani, 2014], a combination of a rotated gradient with a force driving the source is proposed, which keeps the agents rotating on the level curve. The results are satisfactory but require high energy consumption. A different approach [Kingston et al., 2008] is to exchange information regarding the perimeter length and number of team members. For this method, a decentralized algorithm is proposed, where each agent possess a consistent set of coordination variables. A recent study introduced in [Said and Fumin, 2018] has proposed a different approach that avoids the dependencies of gradient estimation and the shared field's measurements. Using principal component analysis (PCA) of the relative positions of its neighbors in addition to local measurements to compute the local body frame, an agent can modulate its speed accordingly.

It is important to provide the ability to complete these tasks in the presence of obstacles or noisy measurements. For instance, with obstacles in the region, the agents are required to continue their tasks while avoiding collisions. The topic of obstacle avoidance for multi-agent systems has been investigated thoroughly. For example, [Ahmadi Barogh et al., 2015] offers distributed formation control and collision-avoidance control laws for reaching a consensus of a group of non-holonomic agents with limited communication. Each agent's controller requires information only from its local neighbors. [Wang and Xin, 2011] propose an optimal control approach that involves a non-quadratic penalty function to achieve consensus with obstacle-avoidance capability. To provide a solution to the source-seeking problem in a complex environment, [Zou et al., 2015] propose strategies for adaptation to real-life environments, such as obstacles and collision with objects, using particle-swarm optimization (PSO). The objective of the seekers is to communicate, and move in a manner so as to reach the global minimum of the cost function. A second enhancement is providing noise robustness under corrupted measurements. [Young et al., 2010] investigates robustness of consensus in networks driven by white noise and its dependencies on the graph topology, while [Li and Zhang, 2009] uses time-varying gains in the consensus protocol dependent on the measurement noise levels.

Multiple-Extrema

A more realistic approach is to track and monitor a field with *multiple extrema*. This requires an intelligent algorithm that possesses hybrid mission-control characteristics. Whereas a single isolated maximum is being investigated thoroughly, the problem of finding multiple extrema has received little attention. In this work, we follow the growing line of bio-inspired approaches imitating natural swarm behavior. Such optimizations were proposed by several researchers (e.g., [Leitao et al., 2012]), or, for instance [Dorigo and Caro, 1999,Dorigo et al., 2006,Xiang and Lee, 2008], where ant-colony optimization (ACO) is introduced, which uses shared information between agents regarding visited sites/nodes to find an optimal solution for the shortest route. PSO is a population-based stochastic technique, first introduced by [Kennedy and Eberhart, 1995], that can be used for various applications, such as source seeking and power systems [Zhao et al., 2005, del Valle

et al., 2008, Zou et al., 2015]. Our proposed algorithm is based on the work conducted by Krishnanand and Ghose [Krishnanand and Ghose, 2009] regarding the glowworm-swarm optimization (GSO) technique. Similar to glowworms in nature, the agents possess a luminescence agent called *luciferin*, which defines a level of "attraction" to other agents. Solutions for different problems based on the GSO technique were proposed [Wu et al., 2012, Gong et al., 2011, He and Huang, 2016] in the past several years. For instance, in [Liao et al., 2011], a sensor-deployment scheme based on GSO is presented for better coverage to increase the effectiveness of a wireless sensor network. An important part of the solution is developing efficient strategies and algorithms. For example, in [Casbeer et al., 2006], a fire-monitoring solution using cooperative control of multiple unmanned aerial vehicles (UAVs) is proposed. The UAVs, equipped with infrared sensors, monitor the behavior of fire using a distributed load-balancing algorithm. The distributed algorithm is a cooperative surveillance strategy that minimizes the latency of fire perimeter measurements delivered to the base station. The algorithm converges for any changes in the perimeter size and length. In most cases, such algorithms require switching topologies [Olfati-Saber and Murray, 2004], [Xiao and Wang, 2008], [Ni and Cheng, 2010], [Bartels and Werner, 2014] and splitting formations [Olfati-Saber and Murray, 2002], [Chen et al., 2010].

Formation vs. Flocking

In the world of multi-agent systems (MAS), cooperative strategies are at the core of all applications. Keeping the swarm together, in a collective behavior, is mandatory for performing different navigational tasks. Two key frameworks are most commonly used: formation and flocking. Formation control is mainly based on graph-theory tools [Mesbahi and Egerstedt, 2010]. By defining a network connectivity (un/directed graph) in terms of an adjacency matrix, which then constructs the Laplacian matrix, to describe the topological communication, one can apply a structure on a swarm using distributed schemes [Fax and Murray, 2004, Olfati-Saber and Murray, 2004]. A rigid formation guarantees stability and robust performance for different types of linear and nonlinear agent models. For instance, in [Gonzalez et al., 2015], a group of non-holonomic agents reach consensus under switching topologies by representing the agents as a class of decomposable homogeneous linear parameter-varying (LPV) models. A distributed controller is then synthesized by solving standard linear matrix inequalities (LMIs). This is only one complex example of many to present the broad applications of formation control.

However, for certain tasks, such as dynamic tracking, split and rejoin, or navigation in a constrained environment, an explicit formation structure limits the swarm maneuverability (although solutions are provided, e.g., [Olfati-Saber and Murray, 2002, Hu, 2012, Kan et al., 2012, Barogh and Werner, 2016a], they contain strict constraints and conservative assumptions). Thus, a solution may reside in an animal-imitation technique. Reynolds rules, from 1986, were later established in consensus protocol by Saber in [Olfati-Saber, 2006] to dictate the flocking framework. Separation (collision avoidance), alignment (average velocity), and cohesion (average position) are controlled to guarantee the swarm's flocking behavior. An additional navigational function is added to perform different tracking tasks (e.g., [Tanner et al., 2005, Li et al., 2013]). The initial flocking framework is based on a double-integrator agent's model and extensions to the nonholonomic model are proposed; however, for more complex models or advanced techniques (such as LPV), the analysis becomes difficult. This motivates us to provide a solution that combines both flocking and formation. Another motivation is to address problems where a small group with fixed structure provides sufficient information for processes such as gradient climbing or noise reduction; however, the whole swarm behaves as a flock for enhanced maneuvers

or global tasks.

The connection between flocking and formation has been studied thoroughly. For example, in [Dimarogonas and Kyriakopoulos, 2005] and [Dimarogonas and Kyriakopoulos, 2006], when formation is infeasible, the authors show that the swarm still possesses flocking behavior in the sense of matching velocities and orientations. In [Lu et al., 2010], the agents perform formation with flocking. A velocity consensus is achieved (alignment) to keep the mobile agents moving in a fixed formation. Experimental results for outdoor flight with autonomous aerial robots are presented in [Vásárhelyi et al., 2014]. Therein, a velocity-tracking combination with flocking and formation is used to generate a full dynamic equation controlling the flying robots. None of the above propositions explicitly involve cooperative control between the flocking behavior and formation control. Here, we wish to establish a hierarchical framework of coordinates between these two techniques, where in the lower level, agents reach formation consensus and act as small group of sensors, and in the higher level, a set of virtual leaders (i.e., γ-*agents*) behaves as a flock. The hierarchy separation reduces the analysis and synthesis complexity of a unified law, which enables the use of a complex agent model but still benefits from flocking. The different agents' models (double integrator represents a γ-*agent* and unicycle for an agent) involve the possibility of divergence, where the fast, unconstrained dynamics of a γ-*agent* can separate it from its group. A recent result in [Awad et al., 2018] proposed a time-scale separation to distinguish between fast and slow dynamics. Here, our solution is to add feedback from the lower-hierarchy agents to their corresponding γ-*agent*, providing adaptive tuning with respect to the agents' convergence status.

1.1 Contributions

The present dissertation proposes different mission-control strategies for challenging applications that arise in the field of source seeking. Using only local knowledge (without the need for a global coordinate system—i.e., *displacement formations*), such as substance concentration or distance to close neighbors, agents are required to search and locate an unknown field's extrema in the presence of obstacles and noisy measurements. The latter requires advanced and sophisticated methods to reach consensus among agents in different areas, such as formation, flocking, and source location. The following are the main contributions.

- **Level Curve Strategy.** A novel mission-control strategy for source seeking and level curve tracking in different environment is presented. A distributed control scheme based on hierarchy formation and reduced topology is proposed, where the lower level represents mobile sensors and the higher-level agents are in charge of the mission process. Without prior knowledge of the field, several agents, equipped with local sensors, navigate in $\mathbb{R}^m$ using an estimated gradient method. The contributions are twofold. First, we propose a finite iteration process to reach a discrete consensus between all agents for switching from one task to the next. Each group of agents determines their current task according to the status of the other groups in the network. Proof of consensus is introduced in Theorem 3.1. Second, a 4-task algorithm is proposed to explore a time-varying, noisy field. In addition, the agents are provided with the ability to avoid obstacle collision during the whole field-exploration process. Thus, the agents avoid collision not only when seeking the source but also while tracking a level curve. Convergence to the location of the field's maxima under different conditions is introduced in Proposition 3.1 and 3.2

- **Gradient Free Flocking.** A novel scheme that allows a group of mobile agents equipped with sensing capabilities to locate the unknown maximum of a scalar field. This scheme avoids the restrictions associated with gradient estimation and imposing predetermined formations on the agents. Instead, the flocking approach is combined with a technique inspired by GSO. Under mild assumptions, Theorem 4.2 proves the stability and convergence of this approach using the joint work conducted with Datar. A 3D simulation and 2D experimental results illustrate that the proposed method outperforms other techniques in terms of the smoothness of the trajectories.
- **Multiple Source Seeking.** We propose a complete solution for realistic scenarios, such as agent malfunction or time-varying topology. Here, we present the multiple-extrema-seeking algorithm (MESA), where a group of autonomous agents are able, from any arbitrary initial location in a bounded area, to locate multiple, unknown extrema. The proposed algorithm includes a combination of bio-inspired attraction with estimated gradient and formation control, where the task-switching methodology is performed under the specification of the linear temporal logic formula.
- **Cooperative Formation and Flocking.** An approach combining two fundamental frameworks—flocking and formation—in the field of multi-agents is presented. Motivated from the advantages in both techniques we establish a unique hierarchy framework where low-level agents achieve formation (Proposition 5.3) and virtual leaders in a high-level hierarchy flock to locate the unknown extremum. The two-level hierarchies are synchronized by coupling the dynamics using a bump function.

In this thesis, different assumptions are applied. Throughout the thesis, we assume that the agents know their local coordinate system and can measure a limited distance from each other, and that the field is time-invariant for the analysis part. In Sections 3.1 and 3.2, the field is assumed to have a single maximum, whereas in Section 3.3, the field can have multiple extrema within the bounded search area. The estimated gradient is bounded and all obstacles are convex and time-invariant In Chapter 4, the scalar field is concave and its gradient is well-defined.

1.2 Thesis Structure

Cooperative control techniques based on different results from graph theory are introduced in Chapter 2, as well as the LTL framework to formulate hybrid tasks. This chapter also discuss the different formation-control approaches and the flocking framework.
Chapter 3 introduces the formation-based mission-control strategy under different tasks of level-curve tracking and multiple extrema. Complex environments involving obstacles and noise are also addressed using temporal potential functions and varying the formation structure with respect to the measured noise.
Bio-inspiration techniques based on flocking and glowworms are introduced in Chapter 4. Here, a unified, gradient-free rule is proposed to achieve fluent and robust behavior in the search for the source; furthermore, a solution for the multiple-extrema case is also presented. Chapter 5 evaluates both techniques by comparing them under different conditions. In addition, we relax the initial distribution assumption, where an agent can be deployed outside the region of interest. Next, we propose a cooperative scheme showing that flocking and formation can be used together to achieve the benefits of both.
Finally, Chapter 6 provides a number of comprehensive application examples using mobile robots. The novel multiple-extrema technique is tested under different scenarios, as well as flocking for a time-varying field with obstacles and the cooperative technique.

Chapter 2

Preliminaries

This chapter briefly reviews different frameworks, which are used later. Here, we introduce several definitions from graph theory, as well as a discussion on the different approaches for formation control. In addition, the LTL framework is set as the foundation for other relevant parts in this thesis. The remainder of the chapter discuss flocking and the contribution of [Olfati-Saber, 2006] in setting a generalized framework as the basis of controlling multi-agent systems under flocking constraints.

2.1 Graph Theory

The communication structure in a group of agents can be represented by a graph, where the cooperative control scheme is a combination of control and graph theories. Here, we describe several definitions, as introduced by [Mesbahi and Egerstedt, 2010] and concepts from graph theory.
Let $G = (\mathcal{V}, \mathcal{E})$ be a graph that consists of a set of vertices $\mathcal{V} = \{1, 2, \ldots, N\}$ and set of edges $\mathcal{E} \subseteq \{(i, j) : i, j \in \mathcal{V}, i \neq j\}$, and we assume that the graph is undirected.

Definition 2.1 (Undirected Graph)**.** *A graph is undirected if*

$$(i, j) \in \mathcal{E} \;\Leftrightarrow\; (j, i) \in \mathcal{E}, \forall i, j \in N;$$

otherwise, it is directed

The communication topology is represented by the adjacency matrix defined as follows:

Definition 2.2 (Adjacency Matrix)**.**

$$\begin{aligned} A &= [\hat{a}_{ij}] \in \mathbb{R}^{N \times N} \\ \hat{a}_{ij} &= \begin{cases} 1, & (i, j) \in E \\ 0, & else \end{cases} . \end{aligned} \tag{2.1}$$

Let $\Delta = \text{diag}(A \cdot \mathbf{1})$ be the *degree matrix* of G. We can then define the Laplacian matrix.

Definition 2.3 (Laplacian Matrix)**.**

$$L = \Delta - A, \tag{2.2}$$

where $\mathbf{1} = [1, \ldots, 1]^T \in \mathbb{R}^N$.
In addition, we define $\hat{L} = L \otimes I_m$, where $I_m \in \mathbb{R}^{m \times m}$ is the identity matrix and $\otimes$ is the Kronecker product. The following theorem holds.

Theorem 2.1. *Given an undirected graph G, the following statements are equivalent:*

i) G is connected

ii) The null space of the graph Laplacian is the agreement space

iii) $\lambda_1 = 0$ *and* $\lambda_i > 0$, $i = 2, \ldots, N$.

Note that the *agreement space* is the state where all agents' locations are equal, i.e., $\{q_i = q_j, \forall i, j \in N\}$.

Proof. A proof of all equivalences can be found in [Mesbahi and Egerstedt, 2010]. □

We define the set of neighbors of agent i as

$$\mathcal{N}_i = \{j \in \mathcal{V} : ||q_j - q_i|| < r_s\}, \tag{2.3}$$

where r_s is the communication sensing range.

2.1.1 Formation Control

The concept of a distributed control scheme is where, based on partial and relative information, one can control a group of agents using a formation-control scheme. To design such a scheme, one can use a *consensus protocol*. The latter behaves as a local control law with which each agent is equipped, in addition to a communication topology governed from the Laplacian matrix. For instance, given a single integrator dynamic, let $q_i(t) \in \mathbb{R}^m$ be the position of agent i and let $u_i(t)$ be a local control law for agent i; the applied consensus protocol is then

$$\begin{aligned} \dot{x}_i(t) =& u_i(t) \\ u_i(t) =& \sum_{j \in \mathcal{N}_i} (q_j(t) - q_i(t)). \end{aligned} \tag{2.4}$$

The different formation-control methods proposed in the literature can be divided into three groups: position, displacement, and distance-based approaches. To characterize the differences among the three, [Oh et al., 2015] offers an observation in terms of their sensing capability over interaction topology (Figure 2.1).

- **Position-based**. The agents are required to have a common global coordinate system where they sense their absolute position. This yields high sensing capabilities. Thus, the requirement for interaction topology is low, where the formation achieved by each agent's position control.

- **Displacement-based**. The agents are not required to know the origin of the global coordinate system, just their own local coordinate system, and sense relative positions of their neighbors with respect to the global coordinate system. By controlling the displacement of their neighbors, the formation is achieved using the interaction graph.

- **Distance-based**. The agents are required to sense the relative positions of their neighbors and carry only their own local coordinate systems. Thus, there is no need for common orientation or any knowledge of the global coordinate system. This requires a rigid interaction graph (see [Anderson et al., 2008]) where the desired formation is specified by the required distance between pairs of neighbors.

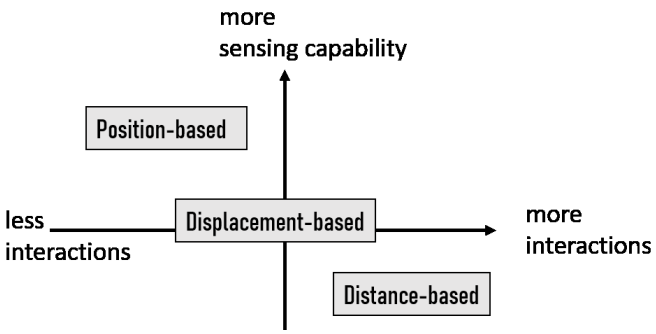

Figure 2.1. Sensing capability vs. interaction topology with respect to different formation techniques, as suggested in [Oh et al., 2015].

In the following subsections, we provide a literature survey of the different formation-control methods.

Position Based

A control law example for the position-based method under single-integrator dynamics can be expressed in the form

$$\begin{aligned} \dot{q}_i =& u_i \\ u_i =& k(\tilde{q}_i - q_i) = ke_i \\ \dot{e} =& -ke - (L \otimes I_m)e,\ e = [e_1, \ldots, e_N]^T, \end{aligned} \tag{2.5}$$

where q_i, u_i, and $\tilde{q}_i$ are the position, control input, and objective of agent i, respectively, and k is a static gain. From the absolute position measurements with respect to the global coordinate, we obtain $q_j - q_i = \tilde{q}_j - \tilde{q}_i$. The authors of [Ren et al., 2007] show sufficient conditions under which each information variable and its higher-order derivatives converges to a common value. The common first-order consensus protocol, also proposed in [Olfati-Saber and Murray, 2004], [Jadbabaie et al., 2003], is

$$\begin{aligned} \dot{q} =& -Lq \\ u_i =& -\sum_{j=1}^{N} a_{ij} k(q_i - q_j). \end{aligned}$$

In [Ren and Atkins, 2007] the agents are assumed to sense their absolute position, velocity, and their neighbors' relative positions. A second-order consensus protocol is then

introduced under communication constraints or sensor limitations.

$$\begin{aligned}\dot{q}_i =& p_i \\ \dot{p}_i =& u_i \\ u_i =& -\sum_{j=1}^{N} a_{ij} k_{ij} [(q_i - q_j) + \gamma(p_i - p_j)],\end{aligned}$$

where $k_{ij}, \gamma > 0$ are uniformly bounded. A general case for a linearly modeled agent is introduced in [Fax and Murray, 2004] with the following dynamics:

$$\begin{aligned}\dot{x}_i =& P_A x_i + P_B u_i \\ y_i =& P_{C_1} x_i \\ z_{ij} =& P_{C_2}(x_i - x_j), j \in \mathcal{N}_i,\end{aligned} \tag{2.6}$$

where y_i and z_{ji} represent internal and external state measurements relative to other agents, respectively, with the following decentralized control law:

$$\begin{aligned}\dot{v}_i =& K_A v_i + K_B y_i + K_{B_2} z_i \\ u_i =& K_C v_i + K_{D_1} y_i + K_{D_2} z_i.\end{aligned} \tag{2.7}$$

The following theorem now holds.

Theorem 2.2. *A local controller (2.7) marginally stabilizes the formation dynamics of* $(\dot{x}, \dot{v})^T = \mathcal{M} \cdot (x, v)^T$ *iff it simultaneously marginally stabilizes the set of* N *systems*

$$\begin{aligned}\dot{x} =& P_A x + P_B u \\ y =& P_{C_1} x \\ z =& \lambda_i P_{C_2} x,\ i \in [1, N],\end{aligned} \tag{2.8}$$

where λ_i *are the eigenvalues of* L.

Proof. See the proof for Theorem 4 in [Fax and Murray, 2004]. □

This fundamental result is used in several applications and with different agent dynamics, such as those proposed in [Pilz et al., 2011, Gonzalez Cisneros, 2014]. For instance, in [Pilz et al., 2012, Bartels and Werner, 2014], an information-flow filter design is used to control a group of autonomous quadcopters. The concept is to consider the separate synthesis of two parts: formation and the local controller (see Figure 2.2). They pro-

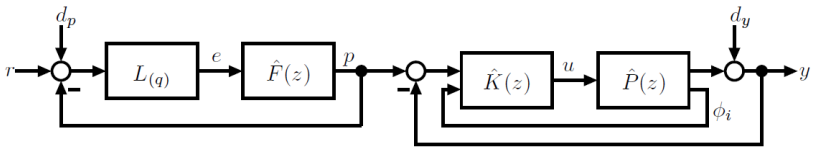

Figure 2.2. Separated formation-control scheme [Pilz et al., 2011].

vided the following result. Using a generalized plant $\hat{P}(z)$ and $\mathcal{H}_\infty/l_1$ synthesis method for calculating $\hat{K}(z)$, the following can be stated about the stability of the MAS.

Theorem 2.3 (IFF stability [Pilz, 2013])**.** *Assuming that $\hat{K}(z)$ stabilizes $\hat{P}(z)$, a MAS, as shown in Figure 2.2, is stable for any number of agents N and arbitrary switching communication topologies with any time-varying communication delays if there exists an invertible matrix $D \in \mathbb{R}^{q\times q}$ s.t. $||DT_{z_1w}D^{-1}||_1 < 1$ and $\min||T_{z_2r}||$, where T_{z_1w} denotes the closed-loop transfer function from w_i to z_1 and that T_{z_2r} from r_i to z_2.*

Proof. The proof is given in [Pilz, 2013]. □

Displacement Based

Displacement-based formation control is similar to position-based but the objective $\tilde{q} \in \mathbb{R}^{mN}$ does not comprise absolute desired positions, but specified desired displacements. For instance, in the control law (2.7), if y_i does not depend on absolute measurements, it can be considered displacement-based. A general consensus protocol for single-integrator dynamics is in the form

$$\begin{aligned} u_i =& k\sum_{j\in\mathcal{N}_i} w_{ij}[(q_j - q_i) - (\tilde{q}_j - \tilde{q}_i)] \\ \dot{e} =& k(L \otimes I_m)e. \end{aligned}$$

Definition 2.4 (Formation Feasibility [Dimarogonas and Kyriakopoulos, 2008])**.** *The formation configuration is considered feasible if the set*

$$\Phi = \{q \in \mathbb{R}^{2N} | q_i - q_j = \tilde{q}_i - \tilde{q}_j,\, \forall (i,j) \in \mathcal{E}\}$$

of feasible formation configurations is nonempty.

Whenever the latter does not hold, the formation configuration is called *infeasible*. In [Dimarogonas and Kyriakopoulos, 2008], it is proven that under the above control law, the assumptions that the formation configuration is *feasible* and the graph is connected, the state of the system converges to the desired formation configuration. If the graph is only connected, all agents attain a common velocity vector $\dot{q}_i = \dot{\tilde{q}}$, $\forall i \in N$ given by

$$\dot{\tilde{q}} = \frac{1}{N}\sum_i \sum_{j\in\mathcal{N}_i} (\tilde{q}_j - \tilde{q}_i).$$

Displacement-based formation control of general linear agents, where the information transmission between neighboring agents is assumed to be intermittent in the present framework, is introduced in [Wen et al., 2012]. A detailed convergence analysis for directed spanning tree topology is performed under the condition of the existence of an infinite sequence of uniformly bounded and non-overlapping time intervals.

Distance Based

Complex tasks in confined spaces or indoor arenas involve difficulties when using a common coordinate system for all agents. This encourages several researchers to focus on developing different methods using distance-based formation control for reaching consensus. For instance, [Oh and Ahn, 2014] proposed a gradient-control law using potential function $\phi_i : \mathbb{R}^{n(|\mathcal{N}_i|+1)} \to \bar{\mathbb{R}}^+$

$$\phi_i(q_i^i, \dots, q_j^i, \dots) = \frac{k}{2}\sum_{j\in\mathcal{N}_i} \gamma(||q_j^i - q_i^i||^2 - ||\tilde{q}_j - \tilde{q}_i||^2),$$

where $k > 0$ and $\gamma : \mathbb{R} \to \bar{\mathbb{R}}_+$ is differentiable. The control law is designed as

$$u_i = -\nabla q_i^i \phi_i(q_i^i, \dots, q_j^i, \dots) = k \sum_{j \in \mathcal{N}_i} \frac{\partial \gamma(d_{ji})}{\partial d_{ji}} p_j^i,$$

where $d_{ji} = ||q_j^i - q_i^i||^2 - ||\tilde{q}_j - \tilde{q}_i||^2$. Distance-based formation control requires graph rigidity. For an undirected graph $G = (\mathcal{V}, \mathcal{E})$, and the position of agent i is defined as q_i, where $q = [q_1, \dots, q_N]^T \in \mathbb{R}^{mN}$ and m is the model order. The pair (G, q) is said to be a framework of G in $\mathbb{R}^m$. The edge function $g_G : \mathbb{R}^{mN} \to \mathbb{R}$ is defined as

$$g_G(q) = \frac{1}{2}[\cdots ||q_i - q_j||^2 \dots]^T, \forall (i,j) \in \mathcal{E};$$

the rigidity of the framework is defined as follows:

Definition 2.5 (Graph rigidity [Asimow and Roth, 1979])**.** *Let G be a graph with N vertices and realization q. Let $\mathcal{K}$ be the complete graph with the same vertex set of G. The framework (G, q) is rigid in $\mathbb{R}^m$ if there exists a neighborhood $\mathcal{U}$ of q in $\mathbb{R}^{mN}$ such that*

$$g_G^{-1}(g_G(q)) \cap \mathcal{U} = g_{\mathcal{K}}^{-1}(g_{\mathcal{K}}(q)) \cap \mathcal{U}.$$

In [Barogh and Werner, 2016a] and its companion paper [Barogh and Werner, 2016b] (extension to nonholonomic models), the authors propose a distance-based formation controller that stabilizes both the formation shape and orientation. This way, flip and flex ambiguity is avoided, which prevents the achievement of unique shapes and eliminate the necessity of initial constraint closeness to the desired formation and orientation. Using the quantities of the measured distance and angle between neighbors, a rigid formation is achieved (with comparison to similar techniques, such as those proposed in [Anderson et al., 2008, Sun and Anderson, 2015]).

2.2 Linear Temporal Logic (LTL)

To provide a formal specification for different hybrid control schemes, a common technique is the linear temporal logic (LTL) framework. LTL is a modal-temporal-logic with modalities referring to time. LTL provides an intuitive formalization for expressing complex behavior, such as task switching or temporal processes, where one can encode formula about the future of paths (where condition will eventually be true or until additional fact becomes true). There has been growing use of LTL over the past several years in diverse areas. Task planning under constraints [Kloetzer et al., 2011, Kantaros and Zavlanos, 2016], motion planning [Zhang and Cowlagi, 2016, Guo et al., 2013], and control synthesis [Papusha et al., 2016] are only a few examples. For instance, in [Fainekos et al., 2005], a framework for generating hybrid controllers is proposed to perform high-level tasks or behaviors while satisfying different LTL formulas. The authors present solutions for different tasks (e.g., locating a fish, animal herding) with an individual or group of robots all specified and constrained by LTL formulas. The latest studies offer control strategies for coordinate multi-agent systems to express high-level goals as LTL formulas [Verginis and Dimarogonas, 2018b, Verginis and Dimarogonas, 2018a]. Each agent, subject to connectivity and collision-free status, is required to satisfy a given local temporal logic specification. The control design includes continuous protocols that guarantee the agent's transition and object transportation among the predefined regions of interest. For instance, [Verginis and Dimarogonas, 2018b] provides the following Lemma. Let the sequences σ_i, σ_j^o be the services provided to the agent and the object, respectively, over their trajectories.

Lemma 2.1. *The behaviors b_j, b_j^o satisfy formulas φ_i, φ_{o_j} if $\sigma_i \models \varphi_i$ and $\sigma_j^o \models \varphi_j^o$, respectively.*

The control objectives are given as LTL formulas φ_i, φ_{o_j}, which are satisfied if there exist behaviors b_j, b_j^o of agent i and object j that satisfy φ_i, φ_{o_j}. Here, similar to [Loizou and Kyriakopoulos, 2004], we formulate a control-switching procedure in the form of LTL specifications to guarantee convergence and robustness.

2.2.1 Definition

Syntax

LTL is built up from a finite set of propositional variables $a \in AP$, the logical operators $\wedge - and, \vee - or, \neg - not$, extended with the temporal operators:

$$\Box : always, \Diamond : eventually, O : next, U : until, \rightarrow : implies.$$

For instance, **Until** operator is defined as follows. The until operator specifies that a formula is true until another one is true. There are two parts in the definition of $\varphi_1 \mathcal{U} \varphi_2$:

- formula φ_2 must hold at some position on the path;
- at all previous positions, formula φ_1 must hold.

The above temporal operators define the semantics of the following operators.

- *eventually*: $\Diamond\varphi := \text{true}\,\mathcal{U}\,\varphi$; φ will become true at some point in the future.
- *always*: $\Box\varphi := \neg\Diamond\neg\varphi$; φ is always true; i.e., "never(eventually $(\neg\varphi)$)."

Formally, the set of LTL formulas over AP is inductively defined as follows:

- if $a \in AP$, then a is an LTL formula.
- if φ_1 and φ_2 are LTL formulas, then $\neg\varphi_1, \varphi_1 \vee \varphi_2, O\varphi_1$ and $\varphi_1 \mathcal{U} \varphi_2$ are LTL formulas.

Consider the following LTL formula:

$$\varphi := \text{true} | a | \varphi_1 \wedge \varphi_2 | \varphi_1 \vee \varphi_2 | \neg\varphi | O\varphi | \varphi_1 \mathcal{U} \varphi_2$$

The following is defined as well-formed formulas (wff):

- **true**,**false**,a,$\neg a$ are wff $\forall a \in AP$.
- if φ_1 and φ_2 are wff, then $\varphi_1 \wedge \varphi_2$ and $\varphi_1 \vee \varphi_2$ are wff.
- if φ_1 and φ_2 are wff, then $O\varphi$ and $\varphi_1 \mathcal{U} \varphi_2$ are wff formulas.

Examples of LTL formula evaluation over a sequence of states (path) follow.

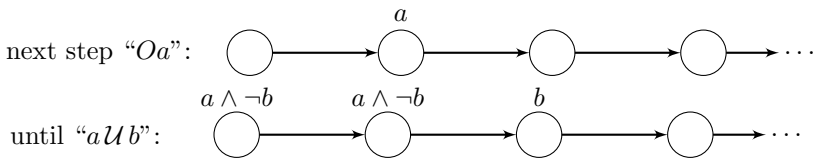

Semantics

An LTL formula can be satisfied by an infinite sequence of truth evaluations of variables in AP. These sequences can be viewed as a word on a path of a Kripke structure (an ω-word over alphabet 2^{AP}).

Definition 2.6. *Let $\sigma = a_0, a_1, a_2, \ldots$ be such an ω-word, and let $\sigma(i) = a_i; \sigma^i = a_i, a_{i+1,\ldots}$. Formula φ is satisfiable if there exist an ω-word σ, such that $\sigma \models \varphi$.*

The satisfaction relation $\models$ between a word $\sigma \in (2^{AP})^\omega$ and an LTL formula is defined as follows:

- $\sigma \models a$ iff $a \in \sigma(0)$.
- $\sigma \models \varphi_1 \wedge \varphi_2$ iff $\sigma \models \varphi_1$ and $\sigma \models \varphi_2$.
- $\sigma \models \neg\varphi$ iff $\sigma \not\models \varphi$.
- $\sigma \models O\varphi$ iff $\sigma^1 = a_1 a_2 a_3 \ldots \models \varphi$.
- $\sigma \models \varphi_1 \mathcal{U} \varphi_2$ iff $\exists j \geq 0$, s.t. $\sigma^j \models \varphi_2$, and $\forall 0 \leq k < j$, $\sigma^k \models \varphi_1$.
- $\sigma \models \Diamond\varphi$ iff $\exists j \geq 0$, s.t. $\sigma^j \models \varphi$.
- $\sigma \models \Box\varphi$ iff $\forall j \geq 0$, s.t. $\sigma^j \models \varphi$.

Remark 1: Note that one state can be defined with different words; thus, the formula is not unique. For instance, $\varphi_1 \rightarrow \varphi_2$ can be described as $\varphi_1 \mathcal{U} (\neg\varphi_1 \vee \varphi_2)$.
Remark 2: Some authors also define a *weak until* binary operator, with semantics similar to that of the until operator but the stop condition is not required to occur.

It is common to represent an LTL formula using a **Büchi automaton**. The latter is a type of ω-automaton, which extends a finite-state machine to infinite inputs. A deterministic Büchi automaton (DBA) is a tuple $A = (Q, \Sigma, \delta, q_0, F)$ consists the following:

- Q is a finite set where its elements are the states of A.
- Σ is a finite set called the *alphabet* of A.
- $\delta : Q \times \Sigma \rightarrow Q$ is the transition function of A.
- q_0 is the initial state of A.
- $F \subseteq Q$ is the acceptance condition.

Note that DBA does not support "eventually forever"($\Diamond\Box\varphi$) and the accepting state is visited "infinitely often".
For a non-deterministic Büchi automaton (NBA) the transition function δ becomes a set of states (noted as Δ), and the initial state q_0 replaced with set of initial states Q_0.

Lemma 2.2. *An ω-language is recognizable by a deterministic Büchi automaton if it is the limit language of some regular language (can be expressed using a regular expression).*

Closure properties:

Let A, B be a Büchi automata and C a finite automaton where $i = (Q_i, \Sigma_i, \delta_i, Q_{0_i}, F_i)$, $i = A, B, C$. The set of Büchi automata is closed under the following operations:

- Union: Exists a Büchi automaton that recognizes the language $L(A) \cup L(B)$.
- Intersection: Exists a Büchi automaton that recognizes the language $L(A) \cap L(B)$.
- Concatenation: Exists a Büchi automaton that recognizes the language $L(C) \cdot L(A)$.
- ω-closure: If $L(C) \notin \emptyset$, then exists a Büchi automaton that recognizes the language $L(C)^\omega$.
- Complementation: Exists a Büchi automaton that recognizes the language $\Sigma^\omega / L(A)$.

Example:

Let the LTL formula defined as

$$\varphi = \Box(a \rightarrow \Diamond b),$$

such that $\mathcal{L}_\omega(A_\varphi) = \text{Words}(\varphi)$, then the corresponding Büchi automaton is in the form of

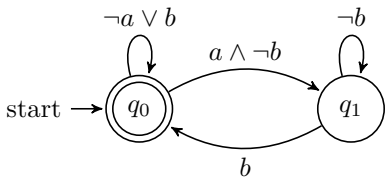

2.3 Flocking

Here, we review fundamental results regarding the flocking framework, which will be referred to in future chapters. This section quotes the definitions introduced in [Olfati-Saber, 2006] for achieving Reynolds rules. Consider a multi-agent system of N mobile, autonomous agents, where i represents an agent that is governed by

$$\begin{aligned} \dot{q}_i &= p_i \\ \dot{p}_i &= u_i, \end{aligned} \tag{2.9}$$

where $q_i, p_i, u_i \in \mathbb{R}^m$, and $q_i \in \mathbb{R}^m$ and $p_i \in \mathbb{R}^m$ can be seen as position and velocity, respectively, of agent i, where the notation $q = [q_1^T, \ldots, q_N^T]^T$ and $p = [p_1^T, \ldots, p_N^T]^T \in \mathbb{R}^{Nm}$ are the position and velocity of the whole network of agents stacked up. Let d denote a desired distance between two neighbor agents.

Definition 2.7 (α-*Lattice*)**.** *An α-Lattice is a configuration q satisfying the set of constraints*

$$||q_j - q_i|| = d, \, \forall j \in \mathcal{N}_i. \tag{2.10}$$

Let $G(q) = (\mathcal{V}, \mathcal{E}(q))$ be a *proximity net* defined by the set of vertices $\mathcal{V} = [1, \ldots, N]$ and the set of edges

$$\mathcal{E}(q) = \{(i,j) \in \mathcal{V} \times \mathcal{V} : ||q_j - q_i|| < r_s, i \neq j\}.$$

Next, we define a *flock*.

Definition 2.8 (Flocks)**.** *A group of α-agents is called a flock over the interval $[t_0, t_f]$, $t_f \geq t_0$ if the proximity net $G(q)$ is connected over that interval.*

To construct a differentiable (smooth) flocking potential function and weighted adjacency matrix, we use the σ-norm definition [Olfati-Saber, 2006]. The σ-norm is a nonnegative map $\mathbb{R}^m \to \mathbb{R}_{\geq 0}$ defined as

$$||z||_\sigma = \frac{1}{\epsilon}(\sqrt{1 + \epsilon||z||^2} - 1),\ \epsilon > 0 \tag{2.11}$$

with a corresponding gradient of

$$\sigma_\epsilon(z) = \nabla||z||_\sigma = \frac{z}{\sqrt{1 + \epsilon||z||^2}} = \frac{z}{1 + \epsilon||z||_\sigma}. \tag{2.12}$$

For the construction of smooth potential functions with finite cut-offs and smooth adjacency matrices, we use the bump function [Saber and Murray, 2003] (Figure 2.3) defined by

$$\rho_h(z) = \begin{cases} 1 & ,z \in [0,h) \\ \frac{1}{2}(1 + \cos(\pi \frac{z-h}{1-h})) & ,z \in [h,1] \\ 0 & ,else \end{cases}, \tag{2.13}$$

where z is the distance from a given agent and $h \in (0,1)$ is a tuning parameter that determines the slope. We use an algebraic sigmoid-based function to describe the repul-

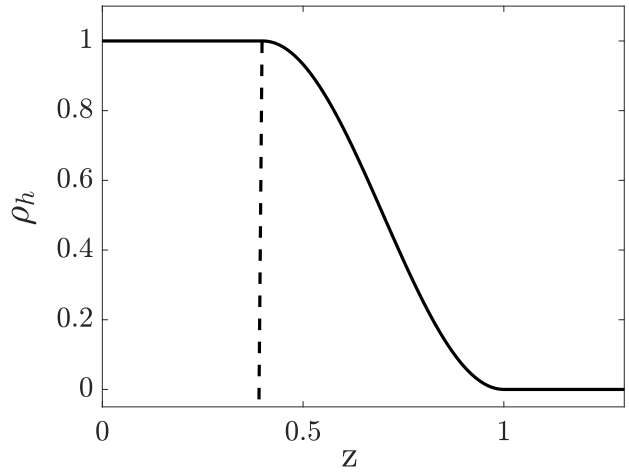

Figure 2.3. *$\rho_h(z)$ bump function* with $h = 0.4$

sive/attractive force.

$$\phi_s(z) = \frac{1}{2}\left[\frac{(a+b)(z+c)}{\sqrt{1 + (z+c)^2}} + (a-b)\right], \tag{2.14}$$

where $0 < a \leq b, c = |a-b|/\sqrt{4ab}$. From graph theory, the Laplacian matrix L of an undirected graph is always positive semidefinite and satisfies, for all $z \in \mathbb{R}^N$,

$$z^T L z = \frac{1}{2} \sum_{i,j \in \mathcal{E}} a_{ij}(z_j - z_i)^2, \tag{2.15}$$

and its second smallest eigenvalue $\lambda_2(L)$ determines the speed of convergence.
The flocking protocol proposed in [Olfati-Saber, 2006] (eq. (23)) is based on two terms: a *gradient-based term* and a *consensus term*, which satisfy all three Reynolds rules: separation (collision avoidance), alignment (average velocity), and cohesion (average position). Let $d_\alpha = ||d||_\sigma$, and replace the set of constraints in (2.10) with

$$||q_j - q_i||_\sigma = d_\alpha, \, \forall j \in \mathcal{N}_i. \tag{2.16}$$

The modified rule in (2.16) induces a smooth collective potential function

$$V = \frac{1}{2} \sum_i \sum_{j \neq i} \Phi_i^j(q_{ji}), \tag{2.17}$$

where

$$\Phi_i^j(q_{ji}) = \int_{d_\alpha}^{q_{ji}} \phi_i^j(s) ds$$
$$q_{ji} = ||q_j - q_i||_\sigma \in \mathbb{R}_{\geq 0}.$$

The term $\phi_i^j : \mathbb{R} \to \mathbb{R}$ is the action function; using (2.13) and (2.14), we obtain a repulsive/attractive force

$$\phi_i^j(q_{ji}) = \rho_h(q_{ji}/r_\alpha)\phi_s(q_{ji} - d_\alpha), \tag{2.18}$$

where $r_\alpha = ||r_s||_\sigma$. The velocity consensus is achieved by defining a weighted adjacency matrix

$$a_{ij} = \rho_h(q_{ji}/r_\alpha) \tag{2.19}$$

and using the flocking protocol.
Control law I:

$$u_i^\alpha = \sum_{j \in \mathcal{N}_i} \phi_i^j(q_{ji}) n_{ji} + \sum_{j \in \mathcal{N}_i} a_{ij}(p_j - p_i), \tag{2.20}$$

where $n_{ji} = \sigma_\epsilon(q_j - q_i) \in \mathbb{R}^m$ is a vector along the line connecting q_i to q_j.
A second protocol includes adding a *navigational feedback* element. This way, the authors relax assumptions regarding group cohesion or connectivity of the proximity net of the agents, and it holds for a generic set of initial states (where the former protocol can yield fragmentation instead of flocking). The navigational term is in the form

$$u_i^\gamma = f_i^\gamma(q_i, p_i, q_r, p_r) = -c_1(q_i - q_r) - c_2(p_i - p_r), \; c_1, c_2 > 0, \tag{2.21}$$

which yields
Control law II:

$$\begin{aligned} u_i &= u_i^\alpha + u_i^\gamma = \\ &= \sum_{j \in \mathcal{N}_i} \phi_i^j(q_{ji}) n_{ji} + \sum_{j \in \mathcal{N}_i} a_{ij}(p_j - p_i) + f_i^\gamma(q_i, p_i, q_r, p_r). \end{aligned} \tag{2.22}$$

The problem with the current protocol is that one must equip the agents with an explicit target set, which is not guaranteed to be available. The significant differences in group

behaviors created by control laws I and II are due to the considerable differences in the structural dynamics induced by the two protocols. Let Σ_1 be the structural dynamics of control law I:

$$\Sigma_1 : \begin{cases} \dot{x} = v \\ \dot{v} = -\nabla V(x) - \hat{L}(x)v \end{cases}, \tag{2.23}$$

where x, v is a moving frame (origin at q_c, p_c) applying

$$x_i = q_i - q_c,\ v_i = p_i - p_c$$

and $\hat{L} = L \otimes I_m$ is the Laplacian matrix. In comparison, let Σ_2 be the structural dynamics of control law II:

$$\Sigma_2 : \begin{cases} \dot{x} = v \\ \dot{v} = -\nabla(V(x) + c_1 J(x)) - (\hat{L}(x) + c_2 I_m)v \end{cases}, \tag{2.24}$$

where $J(x) = \frac{1}{2}\sum_{i=1}^{N} ||x_i||^2$ is the moment of inertia and the second term of $\dot{v}$ is a damping matrix. The corresponding Hamiltonians are

$$\begin{aligned} H_1(x, v) =& V(x) + K(v), \\ H_2(x, v) =& U(x) + K(v), \end{aligned} \tag{2.25}$$

where $U(x) = V(x) + c_1 J(x)$ and $K(v) = \frac{1}{2}\sum_{i=1}^{N} ||v_i||^2$ is the kinetic energy.
The goals of the proposed control laws are the following:

i. Convergence to an equilibrium $(x^*, 0)$.

ii. All agents asymptotically move with the same velocity.

iii. No inter-agent collisions occur.

The proofs are based on the La Salle's invariance principle using the Hamiltonian's definitions in (2.25).

Chapter 3

Formation-Based Source Seeking

This chapter proposes different methods for field exploration using formation-control tools. By reaching consensus and different gradient climbing approaches, agents form groups for field exploration. Here, we demonstrate a level-curve strategy in neutral and complex environments where, by applying the 4-task algorithm, agents are divided into two main groups of anchors and patrols. The former subgroups are quasi-static and set to monitor the field's extremum, and the latter track the corresponding level curve by traveling along it between the *anchors*. This technique allows the level curve to continue being tracked, even in the presence of obstacles or noisy measurements. A more realistic approach is the solution we propose for exploring a multiple-extrema field. This complex task requires multiple conditions and terms where the LTL framework and a bio-inspiration technique are applied. A definition for the occupied extremum is set in addition to the source density for evaluation of the agents' state and future steps. This way, we guarantee, under a certain assumptions, that all existing extrema are explored and monitored. In section 3.1 and 3.2 we use single integrator agents exploring a single extremum, where in section 3.3 the agents are modeled as unicycles (kinematic model) and search for multiple extrema.

3.1 Level-Curve Strategy

A full exploration of a field involves not only the source (i.e., extremum) location but its structure as well. Here, we propose a 4-task algorithm that enables a group of N agents to first locate the highest concentration and then, by decomposition into several search groups, locate and track the field's level curves. Moreover, a finite iteration process to reach a discrete consensus between all agents for switching from one task to the next is introduced. Each group of agents determines their current task according to the status of the other groups in the network.

3.1.1 Distributed Gradient Estimation

A key element for solving the source-seeking problem is a technique that navigates agents toward the extremum location. The gradient direction-based method is, perhaps, the most common type. For instance, in [Ogren et al., 2004], the agents are considered to be mobile sensors, where the distributed formation control is based on virtual bodies

and artificial potentials, and the agents adapt their sensing resolutions based on gradient estimation and formation geometry. In [Brinon-Arranz et al., 2011], by rotating agents around their center of mass and using all-to-all communication, the gradient is estimated at this location. Here, we use a distributed technique proposed in [Rosero and Werner, 2014a].
For the general case, let $q_i \in \mathbb{R}^m$ be the position of a single agent, where $m = 2/3$ is the space dimensions, and let $\psi : \mathbb{R}^m \to \mathbb{R}^+$ describe the level of concentration at q_i. Each agent $i = 1, \ldots, N$ measures the signal strength $\psi(q_i)$ at position q_i. We assume the following.

Assumption 3.1. *ψ has a single maximum in q_s and is time-invariant. Each agent knows its current position and the local value of $\psi(q_i)$.*

Approximation by Taylor series, neglecting higher-order terms, leads to

$$\psi(q_j) = \psi(q_i) + (q_j - q_i)^T \nabla\psi(q_i), \tag{3.1}$$

where $j \in \mathcal{N}_i$ and $\mathcal{N}_i$ is the set of neighbors of agent i and $\nabla\psi(q_i) \in \mathbb{R}^{m\times 1}$ is the real gradient. To assess the robustness to noise, a modified model for noisy field measurements, proposed in [Olfati-Saber and Shamma, 2005] and improved by [Rosero and Werner, 2014b], is used. Each agent measures a field signal $s_{\psi,i} = \psi_i + n_{\psi,i}$, corrupted by a zero-mean Gaussian noise $n_{\psi,i} \in \mathbb{R}$. The signal is then estimated according to a distributed consensus filter,

$$\dot{\hat{\psi}}_i = \beta_\psi \Bigg[\sum_{j\in\mathcal{N}_i} a_{ij}(s_{\psi,i} - s_{\psi,j}) - \sum_{j\in\mathcal{N}_i} a_{ij}(\hat{\psi}_i - \hat{\psi}_j) + (1 + d_i)(s_{\psi,i} - \hat{\psi}_i) \Bigg], \tag{3.2}$$

where $\hat{\psi}_i$ is the estimate of ψ_i, β_ψ is a scalar tuning parameter and d_i is the agent's degree. The shared information is in the form of the computed slope between agent i and the group of its neighbors in $\mathcal{N}_i := \{i_1, \ldots, i_{|\mathcal{N}_i|}\}$, where i_1 is the first neighbor j of agent i. Define $\bar{q}_i = [q_{i_1}, \ldots, q_{i_{|\mathcal{N}_i|}}]^T$,

$$\underbrace{\begin{bmatrix} \hat{\psi}(q_{i_1}) - \hat{\psi}(q_i) \\ \vdots \\ \hat{\psi}(q_{i_{|\mathcal{N}_i|}}) - \hat{\psi}(q_i) \end{bmatrix}}_{b_i} = \underbrace{\begin{bmatrix} (q_{i_1} - q_i)^T \\ \vdots \\ (q_{i_{|\mathcal{N}_i|}} - q_i)^T \end{bmatrix}}_{R_i} \nabla\hat{\psi}(\bar{q}_i), \tag{3.3}$$

where $b_i \in \mathbb{R}^{|\mathcal{N}_i|\times 1}$ and $R_i \in \mathbb{R}^{|\mathcal{N}_i|\times m}$. The distributed estimated gradient is then computed using least squares as

$$\hat{g}_i = (R_i^T R_i)^{-1} R_i^T b_i, \tag{3.4}$$

where $\hat{g}_i \in \mathbb{R}^{m\times 1}$. The inverse of $(R_i^T R_i)^{-1}$ exists iff R_i is full-column rank, which requires $m \leq |\mathcal{N}_i|$.

3.1.2 Formation Hierarchy

The motivation of using different two hierarchy layers is to reduce the communication complexity by decomposing the tasks. As described later in this chapter, our algorithm contains a repeated iteration process, where minimization of the computation time is crucial. Thus, we use formation hierarchy to describe our graph topology as two layers, leaders and followers. Let G_1 be the lower level considered as a mobile, diamond-shaped sensor for enhanced measurements and let the higher level G_2 be the leaders (Figure 3.1). The combination of the two layers is a *hierarchical product graph*.

Definition 3.1 (Hierarchical Product Graph [Glavaški et al., 2008])**.** *Given n graphs, we call $G = G_1 \times \cdots \times G_n$ their hierarchical product graph if the vertices of G_{i+1} are replaced by a copy of G_i such that only the leader from each G_i replaces each of the vertices of G_{i+1} for all $1 \leq i \leq n-1$.*

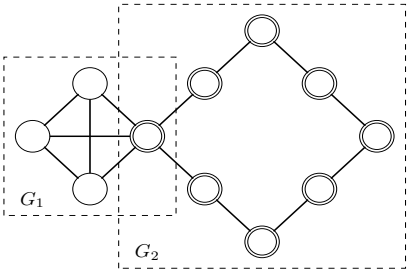

Figure 3.1. Hierarchical formation. The lower hierarchy is defined as $G_1(N_1 = 4)$ and the higher as $G_2(N_2 = 8)$. The leaders are marked with two circles.

Assume $G_1 = (V_1, E_1)$, $|V_1| = N_1$ and $G_2 = (V_2, E_2)$, $|V_2| = N_2$; then, the hierarchical product graph is defined as $G = (V, E)$, $|V| = N = N_1 \cdot N_2$, $|E| = |E_1| \cdot |V_2| + |E_2|$, and its Laplacian matrix is given by

$$L = I_{N_2} \otimes L_{G_1} + L_{G_2} \otimes O_{N_1}, \tag{3.5}$$

where L_{G_i} is the Laplacian of G_i, $I_{N_2} \in \mathbb{R}^{N_2 \times N_2}$ is the identity matrix, and O_{N_1} is a $N_1 \times N_1$ matrix with only the $(1,1)$ entry equal to 1 and the rest zero.
For example, assume that in the lower hierarchy, a group of $N_1 = 3$ agents obtain the topology

$$L_{G_1} = \begin{bmatrix} 1 & -1 & 0 \\ -1 & 2 & -1 \\ 0 & -1 & 1 \end{bmatrix},$$

and the number of leaders in the higher hierarchy is set to $N_2 = 2$, s.t.

$$L_{G_2} = \begin{bmatrix} 1 & -1 \\ -1 & 1 \end{bmatrix}.$$

Then, defining

$$I_{N_2} = \begin{bmatrix} 1 & 0 \\ 0 & 1 \end{bmatrix}, O_{N_1} = \begin{bmatrix} 1 & 0 & 0 \\ 0 & 0 & 0 \\ 0 & 0 & 0 \end{bmatrix}$$

from (3.5), the complete Laplacian matrix is

$$L = \begin{bmatrix} 1 & 0 \\ 0 & 1 \end{bmatrix} \otimes \begin{bmatrix} 1 & -1 & 0 \\ -1 & 2 & -1 \\ 0 & -1 & 1 \end{bmatrix} + \begin{bmatrix} 1 & -1 \\ -1 & 1 \end{bmatrix} \otimes \begin{bmatrix} 1 & 0 & 0 \\ 0 & 0 & 0 \\ 0 & 0 & 0 \end{bmatrix}$$
$$= \begin{bmatrix} 2 & -1 & 0 & -1 & 0 & 0 \\ -1 & 2 & -1 & 0 & 0 & 0 \\ 0 & -1 & 1 & 0 & 0 & 0 \\ -1 & 0 & 0 & 2 & -1 & 0 \\ 0 & 0 & 0 & -1 & 2 & -1 \\ 0 & 0 & 0 & 0 & -1 & 1 \end{bmatrix}.$$

Figure 3.2 illustrates the complete graph topology of the example.

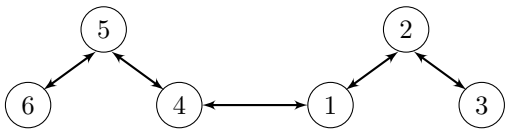

Figure 3.2. Hierarchical communication graph example.

3.1.3 Level-Curve Strategy Algorithm

The following section describes the algorithm and the discrete consensus protocol for switching between the tasks.

Algorithm Description

For complete exploration of the field and its concentration levels, we propose a 4-task algorithm (Figure 3.3), as follows:

Task I—*Locating the extremum*: The agents start by forming a diamond shape, and by exploiting the formation hierarchy topology, use the distributed gradient-estimation method to locate the extremum.

Task II—*Finding the level curve*: Once the agents reach the maximum and a discrete agreement is achieved, the agents switch to their second task: locating a specified level curve by searching in different directions.

Task III—*Even distribution*: Again, once agreement is reached, the groups start a process to distribute themselves evenly along the level curve by measuring the distance to their neighbors.

Task IV—*Anchors and patrols*: In this final task, two different roles are assigned. The groups are separated according to odd (for *anchors*) and even (for *patrols*) group numbers. The *anchors* are in charge of tracking the level curve and maintaining formation, whereas the *patrols* are in charge of exploring the level curve shape between their anchors. This way, the agents are able to map the structure of the field and react properly according to its changes.

Discrete Agreement Consensus

To switch evenly between tasks, we propose a distributed discrete consensus protocol. Here, the hierarchy formation enables a fast iteration process by averaging over G_1 and iterating only on the leaders in G_2. Let $c \in \{0, \ldots, \bar{c}\}$ represent the number of performed iterations, where $\bar{c} = \max_{u,v} d(u, v)$ is the *graph's diameter* (the "longest shortest path" between any two graph vertices (u, v), $d(u, v)$ is a graph distance). The switching value of group $i \in [1, N_2]$ at iteration step l is represented by $S_{i,l}^{(c)} \in \{1, 2, 3, 4\}$. At each step, every agent sets the initial switching value $S_{i,l}^{(0)}$ according to the current task and conditions, so the initial switching vector is defined as $S_l^{(0)} = \left[S_{1,l}^{(0)}, \ldots, S_{N,l}^{(0)}\right]^T$. Then, the iteration process is defined as

$$S_l^{(c+1)} = L \cdot S_l^{(c)}, \tag{3.6}$$

where L is the Laplacian. Using the agent's topology, at each iteration step, the agent's switching value $S_{i,l}^{(c)}$ is affected by more and more layers of its neighbors such that, by

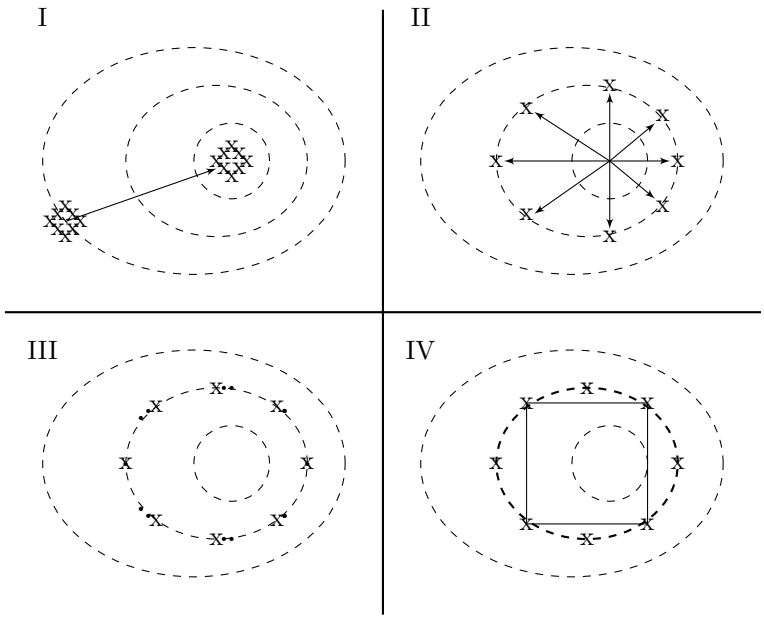

Figure 3.3. The proposed 4-task algorithm for field exploration.

the end of the process (after $\bar{c}$ steps), the whole network is taken into account. Let $P_{i,l} \in \{1, \ldots, N_s\}$, $N_s > 1$ be the selected task of agent i at a time l.

$$\begin{aligned} P_l &= [P_{1,l}, \ldots, P_{N,l}]^T, \\ P_{i,l} &= \begin{cases} S_{i,l}^{(0)} & , S_{i,l}^{(\bar{c})} = 0 \\ P_{i,l-1} & , else \end{cases}, P_0 = \mathbf{1}, \end{aligned} \tag{3.7}$$

where $P_{i,l-1}$ is the previous result of the iteration process. From (3.7), one can see that only when $S_{i,l}^{(\bar{c})} = 0$ an agent changes task; otherwise, no change occurs (and the previous switch value is used).

Definition 3.2 (Agreement Set)**.** *Let $\mathcal{P} = \{1, 2, \ldots, \alpha\}^N$ be the set of all possible switching vectors. Then, $\mathcal{C}$ is defined as the agreement set,*

$$\mathcal{C} = \{S \in \mathcal{P} | S_i = S_j, \forall i, j \in [1, N]\}. \tag{3.8}$$

Once the agents reach the same initial value ($S_l^{(0)} \in \mathcal{C}$), the product in (3.6) produces $S_l^{(1)} = \mathbf{0}$ (where $\mathbf{0} = [0, \ldots, 0]^T \in \mathbb{R}^N$) after the first iteration. However, once $S_l^{(0)} \notin \mathcal{C}$, then the iteration process needs to be completed for the whole network to be aware of the disagreement. This way, the agents are forced to wait until they all reach the same initial value and an agreement is reached.

Theorem 3.1. *If $S^{(0)} \in \mathcal{C}$, i.e., $S^{(0)} = \mathbf{1} \cdot S_i^{(0)}, \forall i$, then, after at most $\bar{c}$ iterations, $S^{(\bar{c})} = \mathbf{0}$ and a discrete consensus is reached. If $S^{(0)} \notin \mathcal{C}$, i.e., $\exists i \neq j, S_i^{(0)} \neq S_j^{(0)}$, then $S^{(\bar{c})} \neq \mathbf{0}$, consensus is not reached, and the previous task holds, i.e., $P_l = P_{l-1}$.*

Proof. First, we prove the equality. From graph theory, the Laplacian matrix has a zero eigenvalue with corresponding eigenvector $\mathbf{1}$, $L \cdot \mathbf{1} = 0 \cdot \mathbf{1} = \mathbf{0}$. Assume a constant $a \in \mathbb{Z}^+$,

which takes a value in $[1, N_s]$. If $S^{(0)} \in \mathcal{C}$ then $S_i^{(0)} = a, \forall i \in [1, N]$, meaning $S^{(0)} = [a, \ldots, a]^T = a \cdot \mathbf{1}$. Therefore, $S^{(1)} = L \cdot S^{(0)} = a \cdot L \cdot \mathbf{1} = \mathbf{0}$, where $S^{(1)}$ is the first iteration. Now, because $L \cdot \mathbf{0} = \mathbf{0}$, then also after $\bar{c}$ iterations, the result remains $S^{(\bar{c})} = \mathbf{0}$ and a consensus is reached. Proving the inequality requires a closer look at the iteration process. If $S^{(0)} \notin \mathcal{C}$, then there exists at least one agent j for which $S_i^{(0)} \neq S_j^{(0)}, \forall i \neq j \in [1, N]$. For simplicity, assume $S_i^{(0)} = a, S_j^{(0)} = b$, so $S^{(0)} = [a, \ldots, a, b, a, \ldots, a]_{N\times 1}^T$. Define $\mathcal{N}_i$ as the group of neighbors of agent i. Following the first iteration $S^{(1)} = L \cdot S^{(0)}$, if $i \notin \mathcal{N}_j$, then all its neighbors have the value a and $S_i^{(1)} = 0$; otherwise, $S_i^{(1)} \neq 0$. For example, if $i = \{j-1, j+1\} \in \mathcal{N}_j$, then, after the first iteration, $S^{(1)} = [0, \ldots, 0, a-b, 2b-2a, a-b, 0, \ldots, 0]^T$. The second iteration also affects the second layer of neighbors (the neighbors of the neighbors of j). Following our example, the groups of $i \in \mathcal{N}_{j+1}$ and $i \in \mathcal{N}_{j-1}$. In that case, only for $i \notin \{\mathcal{N}_j, \mathcal{N}_{j-1}, \mathcal{N}_{j+1}\}$, $S_i^{(2)} = 0$; otherwise, $S_i^{(2)} \neq 0$. The iteration process proceeds, affecting more and more layers of neighbors, until the path between the farthest agents (*graph's diameter*") $\bar{c}$ is completed. Thus, in the final iteration, it is guaranteed that once $S^{(0)} \notin \mathcal{C}$, $S^{(\bar{c})} \neq \mathbf{0}$. □

The following example examines two possible iteration steps, one where discrete consensus is achieved and one where it is not. Given the graph topology depicted in Figure 3.4, the corresponding Laplacian matrix is

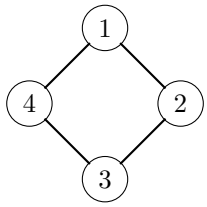

Figure 3.4. Discrete consensus protocol example.

$$L_0 = \begin{bmatrix} 2 & -1 & 0 & -1 \\ -1 & 2 & -1 & 0 \\ 0 & -1 & 2 & -1 \\ -1 & 0 & -1 & 2 \end{bmatrix}.$$

Thus, the number of iteration needed in each step is $\bar{c} = \max_{u,v} d(u, v) = 2$. For the consensus case, assume that all agents agreed on task II, where

$$S_l^{(0)} = \begin{bmatrix} 2 \\ 2 \\ 2 \\ 2 \end{bmatrix} \in \mathcal{C}.$$

Then, at the first iteration, consensus is already achieved, so the second iteration is redundant:

$$S_l^{(1)} = L_0 \cdot S^{(0)} = \begin{bmatrix} 0 \\ 0 \\ 0 \\ 0 \end{bmatrix}, S_l^{(2)} = \begin{bmatrix} 0 \\ 0 \\ 0 \\ 0 \end{bmatrix} = \mathbf{0}$$

and we receive $P_{i,l} = S_{i,l}^{(0)} = 2$. Now, we set agent 4 status in task I, where the rest satisfy the conditions for task II. This disagreement shall cause no change in the value of $P_{i,l}$.

$$S_l^{(0)} = \begin{bmatrix} 2 \\ 2 \\ 2 \\ 1 \end{bmatrix} \notin \mathcal{C}$$

Now, the iteration values of S_l^c are calculated as

$$S_l^{(1)} = \begin{bmatrix} 1 \\ 0 \\ 1 \\ -2 \end{bmatrix}, S_l^{(2)} = \begin{bmatrix} 4 \\ -2 \\ 4 \\ -6 \end{bmatrix} \neq \mathbf{0},$$

where consensus is not achieved and $P_{i,l} = P_{i,l-1} = 1, \forall i \in N$. One can see that, without completing all iteration steps (pausing after the first in the example), agent 2 will mistakenly believe that the swarm has reached consensus.

Algorithm Formulation

After presenting the agreement process, we can now describe the algorithm. All agents start in Task I, i.e., $P_0 = \mathbf{1}$ where here we assume that each agent is represented as a single integrator ($m = 2$)

$$\dot{q}_i = u_i, \tag{3.9}$$

where $i = [1, \ldots, N]$, $q_i = [x_i, y_i]^T$ is the position vector and $u_i \in \mathbb{R}^2$ is the control input of agent i. The control law is then

$$\begin{aligned} u_i =& k_f \sum_{j \in \mathcal{N}_i} a_{ij}[(q_{f_i} - q_{f_j}) - (q_i - q_j)] + k_g \tilde{g}_i = \\ =& k_f \sum_{j=1}^{N} L_{ij}(q_{f_j} - q_j) + k_g \tilde{g}_i, \end{aligned} \tag{3.10}$$

where $k_f, k_g > 0$ are tuning parameters for the formation and gradient, respectively; $q_{f_i} = [q_{f_i}^x, q_{f_i}^y]^T, q_{f_j}$ are the reference relative positions of agents i, j, respectively; and a_{ij} is the corresponding element in the adjacency matrix. In addition, we have an upper bound for the field velocity enabling tracking changes.

At every step, the initial iteration value is set according to the following conditions (all conditions are at iteration step l so the notation is dropped):

$$S_{i,l}^{(0)} = \begin{cases} 1 & , e_i > \varepsilon_1,\ P_{i,l-1} = 1 \\ 2 & , e_i \leq \varepsilon_1,\ P_{i,l-1} = 1 \\ 3 & , \Delta\psi_i \leq \varepsilon_2,\ P_{i,l-1} = 2 \\ 4 & , \mathcal{E}_i = 1,\ P_{i,l-1} = 3 \\ P_{i,l-1} & , else \end{cases}, \tag{3.11}$$

where $e_i = \frac{1}{N_1} \sum_{k=1}^{N_1} \left[\hat{L}(q_f - q) + \hat{g}\right]_k$, $\hat{L} = L \otimes I_p$ and $\Delta\psi_i = \frac{1}{N_1} \sum_{k=1}^{N_1} \psi_{ik}^{ref} - \psi_{ik}$ are the errors for every group $\{i, \forall k\}$. The even distribution process is performed according to

$$\mathcal{E}_i = \begin{cases} 0, |d_i^f - d_i^b| > h \\ 1, else \end{cases}, \tag{3.12}$$

where $d_i^f = ||q_i - q_{i+1}||$, $d_i^b = ||q_i - q_{i-1}||$ are the Euclidean distances between group i and its forward and backward neighbors, where h is a minimum allowed distance. $S_{i,l-1}$ is the previous switch state, $S_{i,l}^{(0)}$ is the initial iteration for (3.7), and $\varepsilon_1, \varepsilon_2$ are calibrated thresholds. Figure 3.5 shows the switching topology as a distributed state machine.

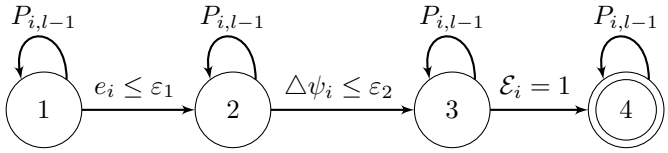

Figure 3.5. The switching sequence can be interpreted as a state machine where the initial state is Task I and, following the conditions, it continues until reaching the accepting state, Task IV.

Once the iteration process is completed (according to (3.7)) and the task is chosen, the estimated gradient is affected accordingly (again, the notation l is dropped).

$$\tilde{g}_{i,l} = \begin{cases} \hat{g}_i & , P_{i,l} = 1 \\ \mathcal{M}_i \hat{g}_i & , P_{i,l} = 2 \\ \mathcal{M}_i \hat{g}_i + \hat{T}\hat{g}_i & , P_{i,l} = 3 \\ \mathcal{M}_i \hat{g}_i + \tilde{T}\hat{g}_i & , P_{i,l} = 4 \end{cases} \tag{3.13}$$

When $P_{i,l} = 1$, $\tilde{g}_i$ is simply calculated according to (3.4). To reach a specified level curve $\psi_{i,ref}$, an additional element is added:

$$\mathcal{M}_i = (\psi_{i,ref} - \psi_i) \cdot \mathcal{D}_i, \tag{3.14}$$

where $\mathcal{D}_i \in \mathbb{R}^{m \times m}$ is the exploring direction for each group i (notice that $\mathcal{D}_i \neq \mathcal{D}_j$, $\forall i, j \in [1, N_2]$). To evenly distribute agents along the level curve, the gradient is rotated using the transformation

$$\hat{T} = \begin{cases} T_{\text{cw}},\ d_i^f > d_i^b + h \\ T_{\text{ccw}},\ d_i^f + h < d_i^b \\ I_2, else \end{cases}, \tag{3.15}$$

where $T_{\text{cw}} = \begin{bmatrix} 0 & -1 \\ 1 & 0 \end{bmatrix}, T_{\text{ccw}} = \begin{bmatrix} 0 & 1 \\ -1 & 0 \end{bmatrix}$ are clockwise and counterclockwise rotations according to the distance conditions. Finally, the role assignments of *anchors* (i_o) and *patrols* (i_e) are

$$\tilde{T} = \begin{cases} T_{\text{cw}},\ d_i^f > h, \delta_T = 1, i \in i_e \\ T_{\text{ccw}},\ d_i^b > h, \delta_T = 2, i \in i_e \\ I_2, i \in i_o \end{cases}, \delta_T = \begin{cases} 1,\ d_i^b \leq h \\ 2,\ d_i^f \leq h \\ \delta_T, else \end{cases} \tag{3.16}$$

where $\{i_e : \mod(i,2) = 0,\ i_o : \mod(i,2) = 1\}$ and $\delta_{T,0} = 1$.

Proposition 3.1. *Consider a group of N agents with dynamics (3.9) applying the control law (3.10). Then, under the described assumptions, the agents converge into formation and complete the sequence of 4 phases using Theorem 3.1.*

Proof. We first proof phase I convergence to source location. Let $\tilde{\psi}_i = -\psi_i$ and $\xi_i = q_i - q_{f,i}$, where $\xi = [\xi_1, \ldots, \xi_N]^T$. Consider the following Lyapunov candidate

$$V = \frac{1}{2}\xi^T \hat{L}\xi + \sum_{i=1}^{N} \tilde{\psi}_i$$

and it is follows that

$$\dot{\xi} = u = -\nabla V.$$

Thus,

$$\dot{V} = \nabla V^T \dot{\xi} = \nabla V^T(-\nabla V) = -||\nabla V||^2 < 0.$$

Since the field posses a single maximum the agents shall converge to source location in formation (where $q_c = q_s$, and q_c its the swarm center of mass). The next step, tracking a level curve invokes from Theorem 3.1 where agents reach discrete consensus and switch to phase II. Here, $\tilde{\psi}_i = -(\psi_{i,ref} - \psi_i)$ and the proof is repeated as for phase I where here the convergence is to an invariant set along the level curve using LaSalle's. Phase III apply evenly distribution where the agents arrange themselves equally along the level curve. This is done by orthogonal gradient such that $\nabla\tilde{\psi}_i = T\nabla\tilde{\psi}_i$. In phase IV, the *anchors* behave as in phase II and the *patrols* behave as in phase III. □

For a time-varying field with constant velocity, one can select the local controller to achieve a specified bound on the steady-state error.

3.1.4 Simulation Results

To present the practicality of the proposed algorithm, a MAS of 32 agents, each modeled as a single integrator, divided into 8 groups of 4 is simulated in formation and topology according to Figure 3.1. In all simulations, the field has a single maximum, and for a more realistic scenario, although not mentioned in the analysis, we add noise to the measurements.
The first simulation assumes a time-invariant field. The scalar field is defined as

$$\psi(q) = A_\psi e^{-((q-q_s)^T H_1 (q-q_s))} + A_\psi e^{-((q-q_s)^T H_2 (q-q_s))}, \tag{3.17}$$

where $H_1 = diag(\frac{1}{2\sigma_{x_1}^2}, \frac{1}{2\sigma_{y_1}^2}), H_2 = diag(\frac{1}{2\sigma_{x_2}^2}, \frac{1}{2\sigma_{y_2}^2})$, $\sigma_{x_1} = 10, \sigma_{y_1} = 50, \sigma_{x_2} = 80, \sigma_{y_2} = 30, A_\psi = 3$, the maximum location is in $q_s = [40, 80]^T$, and the noise has a normal distribution of $n_{\psi,i} \sim \mathcal{N}(0, 0.04)$. Figure 3.6 shows the trajectories of the agents in the $x - y$ plane. At the beginning, the agents start in Task I from a location with low concentration of the field and reach the maximum using the distributed gradient-estimation process. Once the maximum and a discrete consensus are reached, the mission switches to Task II and the agents split into eight groups to find the reference level curve. Once all eight groups find the level curve, the mission switches to Task III, where the groups evenly distribute themselves along the level curve. Finally, the agents switch to Task IV, where the *anchors* position themselves in a formation while the *patrols* explore the shape of the level curve between them. Because of the noisy measurements, one can see that the trajectories are not smooth lines. Nevertheless, the agents are able to perform their tasks (locate the extremum and track the level curve).
Next, we allow the field to be time-varying outside of the assumptions to examine the algo-

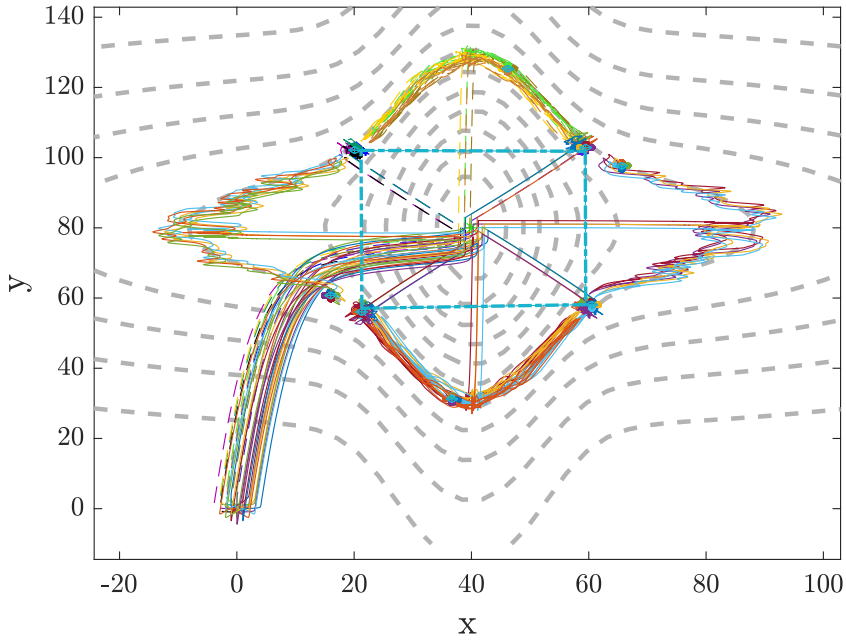

Figure 3.6. Time-invariant scalar field with isolated maximum in [40,80] and a reference level curve with 50% of the highest concentration. Although the measurements are corrupted by noise, the agents locate the extremum and track the desired level curve.

rithm capabilities (Figure 3.7); it is defined as $\psi(q,t)$, so the parameters $\sigma_{x_1}, \sigma_{y_1}, \sigma_{x_2}, \sigma_{y_2}$, A_ψ, q_s are now time-dependent (with respect to the simulation sample step t_s), where

$$\begin{aligned} q_s(t) =& q_s(0) + [0.01, 0.01]^T t_s, \\ \sigma_{x_1}(t) =& \sigma_{x_1}(0) + 0.01 \cdot t_s, \\ \sigma_{y_1}(t) =& \sigma_{y_1}(0) + 0.02 \cdot t_s. \end{aligned}$$

The initial extremum location is in $q_s(0) = [40, 80]$, whereas it moves when $t \in [80 - 120]$ and expands when $t \in [140 - 160]$. The final location of the field's extremum is $q_s(t = 160) = [75, 115]$. Similar to the first simulation, the agents reach the field maximum, find the specified level curve, distribute themselves evenly, and start to explore the curve shape. Throughout this process, the agents reach discrete consensus to switch between the tasks and while keeping formation.

3.2 Level-Curve Strategy in a Complex Environment

The previous section describes a two-level hierarchy of autonomous agents to track a level curve. In this section, we wish to extend the proposed solution to a more complex and realistic environment. By using distribution to groups of *patrols* and *anchors*, a novel solution for level-curve tracking in the presence of obstacles is achieved. To handle noise and errors in measurement, we propose a formation-adapting technique and distributed localization method.

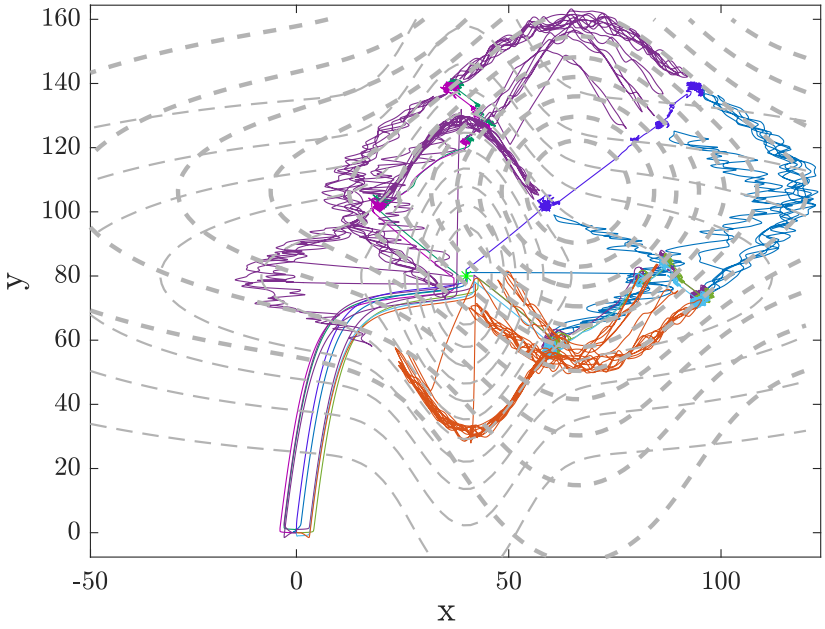

Figure 3.7. Time-varying scalar field with noise-corrupted measurements. The field starts with maximum in [40,80] and level curves in diamond shape, and reaches at t=160 the location [75,115] with a circular level curve. One can see the evolution of the field over time captured by the agents.

3.2.1 Obstacle Avoidance

In this section, we propose a technique for avoiding collision with unknown obstacles when agents navigate toward a source or track level curves by generating a virtual repulsive force around the obstacle via estimation of its center and influence radius. First, we establish the following assumption.

Assumption 3.2. *All obstacles are convex, bounded, and time-invariant.*

Next, we define γ_i as a temporal term, active in the presence of a nearby obstacle, based on potential function (Figure 3.8). Using a potential function as a repulsive force is a common and efficient technique, but requires knowledge of the obstacle's location and radius of influence (the radius of a circle around the obstacle), which, in most cases, is unavailable. Here, we propose a method to estimate an obstacle's location and shape by generating a repulsive virtual potential field around the obstacle using a running-mean method.
Let o be an obstacle index, where $o \in [1, N_{obs}]$ and N_{obs} is the number of detected obstacles, and let ρ_d be the agents' sensing radius. At each $t_k = k \cdot T_s$, where k, T_s are the sampling instant and interval, respectively, an agent i measures a location on the obstacle's surface $q_{io}(t_k) = [x_{io}, y_{io}]^T_{t_k}$. The process is repeated in different locations where the obstacle's shape is revealed. Once an obstacle is detected, $q_o(t_0) = q_{io}(t_0)$, the process continues by estimating a virtual center

$$q_o(t_k) = (q_{io}(t_k) + q_o(t_{k-1}))/2 \tag{3.18}$$

and influence radius

$$\begin{aligned} h_o(t_k) &= \max_{p\in[1,k]} ||q_o(t_k) - q_{io}(t_p)|| \\ \rho_o(t_k) &= \varepsilon_d \cdot \rho_d + h_o, \end{aligned} \tag{3.19}$$

where $\varepsilon_d > 1$ is a tuning parameter. There are several applicable potential functions; here, we choose one similar to that in [Yan et al., 2011]:

$$f_o(\rho_{io}) = \begin{cases} \frac{\varepsilon_{obs}}{2}(\rho_{io}^{-1} - \rho_o^{-1})^2 & , \rho_{io} \le \rho_o \\ 0 & , \text{else} \end{cases}, \tag{3.20}$$

where $\varepsilon_{obs} > 0$ is a scaling factor and $\rho_{io} = ||q_i - q_o||$ is the relative distance between the i-th agent and the o-th obstacle. Then, the repulsive force of obstacle o is given by the negative gradient of the potential function

$$\begin{aligned} \gamma_{i,o} &= -\nabla f_o(\rho_{io}) = \\ &= \begin{cases} \varepsilon_{obs}(\rho_{io}^{-1} - \rho_o^{-1})\rho_{io}^{-3}(q_i - q_o) & , \rho_{io} \le \rho_o \\ 0 & , \text{else} \end{cases}. \end{aligned} \tag{3.21}$$

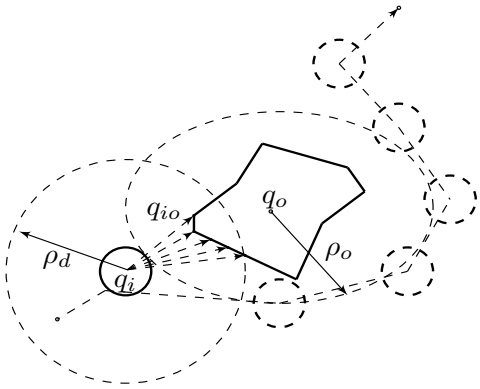

Figure 3.8. Agent q_i, equipped with ρ_d sensing radius, detects obstacle o's surface at several points $q_{io}|_{t_k}^{t_{k+4}}$ and estimates its virtual location q_o and the influence radius ρ_o.

Finally, the contribution of all obstacles is then calculated as

$$\gamma_i = \sum_{o=1}^{N_{obs}} \gamma_{i,o}. \tag{3.22}$$

Obstacles Disturb Level-Curve Path

For the source seeking task, agents encircle obstacles using the gradient climbing element which continues pushing them to the maximum. This is not the case in the level-tracking task where a different solution is required. One solution is to set an arbitrary direction or excitation force for the agents to encircle the obstacle; however, it requires a constant update regarding the desired direction, which becomes inefficient. Furthermore, it does not guarantee continuity of the specified level curve tracking task. Here we present a solution using the proposed field exploration strategy. As described in [Turgeman and Werner,

2017], in Task IV the agents are divided into two groups of *patrols* and *anchors*. Once an obstacle is detected by a *patrol* agent, the destination *anchor* becomes a temporary target which generates an attractive force for encircling the obstacle

$$\begin{aligned} \beta_i =& \sum_{o=1}^{N_{obs}} \beta_{i,o} \\ \beta_{i,o} =& k_o \mathcal{E}_i^o (q_a - q_i), \end{aligned} \tag{3.23}$$

where $k_o > 0 \in \mathbb{R}^{2\times 2}$ and q_a is the position of the target agent. This intervention is only active when an agent is inside the influence region of an obstacle, i.e.,

$$\mathcal{E}_i^o = \begin{cases} 1 & , \rho_{io} \leq \rho_o \\ 0 & , else \end{cases}. \tag{3.24}$$

Now, we can produce the complete control law as

$$u_i = k_f \sum_{j=1}^{N} L_{ij}(q_{f_j} - q_j) + k_g \tilde{g}_i + \beta_i + \gamma_i. \tag{3.25}$$

Proposition 3.2. *Consider the MAS (3.9) with control law (3.25). Then, under the described assumptions, the agents converge into formation and complete the sequence of 4 phases using Theorem 3.1 while avoiding obstacles.*

Proof. Similar as in Proposition 3.1, the Lyapunov candidate is structured as

$$V = \frac{1}{2}\xi^T(\hat{L} + \beta)\xi + \sum_{i=1}^{N} \tilde{\psi}_i + f_{o,i}$$

where $\beta = [\beta_1, \ldots, \beta_N]^T$ and $\dot{\xi} = u = -\nabla V$. Thus

$$\dot{V} = \nabla V(\xi)^T \dot{\xi} = \nabla V(\xi)(-\nabla V(\xi)) = -||\nabla V(\xi)||^2 \leq 0.$$

and the rest of the proof is similar. □

3.2.2 Noise Robustness

We approach the problem of corrupted measurements using two methods: a noise-robustness technique where the agents change their relative distance in relation to the noise level and a distributed localization method where, based on shared information with other neighbors, an agent handles noise-corrupted measurements by using a prediction technique based on a Kalman filter. Different concepts for using a distributed Kalman filter have been proposed in [Aragues et al., 2011] and [Barooah et al., 2010]; here, we use the concept of a central Kalman filter taking the average Kalman gain instead of the inverse covariance and measurements, as suggested in [Olfati-Saber, 2005].

Distributed Kalman Filter

An agent's model described by Kalman filter equations is

$$\begin{aligned} q_{i,t_k} =& A q_{i,t_{k-1}} + B u_{i,t_{k-1}} + w_{i,t_{k-1}}, \\ z_{i,t_k} =& H q_{i,t_k} + v_{i,t_k}, \end{aligned} \tag{3.26}$$

where $q_i \in \mathbb{R}^p$ is the agent's state vector, $z_i \in \mathbb{R}^m$ is the measurement vector, and the variables w, v represent the process and measurement noise, respectively. The latter is assumed to be independent, white, and with normal probability distributions $p(w) \sim N(0, Q)$, $p(v) \sim N(0, R)$, where Q is the process and R is the measurement-noise covariance matrix. The process involves two steps. The first is a *prediction* step using the agent model

$$\begin{aligned} \hat{q}^-_{i,t_k} =& A\hat{q}_{i,t_{k-1}} + Bu_{i,t_{k-1}} \\ P^-_{i,t_k} =& AP_{i,t_{k-1}}A^T + Q, \end{aligned} \tag{3.27}$$

where $P_{i,k}$ is the estimated error covariance matrix. The Kalman gain $K_i \in \mathbb{R}^{p\times m}$ minimizes the error covariance. Thus, averaging over agents' neighbors generates a distributed Kalman gain, which increases the model prediction accuracy according to

$$\begin{aligned} K^-_{i,t_k} =& P^-_{i,t_k}H^T(HP_{i,t_k}H^T + R)^{-1}, \\ K_{i,t_k} =& \frac{1}{1+|\mathcal{N}_i|}\sum_{q=i\cup j\in\mathcal{N}_i} K^-_{q,t_k}. \end{aligned} \tag{3.28}$$

Finally, the *correction* step is

$$\begin{aligned} \hat{q}_{i,t_k} =& \hat{q}^-_{i,t_k} + K_{i,t_k}(z_{i,t_k} - H\hat{q}^-_{i,t_k}) \\ P_{i,t_k} =& (I - K_{i,t_k}H)P^-_{i,t_k}. \end{aligned} \tag{3.29}$$

Signal-to-Noise Ratio

Next, we describe a solution for noisy measurements of level curves, based on modifying the formation structure with respect to the signal-to-noise ratio (SNR). This way, the gradient is measured in locations with a sufficient distance to result in a significant difference between measurements, which reduces the noise effect. Previously, we introduced in (3.2), a distributed consensus filter that improves the accuracy of time-varying signal tracking and attenuates high-frequency noise.
Lower-frequency noise (which can be considered as a sequence of disturbances) is more difficult to filter. Therefore, measurements with significant differences are required. In the source-seeking task, by calculating the gradient in several distant locations, the agents are able to cope with noisy measurements and locate the maximum. From (3.4), the element of the estimated gradient between two neighbor agents is

$$\begin{aligned} b_{i,j} =& s_{\psi,j} - s_{\psi,i} = (\psi_j - \psi_i) + (n_{\psi_j} - n_{\psi_i}) \\ =& \Delta\psi_{i,j} - \Delta n_{\psi_{i,j}} \\ R_{i,j} =& ||q_i - q_j|| = d_{i,j} \\ \hat{g}_{i,j} =& \frac{\Delta\psi_{i,j} - \Delta n_{\psi_{i,j}}}{d_{i,j}}. \end{aligned} \tag{3.30}$$

One can observe that once the distance increases, $\Delta\psi_{i,j}$ and $d_{i,j}$ become larger while $\Delta n_{\psi_{i,j}}$ remains the same. Thus, the varying range for $\hat{g}_{i,j}$ becomes tighter (i.e., more accurate). For this adaptive formation structure, we propose a technique based on an SNR calculation. The agents change their group's structure according to the level of concentration and noise (Figure 3.9). This way, they will extend the search area when the SNR is low and narrow the formation when approaching the maximum. The adaptive element is calculated by

$$\Delta q_{f,i} = 20\log_{10}(\frac{s_{\psi,i}}{\sigma_\psi}), \tag{3.31}$$

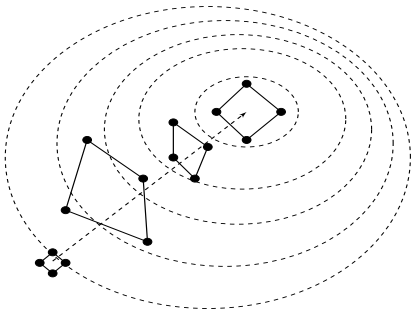

Figure 3.9. Illustration of agents' adapted formation.

where $\sigma_\psi \geq 1$ is a tuning parameter for evaluating the noise level. The formation's behavior depends on the ratio between the signal and the noise evaluation. If the ratio is less than one (i.e., $\sigma_\psi > s_{\psi,i}$), then the distance of agent i to its neighbors increases; otherwise, it decreases. Choosing a low value of σ_ψ will cause small changes in the formation structure, which might not be enough to cope with the noise. On the other hand, choosing a large value will cause an inefficiently large formation at the maximum. Thus, we propose an adaptive noise-evaluation method.

$$\sigma_{\psi,i}(t_k) = \begin{cases} (\sigma_{\psi,i}(t_{k-1}) + |s_{\psi,i}(t_k)|)/2 & , \sigma_{\psi,i}(t_{k-1}) < |s_{\psi,i}(t_k)| \\ \sigma_{\psi,i}(t_{k-1}) & , \text{else} \end{cases}, \tag{3.32}$$

where $\sigma_{\psi,i}(0) = 1$. The value of $\sigma_{\psi,i}$ increases with respect to the signal's highest value, but does not exceed it. Thus, we ensure that the agents will increase their formation size while seeking the source and reduce the size when they approach it. To achieve smooth behavior of $\Delta q_{f,i}$, a second-order filter $\frac{\omega_n^2}{s^2+2\zeta\omega_n s+\omega_n^2}$ is included in the output of (3.32). Let $\Delta q_f = [\Delta q_{f,1}, \ldots, \Delta q_{f,N}]^T$; then, the formation structure is adapted according to

$$\begin{aligned} \Delta q_{fp} =& k_{q_f} \cdot \Delta q_f \otimes [1,1]^T \\ q_f =& \max\{q_f, q_f - \Delta q_{fp} \cdot \text{sgn}(q_f)\}, \end{aligned} \tag{3.33}$$

where $k_{q_f} > 0$ is a scalar tuning gain.
We demonstrate the algorithm capabilities with simulation results.

3.2.3 Simulation Scenarios

Field Exploration with Obstacle Avoidance

A simulation of collision-free motion is presented in Figure 3.10. Similar to that in the previous section, a group of 32 agents, each modeled as a single integrator, is divided into 8 groups of 4. The field is time-varying and is defined as $\psi(q,t)$ where $\sigma_{x_1}, \sigma_{y_1}, \sigma_{x_2}, \sigma_{y_2}, A_\psi, q_s$ are now time-dependent. The field is moving from $q_s = [40, 80]^T$ to $q_s = [60, 120]^T$. The figure shows the trajectories of the agents in the $x-y$ plane where they successfully locate the source (phase I) while detecting and avoiding collision with an obstacle in the way, where the gradient participates as the attractive force. After the agents complete phase IV and start exploring the shape of the field by tracking the desired level curve, one group encounters the second obstacle. Here, depending on their

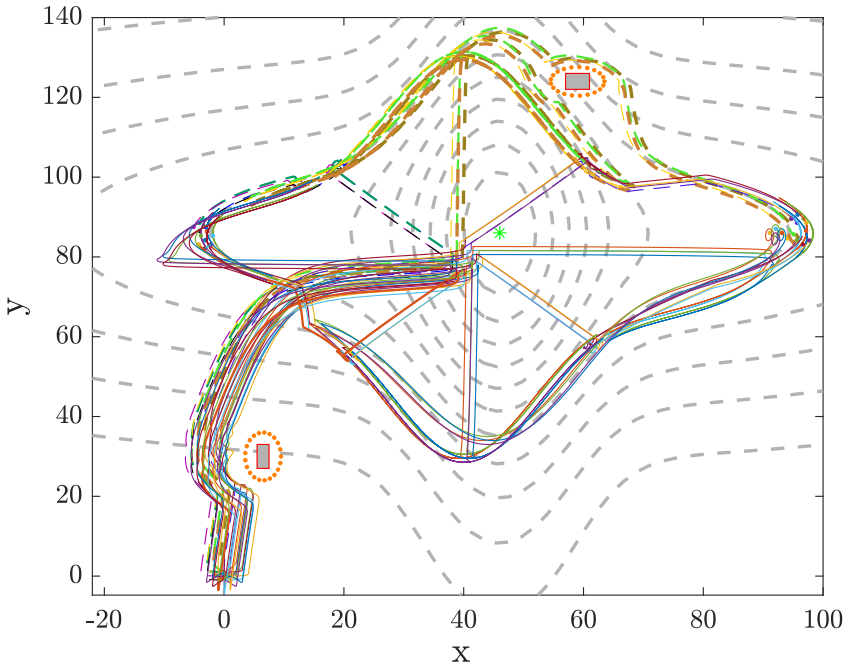

Figure 3.10. Exploration of time-varying field with two obstacles, where the second obstacle interferes with level-curve tracking during the movement of the field.

direction, the *anchor* agent becomes a target with additional attractive force, which enables the agents to encircle the obstacle and continue tracking the level curve. This action is repeated sequentially.

Noise-Corrupted Measurements

In this section, the proposed noise-compensation technique is illustrated. The field's parameters here are $\sigma_{x_1} = 30, \sigma_{y_1} = 30, \sigma_{x_2} = 90, \sigma_{y_2} = 50, A_\psi = 4$ and the maximum location is in $q_s = [80, 100]^T$. Each scenario includes a distributed error of $n_{\psi_i} \sim N(0, 0.5)$ where $s_{\psi_i} = \psi_i + n_{\psi_i}$. As explained, to achieve a smooth change of Δq_f we use a second-order filter with a natural frequency $f_n = 0.25$ Hz and a damping ratio of $\zeta = 0.707$, and we choose $k_{q_f} = 2$. To analyze the quality of the proposed methods, a comparison between three different techniques is shown; using only distributed LPF, SNR and a combination of SNR and the distributed localization method. We evaluate the proposed method by calculating the final error with respect to the source location.

$$\bar{e} = \frac{1}{N} \sum_i ||q_s - q_i||, \tag{3.34}$$

where due to the formation reference, the minimum error is $\bar{e} \geq 5$. To evaluate its efficiency, we also check the swarm total traveled distance (the lower the better), using the following calculation.

$$\bar{d} = \sum_{k=0}^{\Xi} q_{c,k}, \; \Xi = \{k | \, \bar{e} \leq \varepsilon\}, \tag{3.35}$$

where $q_{c,k} = \frac{1}{N}\sum_{i\in N}||q_{i,k}||$ and $\varepsilon = 30$. Table 3.1 summarize the simulation results, concluding that using SNR reduced $\bar{d}$ significantly, whereas the combination of SNR and localization provided the best results. Figure 3.11 illustrates the swarm behavior using

proposition	$\bar{d}$	$\bar{e}$
LPF	691.6	15.8
SNR	357.6	15.6
SNR + Localization	344.7	15.3

Table 3.1: Comparison between different approaches

the adaptive structure proposition for locating the source under noisy measurements. The agents start in relatively close formation, where during motion, increase their structure for better gradient estimation, which eventually drive them toward the unknown maximum.

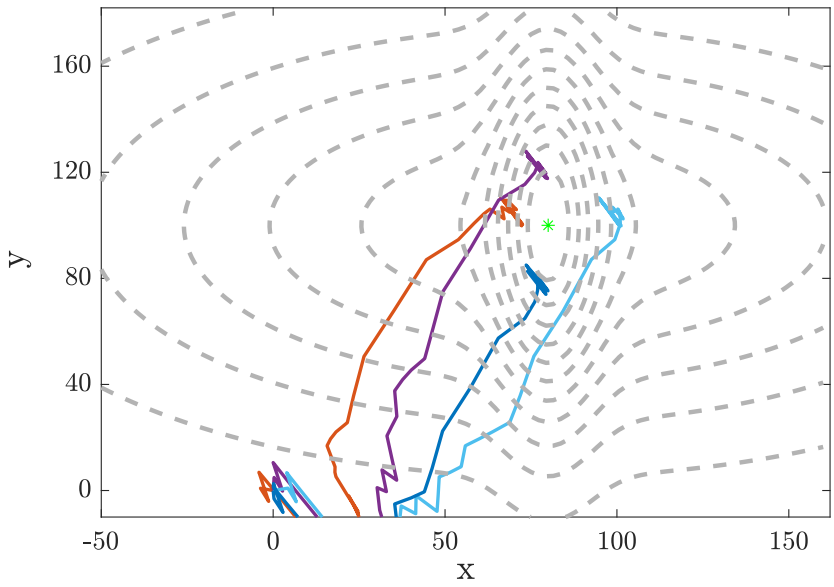

Figure 3.11. Combined technique (consensus filter and adaptive formation) for seeking the source with disturbances, where the agents succeed in locating the maximum and remain there.

3.3 Multiple-Source-Seeking Problem

Considering a realistic scenarios, such as oil tanker damage or pipe explosion, where a large amount of toxic oil is spilled to the ocean. This disaster contains concentration levels that enable exploitation via gradient calculation. In the previous sections, we assumed the field to possess only a single maximum; however, here, the agents encounter several extrema that need to be discovered. Thus, a different approach shall be considered. Furthermore, several studies assume a predefined topology, where agents know their neighbors and a formation is reached. Here, we wish to relax this assumption and let the agents construct groups according to current conditions. This also provides a solution for malfunctioning or lost agents.

3.3.1 Problem Statement

The proposed strategy is compatible with different agent models. Here we consider each agent i as a non-holonomic unicycle with the kinematic model (Figure 3.12)

$$\begin{aligned} \dot{x}_i =& v_i \cos(\theta_i), \\ \dot{y}_i =& v_i \sin(\theta_i), \\ \dot{\theta}_i =& \omega_i, \\ (x_i, y_i) & \end{aligned} \tag{3.36}$$

where, with respect to agent i, $q_i = [x_i, y_i]^T \in \mathbb{R}^2$ is the position in the plane, $\theta_i \in [0, 2\pi]$ is the orientation with respect to the x axis, and $v_i, \omega_i \in \mathbb{R}$ are the control input for linear and angular velocities, respectively. The field vector is described as $\psi = [\psi_1, \ldots, \psi_N]^T$,

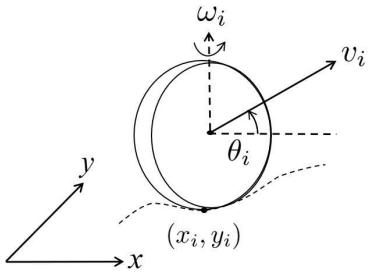

Figure 3.12. agent's unicycle model.

where each agent measures a concentration level at $\psi_i = \psi(q_i)$. An example for such a field, which is examined in our simulation, is the function

$$z = 3(1-x)^2 e^{-x^2-(y+1)^2} - 10(\frac{x}{5} - x^3 - y^5)e^{-x^2-y^2} - \frac{1}{3}e^{-(x+1)^2-y^2}$$

depicted in Figure 3.13, involving 2 minima and 3 maxima.
A single assumption is made regarding the search area size.

Assumption 3.3. *The initial search area is bounded.*

The number of extrema in a field is N_ψ and $\hat{q} = [\hat{q}_1^T, \ldots, \hat{q}_{N_\psi}^T]^T$ is their position vector where the agents, according to the law (3.43) introduced below, can locate both field's minima and maxima. Field exploration requires agents to form groups where a) δ is the

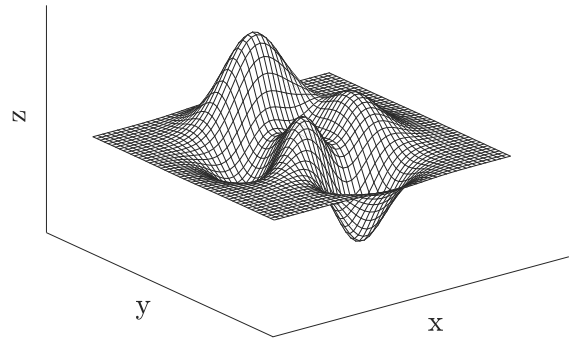

Figure 3.13. Multiple-extrema scalar field function.

maximum allowed number of agents in a single group and b) $\bar{q}_f$ is the offset between agents and the formation. To form such groups, a set

$$\begin{gathered} Q = \{q_1, \ldots, q_w\},\ \mathcal{J}_{\mathcal{Q}} = \{1, 2, \ldots, w\} \\ \max ||q_i - q_j|| \leq 2r_s,\ \forall i, j \in \mathcal{J}_{\mathcal{Q}} \end{gathered} \tag{3.37}$$

of w predefined locations, acting as a "match-maker," is generated by

$$w = \left\lfloor \frac{h_f w_f}{\lceil 2r_s \rceil^2} \right\rfloor, \tag{3.38}$$

where h_f and w_f are the search area maximum height and width, respectively, and r_s is an agent's maximum sensing radius. The number of extrema expected to be detected is determined by $\tilde{N}_\psi$, which set the number of agents

$$N = \delta \cdot \tilde{N}_\psi. \tag{3.39}$$

The task is to split into two parts: locating a single source and swarm field exploration. For the first part, consider $\psi_\alpha = \psi(\hat{q}_\alpha), \alpha \in [1, N_\psi]$ as the concentration level of a source located in $\hat{q}_\alpha$.

Definition 3.3. *The set of all agents which are locating an extremum at $\hat{q}_\alpha$ is defined as*

$$\xi_\alpha = \{i \in N|\ ||\hat{q}_\alpha - q_i|| \leq \bar{q}_f\}. \tag{3.40}$$

Now, for the second part, to evaluate the field exploration performance of a swarm, we define the **source density** as a measure of how many agents are located at the source.

Definition 3.4. *A source density is defined as*

$$p_{\psi_\alpha} = \frac{1}{N} \sum_{i \in \xi_\alpha} e^{-||\hat{q}_\alpha - q_i||}, \tag{3.41}$$

where $p_{\psi_\alpha} \in [0, 1]$, $\alpha \in [1, N_\psi]$.

From (3.41), if $p_{\psi_\alpha} = 1$, then all agents are at the extremum location $\hat{q}_\alpha$. For the case of multiple extrema, it is desired that all densities be leveled (i.e., $p_{\psi_1} = \cdots = p_{\psi_{N_\psi}}$). An additional example is when all agents in a subgroup converge to the same location; this yields a convergence at the source location as well, i.e., $q_i = \hat{q}_\alpha$, $\forall i \in \xi_\alpha$ with a density of $p_{\psi_\alpha} = \frac{\delta}{N}$, $\forall \alpha \in [1, N_\psi]$.
Given a field, and under the assumption that the search area boundaries are known, the problem is to design a mission-control strategy where:
a) the agents are able to locate.
b) the agents are able to locate all extrema as close as possible to equal density.
The agents, based only on local information, must establish communication with nearby neighbors and reach a consensus regarding the formation and source location. For such a mission-control design, we use the specification of an LTL formula φ to control switching between tasks. Here, we use a fragment of LTL, where the formula is constructed over a set of atomic propositions ($\{a\} \in AP$) according to the grammar

$$\varphi := \text{true} | a | \varphi_1 \wedge \varphi_2 | \neg\varphi | \bigcirc \varphi | \varphi_1 \mathcal{U} \varphi_2, \tag{3.42}$$

equipped with traditional ($\wedge, \vee, \neg$) and temporal ($\Box, \Diamond, \bigcirc, \mathcal{U}, \rightarrow$) operators. We use the standard definitions and semantics of LTL, as in [Loizou and Kyriakopoulos, 2004], [Kress-Gazit et al., 2009].

3.3.2 Multiple-Extrema-Seeking Algorithm

In this section we present MESA: a mission-control strategy for the described problem. The idea is that after random deployment of the agents in a bounded area covered by equally distributed predefined match-making points, groups are formed while approaching the nearest match-making location, and search the plane for extrema using gradient climbing and attraction forces. Once an extremum is located, the respective group generates a virtual repulsive force to mark the location to encourage other agents to search for other extrema.

Single-Extremum Seeking

First, we describe the control design for locating a single extremum. Our approach is based on a combination of different elements, such as distributed gradient and *luciferin* level, while keeping formation. Unlike previous methods, where only gradient estimation technique is implemented, here, the GSO element is added for a complete and robust solution. When a group of agents are set "outside" the field (where no concentration is measured) or when a single agent is lost, an attraction relationship is used in addition between neighbors to preserve the agents as a cohesive group. This relaxes the gradient-estimation process requirement $m \leq |\mathcal{N}_i|$ due to the inverse element in (3.4).
A key element in the search procedure is the sensing radius r_s. Thus, connections are made and information is shared. The GSO method [Krishnanand and Ghose, 2009] is based on adjusting agent attractiveness. Let l_i be a property that defines the attraction level of agent i, referred to as *luciferin* and given by

$$l_{i,t} = (1 - \rho) l_{i,(t-\Delta t)} + \zeta |\psi(q_i)|. \tag{3.43}$$

Then, the attraction level of agent j exerted on i is

$$p_{ij} = \frac{l_j - l_i}{\sum_{k \in \tilde{\mathcal{N}}_i} l_k - l_i}, \tag{3.44}$$

where $j \in \tilde{\mathcal{N}}_i$, $\tilde{\mathcal{N}}_i = \{j : d_{ij} < r_s; l_i < l_j\}$ is the set of neighbors of agent i and d_{ij} is the Euclidean distance. Eventually, agent i is attracted to its most attractive neighbor $\{\tilde{j} = j |\ p_{ij} = \max_j(p_{ij})\}$; then,

$$e_i^l = k_l \frac{q_{\tilde{j}} - q_i}{||q_{\tilde{j}} - q_i||}, \tag{3.45}$$

where $e_i^l \in \mathbb{R}^2$ and $k_l > 0$ is a tuning parameter.
As described before, we implement the distributed gradient estimation in (3.4)

$$\hat{g}_i = (R_i^T R_i)^{-1} R_i^T b_i.$$

Here, the agent's neighbors are defined according to the sensing radius r_s and under the limitation of at most δ agents in a group. The gradient law is then

$$e_{i,x}^g = k_g |\hat{g}_{i,x}| \text{sgn}(e_{i,x}^l),\ e_{i,y}^g = k_g |\hat{g}_{i,y}| \text{sgn}(e_{i,y}^l), \tag{3.46}$$

where $e_i^g \in \mathbb{R}^2$ and k_g is a tuning parameter. The $\text{sgn}(e_i^l)$ is added to enable exploration of both the field's minima and maxima such that $|\hat{g}_{i,x}|$ is the gradient's estimated magnitude in the x direction. To estimate the gradient by taking measurements in different locations, each group arranges itself in a specified formation

$$e^f = k_f \hat{L}(q_f - q), \tag{3.47}$$

where k_f is a tuning parameter and q_f is the relative formation vector.

Field Exploration

Next, we describe the second part concerning the field exploration performance of a swarm. Each agent carries a predefined set of reference locations according to (3.37),(3.38). This set's contribution is twofold: neighbor "match-making" and extremum density. While an agent is not a part of a group, it keeps searching for neighbors by traveling between the reference locations according to

$$\begin{aligned} q_p^i &= \arg \min_{p \in \mathcal{J}_\mathcal{Q}} ||q_p - q_i||, \\ e_i^p &= k_q \frac{q_p^i - q_i}{||q_p^i - q_i||}, \end{aligned} \tag{3.48}$$

where $k_q > 0$ is a tuning parameter. If an agent reaches q_p without finding a neighbor, then this location is excluded and the search continues to the next nearest reference location $q_b \in Q$, $b \neq p \in \mathcal{J}_\mathcal{Q}$. The same is applicable to locating all possible extrema. Once a group locates an extremum ψ_α, if another agent i approaches and

$$||q_j - q_i|| \leq r_s,\ j \in \xi_\alpha,\ i \notin \mathcal{N}_j, \tag{3.49}$$

then a virtual repulsive force is generated by compelling the approaching agents to search for the nearest reference location according to (3.48), and the searching procedure is repeated. The overall error with respect to agent i is

$$e_i = \rho_i^p e_i^p + \rho_i^l e_i^l + \rho_i^g e_i^g + \rho_i^f e_i^f, \tag{3.50}$$

where $e_i \in \mathbb{R}^2$, $e = [e_1, \ldots, e_N]^T \in \mathbb{R}^{2N}$ and

$$\begin{aligned} \rho_i^p &= \begin{cases} 0, \, |\mathcal{N}_i| = \delta - 1 \wedge ||\hat{g}|| > 0 \\ 1, \text{ else} \end{cases} ; \rho_i^l = \begin{cases} 0, \, (3.49) \text{ holds} \\ 1, \text{ else} \end{cases} \\ \rho_i^g &= \begin{cases} 0, \, |\mathcal{N}_i| < 2, (3.49) \text{ holds} \\ 1, \text{ else} \end{cases} ; \rho_i^f = \begin{cases} 0, \, |\mathcal{N}_i| = 0 \\ 1, \text{ else} \end{cases} . \end{aligned} \tag{3.51}$$

The local control law that stabilizes and navigates the non-holonomic unicycle is similar to [Ahmadi Barogh et al., 2015]

$$\begin{aligned} u_i =& [v_i, \omega_i]^T \\ v_i =& k_v D_i cos(e_{\theta_i}) \\ \omega_i =& k_\omega e_{\theta_i} + \dot{\theta}_{d_i}, \end{aligned} \tag{3.52}$$

where $e_i = [e_{x_i}, e_{y_i}]^T$, $D_i = \sqrt{e_{x_i}^2 + e_{y_i}^2}$, $e_{\theta_i} = \theta_{d_i} - \theta_i$, $\theta_{d_i} = \tan^{-1}(\frac{e_{y_i}}{e_{x_i}})$ and $k_\omega, k_v > 0$ are tuning parameters.

Assumption 3.4. *It is assumed that $e_{\theta_i} \neq k\frac{\pi}{2}$, $k \in \{-1, -3, 1, 3\}$ for all agents. In other words, $cos(e_{\theta_i}) \neq 0, \forall i \in N$. When $e_{\theta_i} = k\frac{\pi}{2}$, the orientation error should be perturbed to $e_{\theta_i} = e_{\theta_i} + \varepsilon_\theta$*

The complete control scheme is presented in Figure 3.14 where K is the control law from (3.52).

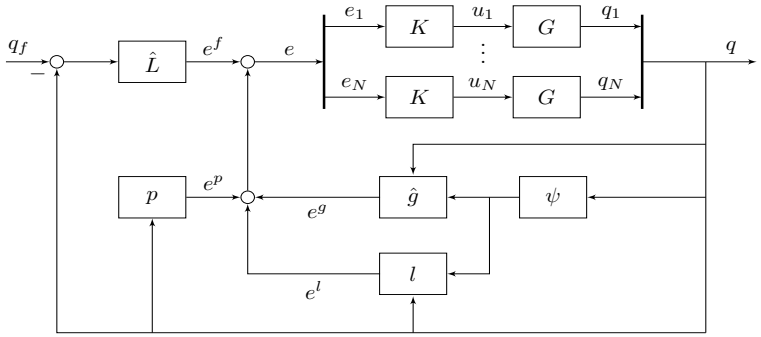

Figure 3.14. Proposed distributed control scheme.

LTL Specification

Here, we formalize MESA using an LTL specification formula. We use (3.51) to define our atomic proposition set $\{a_1, a_2, a_3, a_4, a_5\} \in AP$:

$$\begin{aligned} a_1 :& |\mathcal{N}_i| < \delta - 1 \\ a_2 :& |\mathcal{N}_i| = \delta - 1 \\ a_3 :& ||e_i|| \leq ||k_g |\hat{g}_i(\bar{q}_f)| + k_l|| \\ a_4 :& ||q_j - q_i|| \leq r_s, j \in \xi_\alpha, i \notin \mathcal{N}_j \\ a_5 :& ||q_b - q_i|| > 0. \end{aligned} \tag{3.53}$$

When a_1 is *true*, the neighbor-searching and group-formation procedure is active, which is completed once a_2 is *true*. a_3 is *true* when an agent is near an un-located extremum and a_4 is *true* when agent i approaches an occupied extremum that leads to a_5 and a repulsive force. This can be stated as an LTL specification formula:

$$\varphi_i = \Box[(a_1 \rightarrow \Diamond a_2) \wedge (a_4 \bigcirc a_5 \rightarrow \Diamond a_1)]\mathcal{U}a_3. \tag{3.54}$$

Next we build a relevant Büchi Automaton [Gastin and Oddoux, 2001, Wolper, 2002], $\mathcal{A}_\varphi$, which accepts this specification and consists of four states (Figure 3.15):

- b_0: $\rho_i^p, \rho_{i,|\mathcal{N}_i|\geq 1}^l, \rho_{i,|\mathcal{N}_i|\geq 1}^f, \rho_{i,|\mathcal{N}_i|\geq 2}^g = 1$,
- b_1: $\rho_i^l, \rho_i^f, \rho_i^g = 1$, $\rho_i^p = 0$,
- b_2: $i \in \xi_\alpha$,
- b_3: $\rho_i^l, \rho_i^f, \rho_i^g = 0$, $\rho_i^p = 1$.

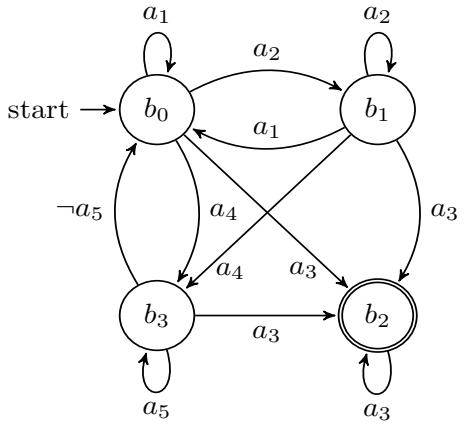

Figure 3.15. Automaton $\mathcal{A}_\varphi$.

From $\mathcal{A}_\varphi$, one can see that the system starts in b_0 where the relevant ρ_i is active for connecting with neighbors; once a full group is completed, the system switches to b_1, where ρ_i^p is canceled. Approaching a source that is already occupied by other groups causes transition to state b_3, where only ρ_i^p is active and the agent is rejected from this extremum. Once the reference location is reached, it returns to b_0 and the procedure is repeated to search for a different extremum. b_2 is defined as the accepting state where an unoccupied extremum is located; it can be reached from b_0, b_1, and b_3 as well. If $\tilde{N}_\psi = N_\psi$, then all extrema are occupied, each with δ agents, all ending in state b_2. Otherwise, if $\tilde{N}_\psi < N_\psi$, then only $\tilde{N}_\psi$ extrema are located. If $\tilde{N}_\psi > N_\psi$, then all N_ψ extrema are located while $\delta(\frac{N}{\delta} - N_\psi)$ agents continue to move around the bounded search area.

Analysis Discussion

In the next sections, the proposed algorithm is tested under different scenarios both in simulations and experiments. Here we wish to discuss the algorithm outline in a sequence manner. First, the deployed agents seek for neighbors by moving toward the closest matching-point (e_i^p) - state b_0. The matching points arrangement guarantee that at least

one neighbor is found ($< 2r_s$ between two points) and the search repeated until the group is complete ($\mathcal{N}_i = \delta - 1$) - state $b_1\,(a_1 \rightarrow \Diamond a_2)$. Then the agents start searching for a source using

$$e_i = e_i^f + e_i^g + e_i^l.$$

The first term reach formation consensus. This can be show with the following Lyapunov candidate

$$V = \sum_{i=1}^{N} \frac{1}{2}(e_{x_i}^2 + e_{y_i}^2 + e_{\theta_i}^2) \quad \text{then,} \quad \dot{V} = -\dot{x}_i e_{x_i} - \dot{y}_i e_{y_i} - k_\omega e_{\theta_i}.$$

Now, by using $v_i = k_v D_i \cos(e_{\theta_i})$ and $\cos(\theta_{d_i}) = \frac{e_{x_i}}{D_i}$, $\sin(\theta_{d_i}) = \frac{e_{y_i}}{D_i}$ in (3.36), we obtain

$$\dot{V} = -k_v(e_{x_i}^2 + e_{y_i}^2)\cos^2(e_{\theta_i}) - k_\omega e_{\theta_i} \leq 0.$$

The source is located using the gradient and luciferin rule where the attractive element is constantly pointing toward a highest (absolute) concentration (e.g. $|\psi_j| > |\psi_i|$ implies $q_i \rightarrow q_j$ until $\psi_c = \psi^*$ where ψ_c is the average concentration level of a group). If the source is not occupied then state $b_2\,(\mathcal{U}a_3)$ is achieved and the sequence is completed. In case it is occupied, i.e. state b_3, then e_i^p is triggered again and the agents move toward a far matching location - state $b_0\,(a_4 \bigcirc a_5 \rightarrow \Diamond a_1)$ and the sequence is repeated.

Next we show that the source density error is bounded. According to Definition 1, a group is belong to an extremum ψ_α as $\xi_\alpha = \{i \in N|\ ||\hat{q}_\alpha - q_i|| \leq \bar{q}_f\}$. Then, the source density is (according to Definition 2)

$$p_{\psi_\alpha} = \frac{1}{N}\sum_{i\in\xi_\alpha} e^{-||\hat{q}_\alpha - q_i||} \leq \frac{1}{N}\sum_{i\in\xi_\alpha} e^{-\bar{q}_f} = \frac{\delta}{N}e^{-\bar{q}_f}. \tag{3.55}$$

This is true $\forall\alpha \in [1, \tilde{N}_\psi]$, i.e., $p_{\psi_\alpha} = p_{\psi_\beta}$, $\forall\alpha, \beta \in [1, \tilde{N}_\psi]$. Therefore, the density error between the different extrema for the case of $\tilde{N}_\psi \geq N_\psi$ is

$$e_{\psi_\alpha} = \frac{1}{N_\psi}\sum_{\beta=1}^{N_\psi}(p_{\psi_\alpha} - p_{\psi_\beta})^2 = 0.$$

We also need to look at the case when $\tilde{N}_\psi < N_\psi$ and show that the error is bounded:

$$\begin{aligned} e_{\psi_\alpha} &= \frac{1}{N_\psi}\sum_{\beta=1}^{N_\psi}(p_{\psi_\alpha} - p_{\psi_\beta})^2 \\ &= \frac{1}{N_\psi}\sum_{\beta=1}^{\tilde{N}_\psi}(p_{\psi_\alpha} - p_{\psi_\beta})^2 + \frac{1}{N_\psi}\sum_{\beta=\tilde{N}_\psi+1}^{N_\psi}(p_{\psi_\alpha} - p_{\psi_\beta})^2. \end{aligned}$$

We distinguish between two cases. When $\psi_\alpha \in [1, \tilde{N}_\psi]$, then, as before, $p_{\psi_\alpha} = p_{\psi_\beta} = \frac{\delta}{N}e^{-\bar{q}_f}$, $\forall\alpha, \beta \in [1, \tilde{N}_\psi]$ and $\forall\beta \in [\tilde{N}_\psi + 1, N_\psi]$, $p_{\psi_\beta} = 0$, so

$$\begin{aligned} e_{\psi_\alpha \in [1,\tilde{N}_\psi]} &= \frac{1}{N_\psi}\sum_{\beta=\tilde{N}_\psi+1}^{N_\psi}(\frac{\delta}{N}e^{-\bar{q}_f})^2 \\ &= \underbrace{\frac{N_\psi - \tilde{N}_\psi - 1}{N_\psi}(\frac{\delta}{N}e^{-\bar{q}_f})^2}_{\kappa_1} \leq \varepsilon_\kappa\kappa_1, \end{aligned} \tag{3.56}$$

where $\varepsilon_\kappa > 1$. When $\alpha \notin [1, \tilde{N}_\psi]$, $p_{\psi_\alpha} = 0$ and

$$\begin{aligned} e_{\psi_{\alpha \in [\tilde{N}_\psi + 1, N_\psi]}} &= \frac{1}{N_\psi} \sum_{\beta=1}^{\tilde{N}_\psi} (-\frac{\delta}{N} e^{-\bar{q}_f})^2 \\ &= \underbrace{\frac{\tilde{N}_\psi}{N_\psi} (\frac{\delta}{N} e^{-\bar{q}_f})^2}_{\kappa_2} \leq \varepsilon_\kappa \kappa_2. \end{aligned} \tag{3.57}$$

These results are evaluated in the following simulations.

3.3.3 Simulation Results

In this section, we present the simulation results of exploring a scalar field with 5 extrema using different numbers of unicycle agents constructing groups of $\delta = 4$. The time-invariant scalar field used here is the *peak* function.

$$\psi(q) = \eta_1 (1-x)^2 e^{-(x^2+(y+1)^2)} - \eta_2 (\frac{x}{5} - x^3 - y^5) e^{-(x^2+y^2)} - \eta_3 e^{-((x+1)^2+y^2)},$$

where $\eta = [3, 10, 1/3]$. The field is constructed of one global maximum in $\psi_1 = (-0.01, 1.6)$ and two local maxima in $\psi_2 = (-0.46, -0.63), \psi_3 = (1.28, 0)$, in addition to one global minimum in $psi_4 = (0.24, -1.65)$ and a local one in $\psi_5 = (-1.35, 0.2)$. First, we study the case where $\tilde{N}_\psi = 5$ and with groups of $\delta = 4$, for which, according to (3.39), the number of agents is taken to be $N = 20$. Figure 3.16 shows the simulation results in the $x - y$ plane. At the beginning, the agents (gray rectangle/black top circle) are distributed arbitrarily in the bounded search area (a). By moving toward the reference locations (red cross marks), the agents locate neighbors (state b_0) and cluster into groups while detecting attractive agents and gradient changes. Then (a_2 is *true* change to state b_1), the agents climb or descend toward an extremum until each group is settled and the mission is completed (b), i.e., a_3 is *true*, and the state changes to the acceptance state b_2. If a single agent or group approaches an occupied extremum, then they are repulsed and navigate to the nearest reference location (i.e., state b_3) until they reach it and repeat the search process (state b_0).

Table 3.2 shows a comparison of the sources' densities according to (3.41) between MESA and distributed gradient climbing (similar to [Rosero and Werner, 2014a] for the same set of initial conditions). One can see that the gradient method, which is satisfactory for locating a single isolated extremum, fails in the multiple-source-seeking mission; whereas ψ_2 has the highest density, ψ_4 and ψ_5 were not discovered. MESA shows equal source density levels and a low standard deviation where the error is almost zero.

Tables 3.3, 3.4 along with Figure 3.17 present the results of two additional simulations: one for $[\tilde{N}_\psi = 4, N = 16]$ and the other for $[\tilde{N}_\psi = 6, N = 24]$.

For the case when $\tilde{N}_\psi < N_\psi$, from Table 3.3, one can notice that ψ_3 was not detected due to the low number of agents. The other extrema were located with equal density. The measured value e_{ψ_α} is almost equal to the calculated one (3.56), (3.57) according to whether an extremum is found or not. For the case where $\tilde{N}_\psi > N_\psi$, the results in Table 3.4 are similar to those of $\tilde{N}_\psi = N_\psi$ with lower source density (due to the larger number of agents in use). Whereas the first 20 agents locate and remain in all extrema locations, the redundant 4 agents keep moving in the region, searching for potential field changes.

Experimental results of the proposed method are presented later, in section 6.1.

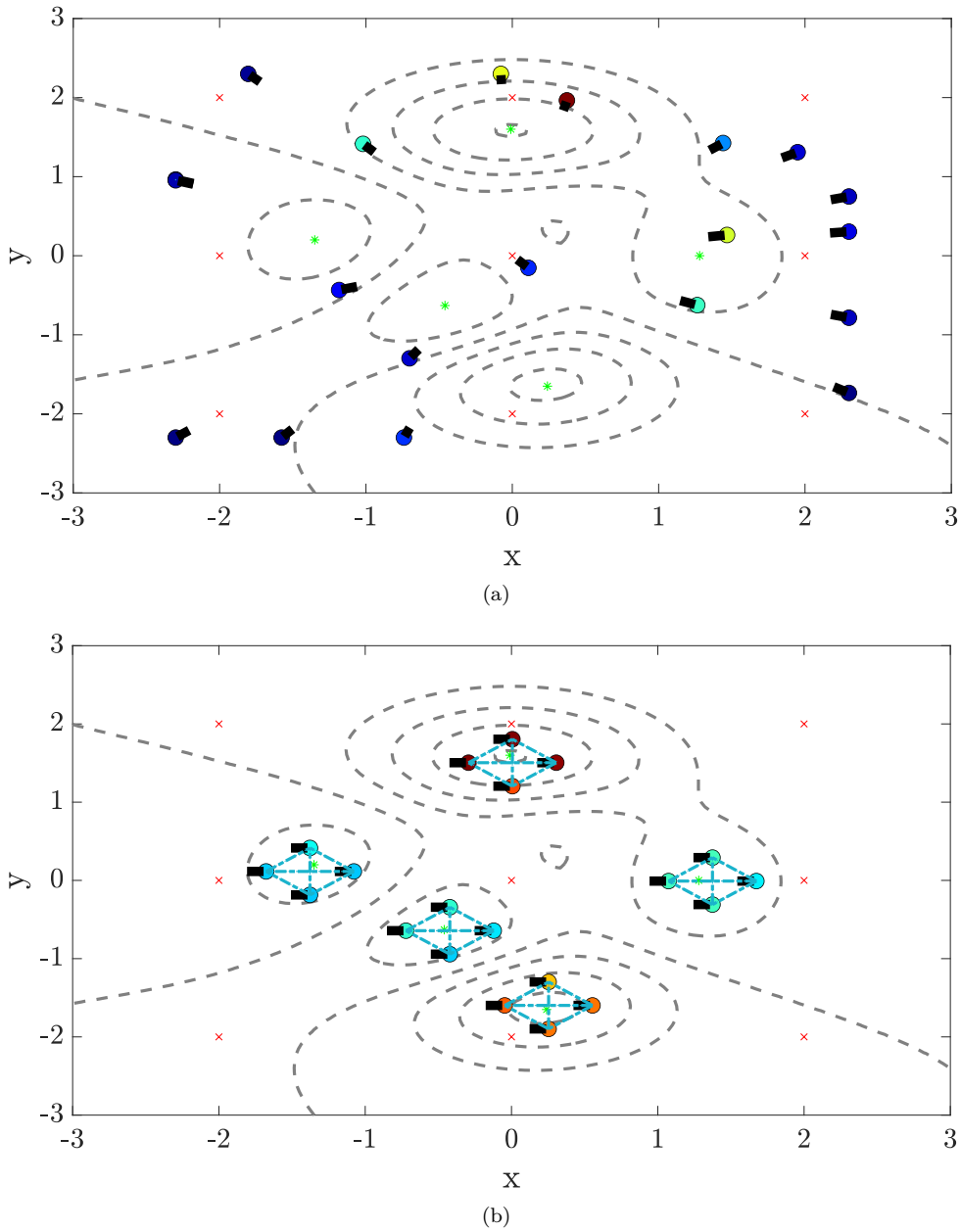

Figure 3.16. The swarm exploration behavior in x–y plot: (a) initial arbitrary distribution of the agents (b) final location. The agents possess each extremum in a desired diamond formation.

		ψ_1	ψ_2	ψ_3	ψ_4	ψ_5
MESA	p_{ψ_α}	0.1665	0.1654	0.1656	0.1666	0.1656
	Eq.(3.55)	0.1637	0.1637	0.1637	0.1637	0.1637
	e_{ψ_α}			$< 1e^{-6}$		
Gradient	p_{ψ_α}	0.2459	0.3268	0.1655	0	0
	e_{ψ_α}	0.0268	0.0492	0.0175	0.0389	0.0389

	Avg. p_ψ	σ_{p_ψ}	Avg. e_{ψ_α}	Max. p_ψ
MESA	0.1659	0.0006	0.0000	0.1666
Gradient	0.1476	0.1463	0.0343	0.3268

Table 3.2: Performance comparison between different methods, $\tilde{N}_\psi = N_\psi = 5, N = 20, \delta = 4$

	ψ_1	ψ_2	ψ_3	ψ_4	ψ_5
p_{ψ_α}	0.2095	0.2074	0	0.2084	0.2067
e_{ψ_α}	0.0088	0.0086	0.0346	0.0087	0.0085
Eq.(3.56)	0.0092	0.0092	-	0.0092	0.0092
Eq.(3.57)	-	-	0.0368	-	-

Table 3.3: For $\tilde{N}_\psi < N_\psi$, $N = 16$, and $\varepsilon_\kappa = 1.1$

	ψ_1	ψ_2	ψ_3	ψ_4	ψ_5
p_{ψ_α}	0.1388	0.1384	0.1380	0.1377	0.1377
Eq.(3.55)	0.1365	0.1365	0.1365	0.1365	0.1365
e_{ψ_α}			$< 1e^{-6}$		

Table 3.4: For $\tilde{N}_\psi > N_\psi$, $N = 24$

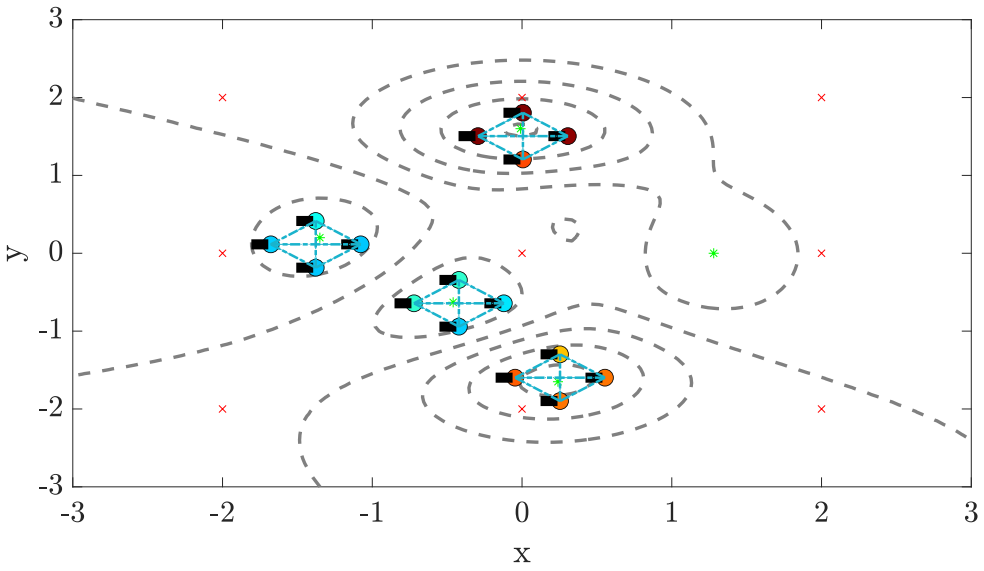

(a)

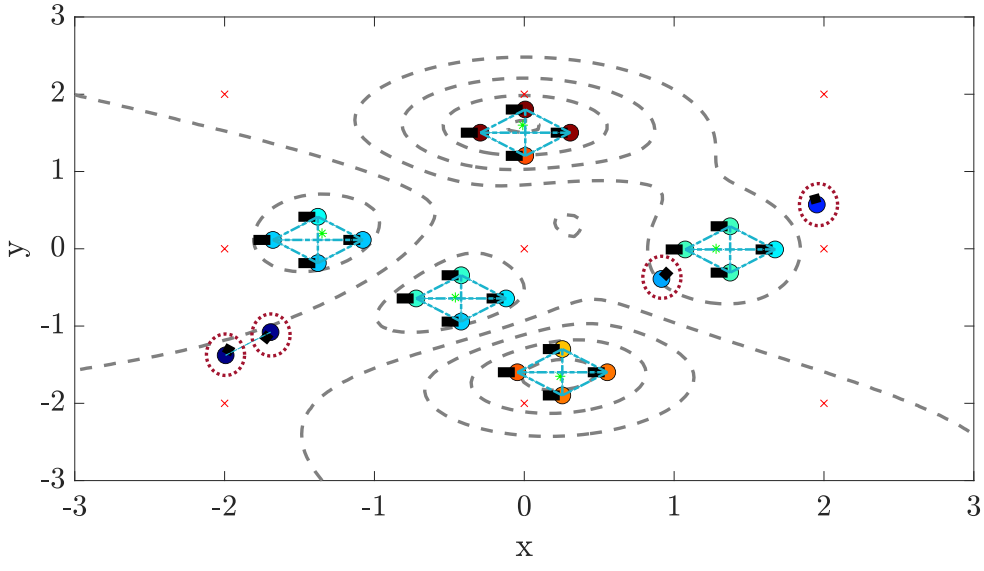

(b)

Figure 3.17. (a) agents' final location for $\tilde{N}_\psi < N_\psi$, $N = 16$ and (b) for $\tilde{N}_\psi > N_\psi$, $N = 24$ (the redundant agents are circled in dashed-red).

Chapter 4

Flocking-Based Source Seeking

In this chapter, we present a source-seeking scheme that is inspired by animal behavior and avoids gradient estimation. The gradient-estimation process is typically based on the underlying formation-control scheme, which can be restrictive. To avoid these restrictions, we employ the flocking framework herein, which provides more flexibility.

4.1 Gradient-Free Source Seeking Using Flocking Behavior

In this section, we propose a novel solution for the source-seeking problem based on flocking and GSO, where we prove the stability and convergence of this scheme under some mild assumptions. Thus, we ensure that a group of autonomous agents locate the unknown extremum while staying together without collision. An alternative solution based on a law that embodies both flocking and an attraction element is introduced in Appendix B.

4.1.1 Protocol

Here, we use the definitions in section 2.3, where the agents are governed as in (2.9). Definition (2.10) sets the distance between agents, and in addition to velocity matching using the weighted adjacency matrix in (2.19), three Reynolds rules are achieved as sketched by algorithm (2.20),

$$u_i^\alpha = \sum_{j\in\mathcal{N}_i} \phi_i^j(q_{ji})n_{ji} + \sum_{j\in\mathcal{N}_i} a_{ij}(p_j - p_i).$$

This alone will converge the agents into a flock (or fragmentation), but for navigational purposes, an additional term is added. Inspired by GSO, where agents with a higher level of attractiveness attract others, we set ψ_i as an agent's level of attractiveness. This way, an agent with larger ψ_j "pulls" an agent with lower ψ_i, which causes a movement of the swarm in the direction of the extremum. The term in the control law that achieves this is

$$u_i^\psi = k \sum_{j\in\mathcal{N}_i} (\psi_j - \psi_i)n_{ji}, \tag{4.1}$$

where $k > 0$ is a tuning parameter and again $n_{ji} = \sigma_\epsilon(q_j - q_i)$.
We assume that the scalar field has a unique stationary point at its maximum and that an *a priori* bound on the gradient of the field is known.

A1 The scalar field $\psi(q)$ is concave with a unique maximum at q_s.

A2 $\exists C > 0 : ||\nabla\psi(q)|| \leq C \ \forall q \in \mathbb{R}^m$.

Note that the gradient of the scalar field is not required for the application of the protocol, but we require it for analysis. A generalization using non-smooth analysis can be carried out for fields whose gradient is not well-defined everywhere.
As explained, the underlying concept is to modify (2.20) to generate an action function that drives agents toward the source in flocking. To do so, we add the term in (4.1) to (2.20) and obtain the control law for agent i:

$$u_i = \underbrace{\sum_{j\in\mathcal{N}_i} \phi_i^j(q_{ji})n_{ji} + \sum_{j\in\mathcal{N}_i} a_{ij}(p_j - p_i)}_{u_i^\alpha} - cp_i + \underbrace{k\sum_{j\in\mathcal{N}_i}(\psi_j - \psi_i)n_{ji}}_{u_i^\psi}, \tag{4.2}$$

where cp_i with $c > 0$ is an additional damping term (due to the double-integrator dynamics). The protocol in (4.2) combines the group objective with flocking behavior and avoids the use of a noise-sensitive gradient-estimation process.

4.1.2 Stability Analysis

The control law (4.2) leads to the closed-loop collective dynamics

$$\begin{aligned} \dot{q} &= p \\ \dot{p} &= -\nabla V(q) - \hat{L}(q)p - c\cdot p + f_\gamma(q), \end{aligned} \tag{4.3}$$

where $f_\gamma(q) \in \mathbb{R}^{Nm}$ is defined as

$$[f_\gamma(q)]_i \in \mathbb{R}^m, \ [f_\gamma(q)]_i = k\cdot\sum_{j\in\mathcal{N}_i}(\psi_j - \psi_i)n_{ji}.$$

We analyze the stability in two steps:
Part A: Define a dissipative Hamiltonian system, assuming that the agents can measure the gradient of the scalar field locally without any communication with neighbors, and analyze this system.
Part B: Show that the proposed protocol leads to a system that can be seen as a perturbed evolution of the dissipative Hamiltonian system defined in Part A and prove that under some assumptions, the states remain bounded.
[Part A]: We consider a scenario where each agent can measure the gradient $\nabla\psi(q_i)$ locally and apply the following control law:

$$u_i^A(t) = \sum_{j\in\mathcal{N}_i}\phi_i^j(||q_j - q_i||)n_{ji} + \sum_{j\in\mathcal{N}_i} a_{ij}(q)(p_j - p_i) - c\cdot p_i + \nabla\psi(q_i), \tag{4.4}$$

where $\nabla\psi(q_i) \in \mathbb{R}^m$ and for the scalar case $\frac{d\psi(q_i)}{dq}$. This leads to the collective dynamics

$$\begin{aligned} \dot{q} &= p \\ \dot{p} &= -\nabla V(q) - \hat{L}(q)p - c\cdot p + \nabla\Psi(q), \end{aligned} \tag{4.5}$$

where $\Psi : \mathbb{R}^{Nm} \to \mathbb{R}$ is the scalar field whose argument comprises the positions of all agents and is defined as $\Psi(q) = \sum_i \psi(q_i)$, and $\nabla\Psi(q) \in \mathbb{R}^{Nm}$ is defined as $\nabla\Psi(q) =$

$[\nabla\psi(q_1), \nabla\psi(q_2), \ldots, \nabla\psi(q_N)]^T$ and for the scalar case, this is reduced to $\nabla\Psi(q) = [\frac{d\psi(q_1)}{dq}, \frac{d\psi(q_2)}{dq}, \ldots, \frac{d\psi(q_N)}{dq}]^T$.

Remark 1: For general scalar fields $\psi(q_i)$, it is not possible to decompose $\nabla\Psi(q)$ as in [Olfati-Saber, 2006]. Hence, the translation and structural dynamics cannot be decoupled and analyzed independently.
Remark 2: For quadratic scalar fields, e.g., $\psi(q_i) = -q^T H q$, where H is symmetric positive definite, we obtain linear forcing terms $\nabla\psi(q_i) = -2Hq$, which allow the decomposition as suggested in [Olfati-Saber, 2006] and facilitates the analysis.

Decoupling the translational and structural dynamics completely, for general case, is difficult. Therefore, to characterize the system's equilibria, we produce the agents center-of-mass dynamics. Let $q_c, p_c \in \mathbb{R}^m$ be two center-of-mass variables, where

$$q_c = \frac{1}{N}(\mathbf{1}^T \otimes I_m)q, \tag{4.6}$$

$$p_c = \frac{1}{N}(\mathbf{1}^T \otimes I_m)p. \tag{4.7}$$

The translational dynamics of the center of mass are then

$$\begin{aligned} \dot{q_c} &= \frac{1}{N}(\mathbf{1}^T \otimes I_m)\dot{q} = p_c \\ \dot{p_c} &= \frac{1}{N}(\mathbf{1}^T \otimes I_m)\dot{p} \\ &= \frac{1}{N}(\mathbf{1}^T \otimes I_m)[-\nabla V(q) - \hat{L}(q)p - c \cdot p + \nabla\Psi(q)] \\ &= \frac{1}{N}(\mathbf{1}^T \otimes I_m) \cdot \nabla\Psi(q) - c \cdot p_c. \end{aligned} \tag{4.8}$$

We can observe that, for the translation dynamics of the center of mass to be in equilibrium, the positions q must satisfy $(\mathbf{1}^T \otimes I_m) \cdot \nabla\Psi(q) = 0$. The following Lemma characterizes the equilibrium for a special case when the scalar field $\psi(q_i)$ is radially symmetric about the stationary point $q_s := \text{argmax}_q \psi(q_i)$.
Let, for a given $q = [q_1^T, q_2^T, \ldots, q_N^T]^T$, convexhull$(q) := \{q \in \mathbb{R}^m | \exists \alpha_1, \alpha_2, \ldots, \alpha_N \in [0,1]$, s.t. $\sum_i \alpha_i = 1$ and $q = \sum_i \alpha_i q_i\}$.

Lemma 4.1. *Assume that the scalar field satisfies assumptions A1,A2. Additionally, if it is radially symmetric, i.e.,* $\psi(x) = \psi(y)\ \forall\ x,\ y,$ s.t $||x - q_s|| = ||y - q_s||$,
then all possible equilibria of the translational dynamics of the center-of-mass correspond to q^* *such that* $q_s \in$ convexhull(q^*).

Proof. Without loss of generality, we assume that the source q_s is at the origin. A radially symmetric scalar field $\psi(q_i)$ can be represented in polar coordinates by a function $\psi_r : \mathbb{R}_+ \to \mathbb{R}$ such that $\psi_r(r) = \psi(q_i)\ \forall\ ||q|| = r$. For $||q|| \neq 0$, $\nabla\psi(q_i) = \frac{d\psi_r(r)}{dr} \cdot \frac{q}{||q||}$ and from concavity of $\psi(q_i)$, we can show that $\psi_r(r)$ is concave with the maximum located at $r = r_s = ||q_s|| = 0$ from our earlier assumption. Similarly, $\frac{d\psi_r(r)}{dr} < 0\ \forall r \neq 0$. Hence, $\nabla\psi(q_i)$ is always in the direction of $-q,\ \forall q \neq 0$.

Let us assume that there exists an equilibrium of the translational dynamics of the center of mass corresponding to q^*, such that $q_s \notin$ convexhull(q^*). Hence, there exists a separating hyperplane such that q_s is located on the opposite half-space to that of $q_i\ \forall i \in 1, 2, \ldots, N$.

Define a unit vector h perpendicular to the separating hyperplane and pointing towards q_s; then, because all agents belong to the opposite side of the hyperplane, note that $q_i^T h < 0 \ \forall i$. The force f_i acting on agent i along h is given by

$$f_i = (\nabla\psi(q_i))^T h = \frac{d\psi_r(r_i)}{dr} \cdot \frac{q_i^T h}{||q_i||} = k_i \cdot q_i^T h,$$

where $k_i := \frac{d\psi_r(r_i)}{dr} \cdot \frac{1}{||q_i||} < 0 \ \forall ||q|| \neq 0$ and $q_i^T h < 0$. Therefore, the force on each agent along h is strictly positive. Hence, the net force f_h on the center of mass along h is

$$f_h = f_1 + f_2 + \cdots + f_N > 0.$$

Therefore, this cannot be an equilibrium of the translational dynamics of the center of mass. We have thus shown by contradiction that for all equilibria, there exists no hyperplane separating the source q_s and the positions of the agents q_i. Then, by considering hyperplanes sequentially, the source must lie in the convexhull(q^*). □

A similar result can be reached by replacing the assumption of radial symmetry with strong concavity of the scalar field ψ, which is weaker. Now, we have the following theorem.

Theorem 4.1. *Under protocol (4.4), almost all trajectories asymptotically converge to the equilibrium $(q^*, 0)$ characterized by $\nabla V(q) - \nabla\Psi(q) = 0$. For the special case when $\psi(q_i)$ is radially symmetric, the trajectory converges to the equilibrium characterized by Lemma 4.1.*

Proof. Straightforward application of La Salle's invariance theorem.
Organize equation (4.5) as

$$\begin{aligned} \dot{q} &= p \\ \dot{p} &= -\nabla U(q) - (\hat{L}(q) + c)p, \end{aligned} \tag{4.9}$$

where $U(q) = V(q) - \Psi(q)$ with the corresponding Hamiltonian

$$H(q, p) = U(q) + K(p).$$

Notice that the Hamiltonian is constructed from the potential $U(q)$ and $K(p) = \frac{1}{2}\sum_{i=1}^{N} ||p_i||^2$ is a dissipative kinetic energy. In this case, the isolated local minima of $U(q)$ correspond to the stable equilibrium point. Derivation of H yields

$$\begin{aligned} \dot{H} =& \dot{q}^T \nabla U + p^T \dot{p} \\ =& p^T \nabla U + p^T(-\nabla U - (\hat{L} + c)p) = -p^T(\hat{L} + c)p \\ =& -\frac{1}{2}\sum_{(i,j)\in\mathcal{E}} a_{ij}||p_j - p_i||^2 - c\sum_{i\in N} ||p_i||^2 \leq 0. \end{aligned} \tag{4.10}$$

Thus, from LaSalle's invariance principle [LaSalle, 1960] ($\dot{H} \leq 0, H(q^*, 0) = 0$), every solution asymptotically converges to an equilibrium q^* a minima of the potential function $U(q)$. □

[Part B]: Now, we relax the assumption that each agent can independently measure the gradient locally. We want to analyze the gradient-free protocol proposed earlier, and show that this protocol leads to dynamics that can be seen as a modification of the

evolution of the collective dynamics shown in Part A.
The dynamics in (4.3) can be written as

$$\begin{aligned}\dot{q} =& p \\ \dot{p} =& -\nabla V(q) - \hat{L}(q)p - c\cdot p + \nabla\Psi(q) + (f_\gamma(q) - \nabla\Psi(q)) \\ =& -\nabla V(q) - \hat{L}(q)p - c\cdot p + \nabla\Psi(q) + e(q),\end{aligned} \tag{4.11}$$

where

$$e(q) := (f_\gamma(q) - \nabla\Psi(q)).$$

Then, we have the following theorem.

Theorem 4.2. *Assume that is possible to tune r_s, d, a, b, and k such that there exists a constant $C > 0$ where $||e||_\infty \leq C\ \forall q$. Then the proposed protocol leads to stable dynamics. Moreover, it behaves qualitatively similar to the protocol proposed in Part A.*

Proof. Consider the total energy of the system.

$$T(q,p) = V(q) - \Psi(q) + \frac{1}{2}p^2 \tag{4.12}$$

By differentiating with respect to time, we obtain

$$\begin{aligned}\dot{T}(q,p) =& (\nabla V(q) - \nabla\Psi(q))^T p + p^T\dot{p} \\ =& (\nabla V(q) - \nabla\Psi(q))^T p \\ &+ p^T(-\nabla V(q) - \hat{L}(q)p - c\cdot p + \nabla\Psi(q) + e(q)) \\ =& -p^T\hat{L}(q)p - p^T cp + p^T e(q).\end{aligned} \tag{4.13}$$

We will now use dissipative arguments. From the fundamental theorem of calculus, we have

$$\begin{aligned}T(q(t),p(t)) =& T(q(0),p(0)) + \int_0^t \dot{T}(q(\tau),p(\tau))d\tau \\ =& T(q(0),p(0)) \\ &+ \int_0^t -p^T(\hat{L}(q) + c\cdot\mathbf{I})pd\tau \\ &+ \int_0^t p^T e(q)d\tau \\ \leq& T(q(0),p(0)) + \int_0^t p^T e(q)d\tau \\ \leq& T(q(0),p(0)) + ||e||_\infty \int_0^t p^T\mathbf{1}d\tau \\ \leq& T(q(0),p(0)) + ||e||_\infty \int_0^t \dot{q}^T\mathbf{1}d\tau \\ \leq& T(q(0),p(0)) + ||e||_\infty (q(t)^T\mathbf{1} - q(0)^T\mathbf{1}) \\ \leq& K_1 + ||e||_\infty \mathbf{1}^T q(t),\end{aligned}$$

where $K_1 = T(q(0),p(0)) - ||e||_\infty q(0)^T\mathbf{1}$.

Now, $-\Psi(q) \leq T(q(t),p(t))$; hence, we have

$$-\Psi(q) \leq T(q,p) \leq K_1 + ||e||_\infty \mathbf{1}^T q(t).$$

Note that $-\Psi(q)$ is a convex function with a maximum slope of C. Therefore, $||e||_\infty \leq C$ and ψ attains slope C for some q. It can be shown that the set of points q satisfying the above inequality is compact. □

Remark 3: This set can be geometrically visualized as the set of points where the hyper-plane $K_1 + ||e||_\infty \mathbf{1}^T q$ is above $-\Psi(q)$. Hence, there exists a bound $q_{\max}$ (supremum over all q along the intersection of the two surfaces mentioned in the above remark) such that $||q|| \leq q_{\max}$ for all time.

Remark 4: It is possible to use the information about the scalar field to develop algorithms that reduce the bound on $||e||_\infty$ using, for example, approximation theory for functions.

4.1.3 Tuning Guidelines

The last theorem requires proper tuning of the control protocol parameters. In this section, we examine the effect of these parameters on the swarm behavior and then conclude the tuning rules. In our example, a proper tuning that provides good behavior is: $r_s = 15; d = 6; a = 1; b = 10$; (see Figure 4.1). The large gap for choosing a, b values is due to the fact

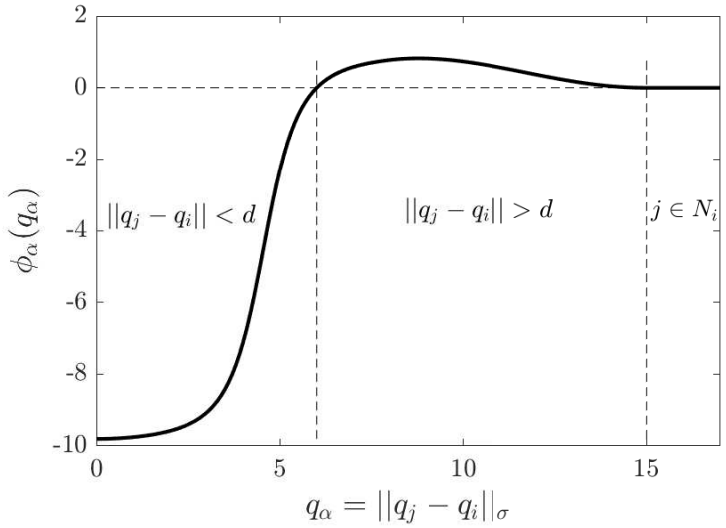

Figure 4.1. Nominal results with short-range and large repulsive area vs. wide-range and small attractive area.

that we have an additional attractive element, the outcome of the field measurements.
The first two parameters are the sensing radius r_s and the desired distance d, which are closely related. From definition $r_s > d$, to check if there exists a limitation on the delta (i.e., $|rs - d|$), we test two extreme cases where d is close to or far from r_s. The effect of different distance values is in the group size, where the performance remains without significant change.
Next, we observe the behavior of the proportional gain k in the field's attractive formula (4.1). As is well known, increasing k increases the speed of convergence, but leads to a poor transient response with low damping ratio, large peak overshoot, and oscillation. This

shall be tuned with respect to the agent representation and the whole swarm requirements (such as settling time and overshoot).
The final two parameters are a, b, which define the sigmoid minimum (b) and maximum (a) values, as well as the slope c (see (2.14)). By definition, $0 < a \leq b$, so we test the behavior for small and equal values of a with respect to b. For both cases, the agents did not diverge, but the swarm structure had an important impact. For a small value, the agents obtain a larger distance than the required d, owing to the small attractive area. For larger values, the distance is too small and collision occurs due to the large impact of the attractive element. Equal values of $a = b$ in addition to the field's attractive element result an aggressive attraction which is not applied to Reynold's rules.
To conclude this section, one should pay attention when tuning k, a in particular. Their impact is determined according to the agent's model as well as the desired distance d and field structure.
Note: For different scenarios, such as oil spills or ideal spheres, the same tuning parameters were applied. This provides strong evidence for the algorithm's robustness and simplicity.

4.1.4 Simulation Results

In this section, we present both simulation and experimental results. All simulations are conducted in 3D space ($m = 3$) with a spherical field characterized by
$\psi(q_i) = 500 - ||q_s - q_i||^2$ under the following chosen parameters.

r_s	d	ϵ	h	a	b	k	c
20.5	8	1	0.5	1	10	0.5	2

Figure 4.2 illustrates the proposed source-seeking scheme with 10 agents (small colored spheres). The right color bar indicates the concentration level $\psi(q_i)$ and the connecting lines indicates the communication topology. The agents' initial arbitrary locations are shown in (a), and (b) presents the final convergence to the extremum location. To evaluate the performance, let $d_s = ||q_s - q_c||$ be the distance between the agents' centers of mass and extremum location. The results are

$$d_s = ||q_s - q_c|| = 0.024$$
$$\psi(q_c) = 500 - ||q_s - q_c||^2 = 499.99,$$

which satisfy source detection under flocking constraints. Observation of the color bar shows that in the initial state (a), the agents' field-level measurements vary, whereas in the final state (b), they reach consensus with a value of $\psi(q_i) = 461$. The case when the field is time-variant is not part of the analysis but the observation is interesting (in such a case the field has constant velocity and the controller should be tuned properly for minimum steady-state error). The tracking ability of the swarm for this case is captured in Figure 4.3. Although the filed is moving, the swarm keeps tracking its maximum in a flocking behavior.
The experimental results of the proposed method are presented later, in section 6.2.

4.2 Flocking: Extension to Nonholonomic Models

In this section, an extension of the proposed gradient-free source-seeking concept to nonholonomic agents is presented. Here, the control law is embedded slightly differently,

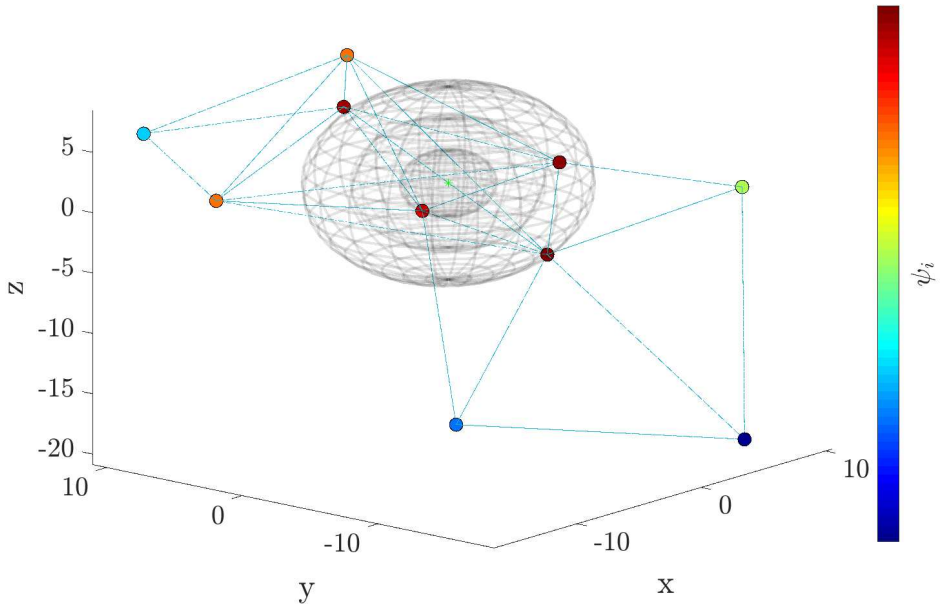

(a)

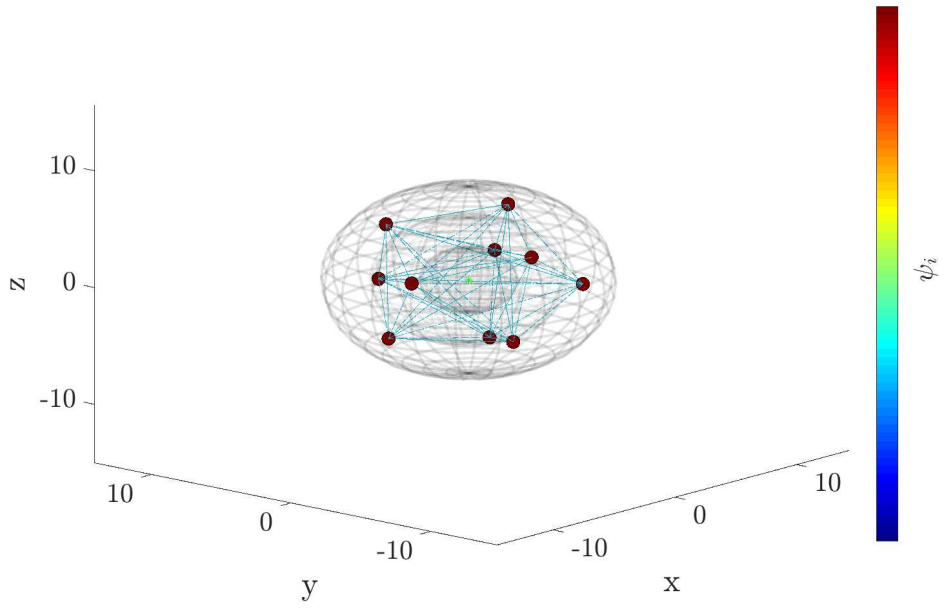

(b)

Figure 4.2. Swarm exploration behavior in a spherical field: (a) agents' initial locations, (b) reaching consensus on source location.

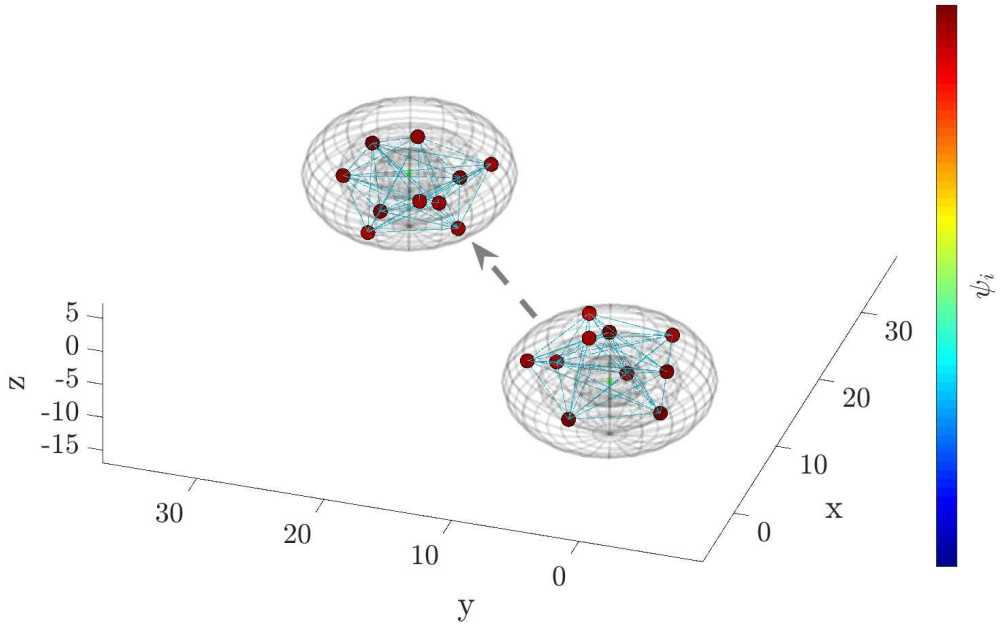

Figure 4.3. Swarm tracking a time-varying source (arrow direction) while flocking. One can see that the agents' concentration level remain the same indicating good tracking capabilities.

owing to the differences in each agent's models. For instance, the damping element, which is unavoidable for the double-integrator case, is omitted here. Two models are shown: kinematic and dynamic. Such cases provide additional sufficient evidence for the algorithm's robustness and efficiency. Protocols and observation results for each technique are presented. The cases are presented as concepts for possible solutions without analysis, but are relevant for realistic scenarios.

4.2.1 Kinematic Model

Each agent is modeled as a kinematic model of a nonholonomic unicycle, similar to (3.36). With respect to agent i, $q_i = [x_i, y_i] \in \mathbb{R}^2$ is the position in the plane, $\theta_i \in [0, 2\pi]$ is the orientation with respect to the x axis, and $v_i, \omega_i \in \mathbb{R}$ are the control inputs for linear and angular velocities, respectively.
Here, we modify the control law in (4.2) such that

$$\begin{aligned} \phi_i^j(q) =& \rho_h(q_{ji}/r_\alpha)\phi_s(q_{ji} - d) + k(\psi_j - \psi_i) \\ n_{ij} =& \sigma_\epsilon(q_j - q_i) \\ \varphi_i =& \sum_{j \in \mathcal{N}_i} \phi_i^j n_{ij}. \end{aligned} \tag{4.14}$$

Interpretation to states $x - y$:

$$\begin{aligned}
&\varphi_{ix} = \sum_{j\in\mathcal{N}_i} \phi_i^j n_{ij}^x,\ \varphi_{iy} = \sum_{j\in\mathcal{N}_i} \phi_i^j n_{ij}^y \\
&n_{ij}^x = \frac{x_j - x_i}{\sqrt{1+\epsilon||q_j - q_i||^2}},\ n_{ij}^y = \frac{y_j - y_i}{\sqrt{1+\epsilon||q_j - q_i||^2}} \\
&\kappa = \frac{1}{\sqrt{1+\epsilon||q_j - q_i||^2}} \\
&\varphi_{ix} = \sum_{j\in\mathcal{N}_i} \kappa\phi_i^j (x_j - x_i),\ \varphi_{iy} = \sum_{j\in\mathcal{N}_i} \kappa\phi_i^j (y_j - y_i)
\end{aligned} \tag{4.15}$$

and θ:

$$\begin{aligned}
\theta_{id} =& \tan^{-1}(\frac{\varphi_{iy}}{\varphi_{ix}}) \\
\varphi_{i\theta} =& \theta_i - \theta_{id}.
\end{aligned} \tag{4.16}$$

Note that the $\varphi_{i\theta}$ argument provides the alignment ability in Reynold's flocking rules; thus, the velocity-matching element is omitted.
The local control law remains as in (3.52).

$$u_i = [v_i, \omega_i]^T$$

$$v_i = k_v d_{iv}\cos(\varphi_{i\theta}),\ d_{iv} = \sqrt{\varphi_{ix}^2 + \varphi_{iy}^2}$$

$$\omega_i = -k_\omega \varphi_{i\theta} + \dot{\theta}_{id}$$

4.2.2 Dynamic Model

The extension to the dynamic model involves changes in the control input. Here, the control law interest is in providing torque commands τ_{i1} and τ_{i2} to control the linear and angular velocities, respectively. We assume that the linear velocity v_i and angular velocity ω_i are measured and fed back to achieve the desired v_{id} and ω_{id} calculated according to the gradient-free flocking protocol, similar to the kinematic case.
The agents' dynamic model is in the form of

$$\begin{aligned}
&\begin{cases}
\dot{z}_i = [\dot{x}, \dot{y}, \dot{\theta}]^T = R_i u_i \\
u_i = [v_i, \omega_i]^T \\
\dot{u}_i = M\tau_i
\end{cases} \\
&R_i = \begin{bmatrix} C_i & 0 \\ 0 & 1 \end{bmatrix},\ C_i = [\cos(\theta_i), \sin(\theta_i)]^T \\
&M = \begin{bmatrix} \frac{1}{m} & 0 \\ 0 & \frac{1}{c} \end{bmatrix},\ \tau_i = [\tau_{i1}, \tau_{i2}]^T,
\end{aligned} \tag{4.17}$$

where m, c are the mass and moment of inertia of agent i.
The control input remains as proposed in (4.14)

$$\begin{aligned}
&\varphi_i = \sum_{j\in\mathcal{N}_i} k\phi_i^j n_{ij} \\
&\varphi_{ix} = \sum_{j\in\mathcal{N}_i} \kappa\phi_i^j (x_j - x_i),\ \varphi_{iy} = \sum_{j\in\mathcal{N}_i} \kappa\phi_i^j (y_j - y_i) \\
&\theta_{id} = \tan^{-1}(\frac{\varphi_{iy}}{\varphi_{ix}}),\ \varphi_{i\theta} = \theta_i - \theta_{id},
\end{aligned}$$

but the local control law is modified to

$$\begin{aligned} u_i =&[\tau_{i1}, \tau_{i2}]^T \\ v_{id} =&k_v d_{iv} \cos(\varphi_{i\theta}),\ d_{iv} = \sqrt{\varphi_{ix}^2 + \varphi_{iy}^2} \\ \omega_{id} =&-k_\omega \varphi_{i\theta} \\ \tau_{i1} =&k_1(v_{id} - v_i),\ \tau_{i2} = k_2(\omega_{id} - \omega_i) \end{aligned} \tag{4.18}$$

such that the torque commands τ_{i1}, τ_{i2} serve as inputs to the motors controlling the vehicle speed and angle.

4.2.3 Simulation Results

Simulation scenarios for the 2D plane are conducted with a group of 6 nonholonomic unicycles. The field is drawn as circles centered at the origin with a function of $\psi_i = 10/||q_i - q_s||$. For the kinematic case, Figure 4.4 (a) shows the agents' trajectories in time and the corresponding field's measurements. The observed peak in the field's concentration level is because one of the agents, while traveling across the field to generate the flocking structure, passes through or near field's maximum, which is expressed as the highest measurement.

The results for the dynamic case are similar to those of the kinematic case, so it is interesting to observe the behavior of the swarm for the time-varying field case. In Figure 4.4 (b) agent's initial and final location are plotted. The agents manage to locate the source, where they all reach concentration level consensus and keep track of the field in time.

4.2.4 Multiple-Extrema Seeking with Flocking

In chapter 3.3, we provide a solution to the complex task of exploring a field with multiple extrema. We use formation control to converge the agents into groups and gradient estimation along with GSO to attract agents toward the different sources. By using fixed match-making locations, agents could meet while seeking potential neighbors or being rejected from occupied extrema. Here, we wish to fulfill this task using the proposed gradient-free flocking protocol. The algorithm proposed in (3.50) is modified, in the flocking method, to

$$e_i = \rho_i^q e_i^q + \rho_i^f \varphi_i, \tag{4.19}$$

where φ_i is the law in (4.14). The simplicity of the law is notable owing to the unified solution of flocking and source-seeking embedded in φ_i. The conditional terms are similar to those in (3.51).

$$\rho_i^q = \begin{cases} 0, \ |\mathcal{N}_i| = \delta - 1 \wedge \psi_i > 0 \\ 1, \text{ else} \end{cases} ; \rho_i^f = \begin{cases} 0, \ ||\hat{q}_\alpha - q_i|| < c \\ 1, \text{ else} \end{cases},$$

where $\hat{q}_\alpha$ is an occupied peak when $i \notin \xi_\alpha$.
The simulation results of the agents' exploration process are presented in Figure 4.5 from the initial distribution (a), and through the seeking process until reaching steady state where five groups in team of four agents are located at each peak, where agents converge in flocking structure (b). Note that the diamond shape is a result of the flocking α-*lattice* characteristic (and not an explicit requirement, as in the formation case).

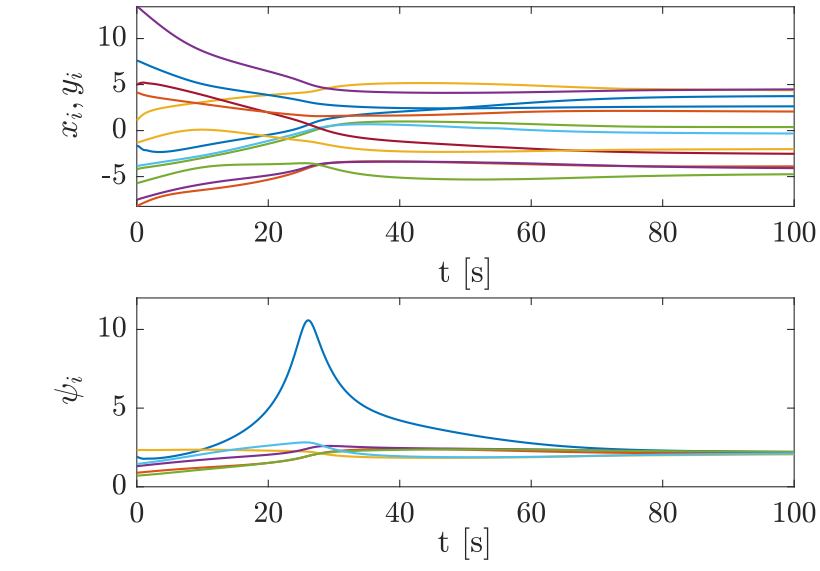

(a)

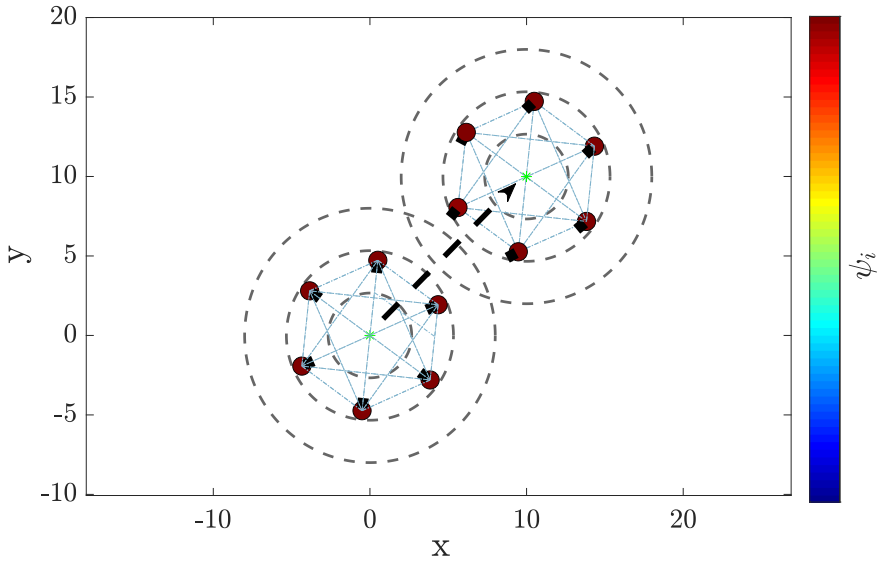

(b)

Figure 4.4. Results for the dynamic representation; (a) agents' trajectories (upper) and corresponding concentration level (lower) in search for a static source. (b) Swarm exploration behavior in time-varying field plotted over the $x - y$ plane.

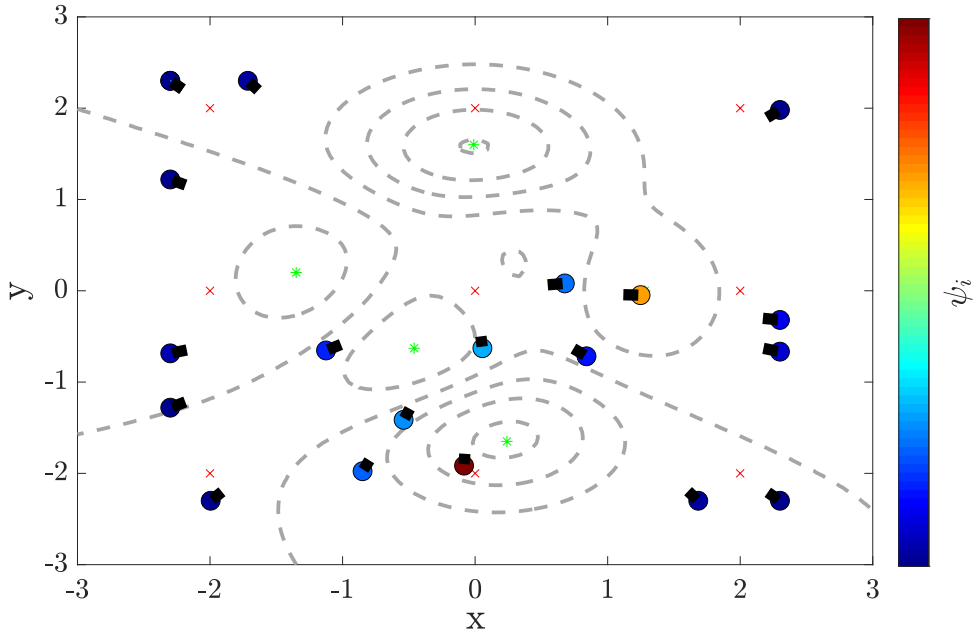

(a)

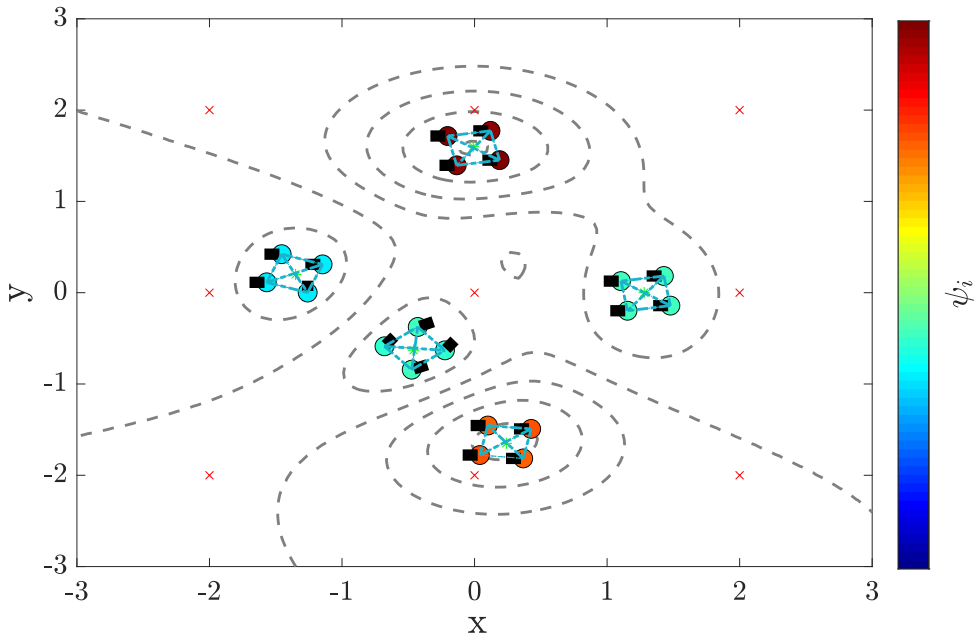

(b)

Figure 4.5. Multiple-extrema-seeking algorithm with flocking; stages from (a)-initial to (b)-final.

Chapter 5

Comparison and Cooperation

In previous chapters, we have focused on the performance and stability analysis of two different cooperative methods: flocking and formation. In this chapter, our intentions are twofold. First, we compare the two methods under a realistic scenario, and then we propose a unified solution that benefits from both. The notation γ-*agent* is an external tracking target which is defined as the match-making location in the first section and described a virtual leader in the second.

5.1 Comparison

This section aims to explain the differences between flocking with glowworm characteristics and formation with the gradient-estimation approach. A numerical representation of an oil spill (can also be considered as a toxic cloud) is used as a complex task where agents are required to locate and monitor the highest concentration by flocking or formation. All agents are modeled as double integrators. In addition, we have added a novel solution for the initial agents' distribution. By using match-making locations, we relax the conservative assumption that for at least one neighbor, $\{\exists j : \psi_j > 0,\, j \in \mathcal{N}_i, \forall i \in N\}$.

5.1.1 γ-Agents as "Match-Making" Locations

Let a γ-agent describes a predefined matching location inside the polluted area (i.e., the area of interest), where $q_{r_i} \in \mathbb{R}^3$ is the location and define Q as the set of all γ-agents.

$$\begin{gathered} Q = \{q_{r_1}^T, \ldots, q_{r_w}^T\},\ \mathcal{J}_\mathcal{Q} = \{1, 2, \ldots, w\} \\ \max ||q_{r_i} - q_{r_j}|| \leq 2r_s,\ \forall i, j \in \mathcal{J}_\mathcal{Q}, \end{gathered} \tag{5.1}$$

where w describes the total number of γ-agents generated according to

$$w = \left\lfloor \frac{h_f w_f d_f}{\lceil 2r_s \rceil^2} \right\rfloor, \tag{5.2}$$

where h_f, w_f and d_f is the field maximum height, width, and depth respectively, and r_s is an agent's sensing radius. The attraction element toward a γ-agent is then set according

to the following f_γ function:

$$\begin{aligned} f_\gamma(q_i, p_i, q_{r_i}) =& - c_1(q_i - q_{r_i}) - c_2 p_i \\ f_{\gamma,i} =& f_\gamma \cdot \rho_i \\ q_{r_i} = \arg\min_{j \in \mathcal{J}_\mathcal{Q}} ||q_{r_j} - q_i||,\ \rho_i =& \begin{cases} 1, \ |\mathcal{N}_i| < n_p \vee \psi_i < \epsilon \\ 0, \text{ else} \end{cases} . \end{aligned} \tag{5.3}$$

Note that q_{r_i} changes sequentially once it is reached (i.e., $||q_{r_i} - q_i|| = 0$) but the conditions still hold.
Let $n_p > 0$ be the lower possible sum of neighbors for a single agent. For example, in a 2D case, this value is set to $n_p = 2$.

Lemma 5.1. *Under the protocol (5.3) and for any arbitrary initial location $q(t = 0) = q_0$, after finite time $t_r > 0$, all agents are inside the field (i.e., $\psi_i > 0$, $\forall i \in N$) and have at least n_p neighbors, $|\mathcal{N}_i| \geq n_p$.*

Proof. First, we show that all agents move toward and remain inside the field. Because all γ-agents are located in areas where $\psi_r > 0$, then it is enough to show that an agent is attract toward a γ-agent. Without loss of generality we assume $c_1 = c_2 = 1$ and define the following.

$$\begin{aligned} \xi =& q_i - q_{r_i} \\ \nu =& \dot{\xi} = \dot{q}_i = p_i \\ \dot{\nu} =& \dot{p}_i = f_\gamma = -\xi - \nu. \end{aligned}$$

Let the following Lyapunov candidate $V(\xi, \nu) = \frac{1}{2}\xi^T\xi + \frac{1}{2}\nu^T\nu$ where

$$\dot{V} = \dot{\xi}^T\xi + \nu^T\dot{\nu} = \nu^T\xi + \nu^T(-\xi - \nu) = -\nu^T\nu \leq 0$$

and $V(\xi^*, 0) = 0$ iff $\xi^* = 0$ when $q_i = q_{r_i}$. For the second part of the proof, let us observe an extreme scenario. Assume that an agent is located at $q_i = q_{r_i}$ with no neighbors, i.e., $|\mathcal{N}_i| = 0$. Thus, all other agents are located near q_{r_j}, $j \notin \mathcal{J}_{\mathcal{Q}_i}$. However, from the definition in (5.1), the distance between two neighbors γ locations is no greater than twice the sensing radius of an agent. Therefore, agent q_i must sense at least one agent located near q_{r_j}, which leads to connectivity. This is true for any other scenario where $0 < |\mathcal{N}_i| < n_p$. □

5.1.2 LTL

Before introducing the two techniques using either formation or flocking, we find the LTL formula that describes the algorithm flow. The possible states are defined as follows:

- b_0: Seek neighbors while moving toward γ-agent,
- b_1: Maintain formation/flocking and use gradient-climbing technique,
- b_2: Peak located.

b_2 is also defined as the *acceptance state*.
Next, the following atomic proposition is defined to describe the transition conditions $a_1, a_2, a_3 \in AP$, where

- $a_1 : |\mathcal{N}_i| < n_p \vee \psi_i < \epsilon$,

- $a_2 : |\mathcal{N}_i| = n_p \wedge \psi_i > \epsilon$,

- $a_3 : u_i \leq \varepsilon_1$,

and n_p is the minimum required number of neighbors.
The LTL specification formula can be stated as

$$\varphi = \Box(a_1 \rightarrow \Diamond a_2) \wedge (a_2 U a_3)$$

with the corresponding Büchi automaton A_φ.

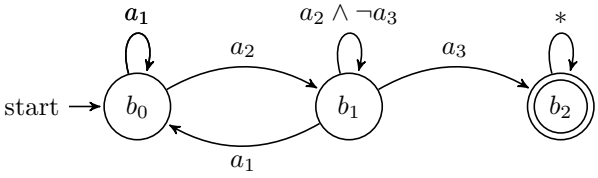

5.1.3 Formation

First, we describe the formation solution. Based on the results from Chapter 3, the control law is in the form of

$$u_i^{fr} = k_f \hat{L}_i (q_f - q) + k_g \cdot \hat{g}_i - cp_i + f_{\gamma,i}, \tag{5.4}$$

where cp_i with $c > 0$ is an additional damping term, $q_f \in \mathbb{R}^{mN}$ is the relative formation vector, and $\hat{L} = L \otimes I_m \in \mathbb{R}^{mN \times mN}$ and $\hat{g}_i$ is defined as in equation (3.4). From Lemma 5.1, the temporal effect of reaching a match-making location is achieved, i.e., $\rho_i = 0$; then, the closed-loop dynamics can be written as

$$\begin{bmatrix} \dot{q} \\ \dot{p} \end{bmatrix} = \begin{bmatrix} 0 & I_N \\ -k_f \hat{L} & -c \end{bmatrix} \begin{bmatrix} q \\ p \end{bmatrix} + \begin{bmatrix} 0 & 0 \\ k_f \hat{L} & k_g \end{bmatrix} \begin{bmatrix} q_f \\ \hat{g} \end{bmatrix}. \tag{5.5}$$

Proposition 5.1. *Consider the MAS (2.9) with control law (5.4). For all $q_i(0) \in \mathbb{R}^m$, the agents converge into formation q_f located at source q_s.*

Proof. From Lemma 5.1 and under the LTL specification, for $t > t_r$, $f_{\gamma_i} = 0$, and from equations (2.9) and (5.4), we have

$$\begin{aligned} \dot{q} =& p \\ \dot{p} =& - k_f \hat{L}(q - q_f) - k_g \hat{g}(q) - cp. \end{aligned} \tag{5.6}$$

Without loss of generality we assume $k_f = k_g = 1$ and let $\xi = q - q_f$ and $\nu = \dot{\xi}$ such that $\dot{\nu} = u_i^{fr} = -\nabla U(\xi)$ where $U(\xi) = -\hat{L}(q - q_f) - \tilde{g}$. Then, the following Lyapunov candidate $V(\xi, \nu) = U(\xi) + \frac{1}{2}\nu^T \nu$, s.t.

$$\dot{V} = \dot{\xi}^T \nabla U + \nu^T \nu = \nu^T \nabla U + \nu^T (-\nabla U - c\nu) = -\nu^T c\nu \leq 0,$$

and $V(\xi^*, 0) = 0$ iff $q - q_f = 0$, $\hat{g} = 0$ so $q^* = q_s$. □

5.1.4 Flocking

Next, we describe the solution based on flocking. Similar to Chapter 4, we generate a gradient-free control law in addition to f_γ tracking capabilities.

$$\begin{aligned} u_i^{fl} &= \underbrace{\sum_{j\in\mathcal{N}_i} \phi_i^j(q_{ji})n_{ji} + \sum_{j\in\mathcal{N}_i} a_{ij}(p_j - p_i)}_{u_i^\alpha} - cp_i + \underbrace{k\sum_{j\in\mathcal{N}_i}(\psi_j - \psi_i)n_{ji}}_{u_i^\psi} + f_{\gamma_i} \\ &= \sum_{j\in\mathcal{N}_i}[\phi_i^j(q_{ji}) + k(\psi_j - \psi_i)]n_{ji} + \sum_{j\in\mathcal{N}_i} a_{ij}(p_j - p_i) - cp_i + f_{\gamma_i} \end{aligned} \tag{5.7}$$

Proposition 5.2. *Consider the MAS (2.9) with the control law (5.7). For all $q_i(0) \in \mathbb{R}^m$ and $t \geq 0$, the agents locate the unknown field's maximum, where all possible equilibria of the translational dynamics of the center of mass correspond to q^* such that $q_s \in$ convexhull(q^*).*

Proof. Similar to the formation proof, once condition a_2 is completed and state b_1 is reached, i.e., $f_\gamma = 0$, equation (5.7) is reduced to

$$u_i^{fl} = \sum_{j\in\mathcal{N}_i}[\phi_i^j(q_{ji}) + k(\psi_j - \psi_i)]n_{ji} + \sum_{j\in\mathcal{N}_i} a_{ij}(p_j - p_i) - cp_i,$$

which is the same as equation (4.2), where the proof is similar, thus omitted. □

Next, we compare the behavior of formation vs. flocking under a controlled scenario, such as a moving sphere and the random noisy behavior of an oil spill. All simulations are conducted using 10 double-integrator agents.

5.1.5 Sphere-Tracking Comparison Results

A sphere model representing a 3D field with maxima at the center is used. Whereas with flocking there is no need for an explicit structure (only the desired distance), with formation, we require the agents to generate a 3D diamond shape. This, as is demonstrated soon, is a disadvantage once level-surface tracking is considered. Figure 5.1 presents the initial (a) and final (b) stages of the agents. As described, the agents' initial distribution is outside the sphere and far from the sensing radius; nevertheless, by using match-making locations, the agents are able to locate the field's maxima and reach formation consensus. For better observation, we provide the field with a repeated motion. In figure 5.2 a comparison of the velocities of agent i is depicted, where with flocking the system behaves more smoothly and has faster reaction as opposed to formation.

Level-Surface Tracking

The need for continuous information regarding the field's size and expansion ratio is crucial in the case of dangerous toxic substances. Flocking characteristics enable such a task to be performed. Whereas the formation is limited by its rigid structure, with flocking, the swarm adapts its structure while maintaining the required distance constraint. Figure 5.3 demonstrates the result of tracking the field structure in addition to time-varying changes. The surface level is detected by increasing the distance d constraint until a surface is reached with a value near zero ($\psi_i \leq \epsilon$, $\epsilon \ll 1$).

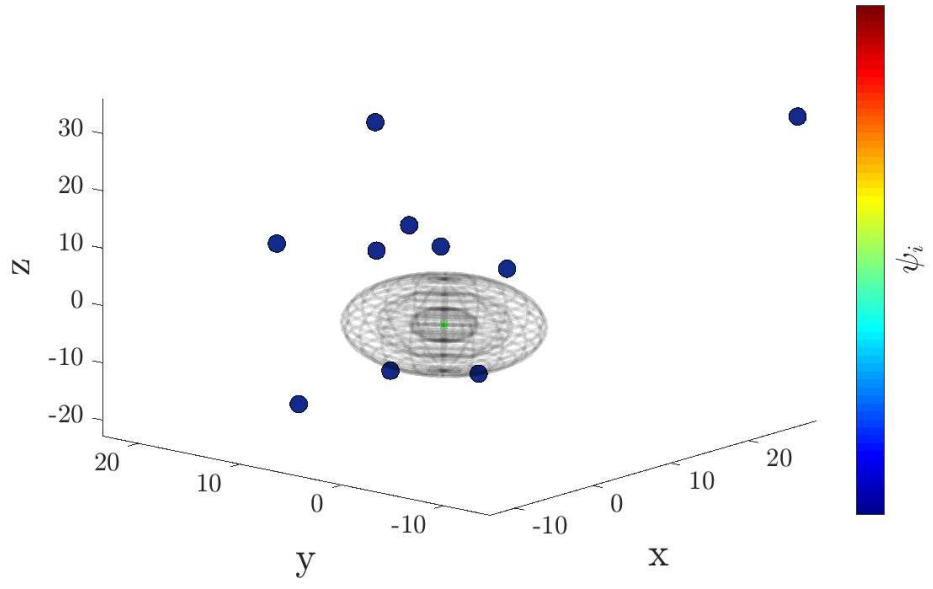

(a)

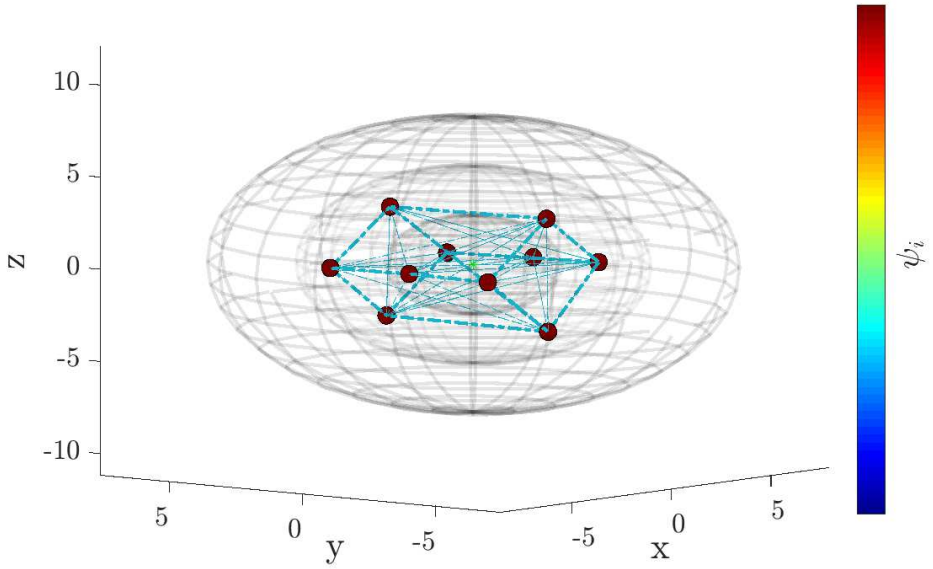

(b)

Figure 5.1. Initial (a) and final (b) state of the agents with the proposed formation algorithm, where agents initially posed outside the field, yet are capable to locate the source.

5.1.6 Oil Spill Exploration

Here, we use numerical models proposed by [Lončar et al., 2012, Stringari et al., 2013] to describe the behavior of oil particles under different conditions, such as diffusion and

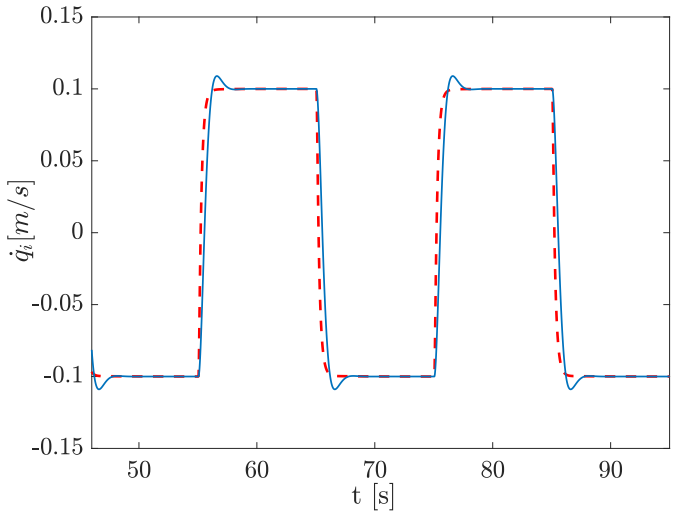

Figure 5.2. Comparison between flocking (red,dashed) and formation (blue,solid) under repeated motion of the field.

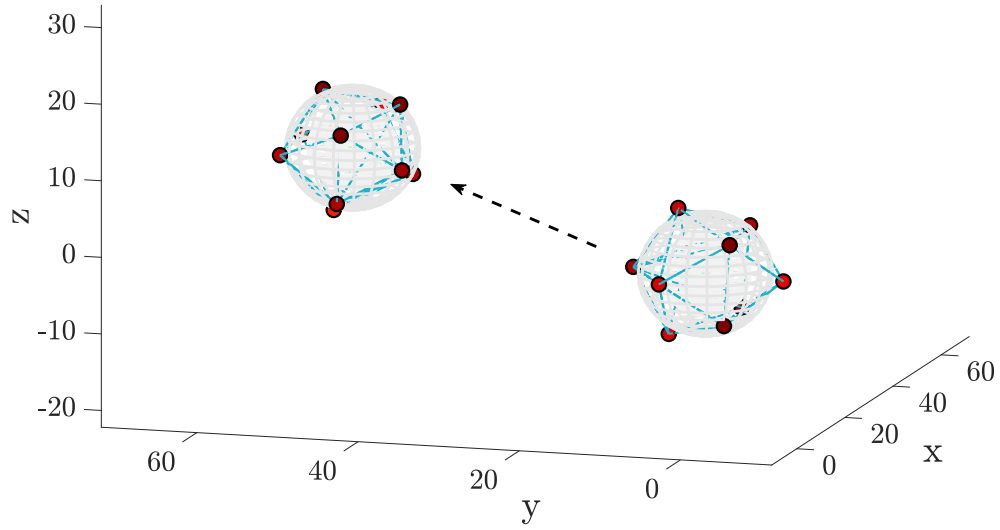

Figure 5.3. Sphere level-surface tracking with flocking and gradient-free approach.

evaporation, along with external effects, such as wind and current. The oil spill model treats the oil as discrete particles using Lagrangian approximation to evaluate the tracer (particles) motion over time. The independent effects (winds\currents) on each particle o

are considered as advective forces and described as

$$\begin{aligned} U_o =& K_c U_c + K_w U_w, \\ V_o =& K_c V_c + K_w V_w, \\ W_o =& K_c W_c + w_o, \end{aligned} \tag{5.8}$$

where U_o, V_o, W_o are the zonal, meridional, and vertical velocity components; U_c, V_c, W_c are the current velocities in each direction; U_w, V_w are the wind velocities; K_c, K_w are current and wind coefficients; and w_o is the particle-buoyancy. Diffusion processes depend on oil's physical–chemical characteristics. Here, we consider two processes: spreading and turbulent diffusion. Spreading is a horizontal expansion effect due to the different superficial tensions between water and oil.

$$U_r = \sqrt{\frac{2D_x}{T_k}},\ V_r = \sqrt{\frac{2D_y}{T_k}}, \tag{5.9}$$

where $D_x = D_y = \frac{\pi k_2^2}{16\sqrt{t}}(\frac{gV_0^2(\rho_w - \rho_0)}{v_w^2 \rho_w})^{1/3}$, V_0 is the tracer volume and T_k is the step interval. The spreading effect is modeled as a random process

$$U_{s,o} = R_1 \cos(2\pi R_2) U_r,\ V_{s,o} = R_1 \sin(2\pi R_2) V_r, \tag{5.10}$$

where $R_1, R_2 \sim \mathcal{N}(0,1)$. Turbulent diffusion has a horizontal effect and is estimated using random-walk methods and the particle's maximum movement ability at a given time (d_s).

$$U_{d,o} = d_s \cos(2\pi R_2),\ V_{d,o} = d_s \sin(2\pi R_2). \tag{5.11}$$

The evaporation process has a vertical effect by controlling the mass balance; it depends on the wind velocity and spill area (Ao).

$$f_{e,o} = \frac{Ao}{V_0} v_w \exp^{-\sqrt{x_o^2 + y_o^2}}. \tag{5.12}$$

Finally, each particle's trajectory is evaluated with time according to

$$\begin{aligned} x_o^{t+\Delta t} =& x_o^t + T_k(U_o^t + U_{s,o}^t + U_{d,o}^t), \\ y_o^{t+\Delta t} =& y_o^t + T_k(V_o^t + V_{s,o}^t + V_{d,o}^t), \\ z_o^{t+\Delta t} =& z_o^t + T_k(W_o^t + w_o^t) + f_{e,o}, \end{aligned} \tag{5.13}$$

where Δt is the time-step interval.

Oil Spill Estimation

As a result of using the particle model to represent the oil spill, one can consider different spatial concentration levels. This allows the oil spill density to be measured based on the number of particles surrounding a vehicle. Each vehicle is equipped with a sphere sensor of range r_{so}, which computes the concentration $\psi_k(q_i) \in \mathbb{R}$
The complex oil spill behavior requires an extension of the previously introduced 3D source-seeking technique so in addition we use a discrete Kalman filter (DKF) to estimate the oil density (which then lead to concentration levels). Let $\hat{\psi}_t(q_i)$ be the estimated

concentration level in q_i, then

$$\begin{aligned}
&\textit{prediction:}\\
&\quad \hat{\psi}_t^- = \hat{\psi}_{t-\Delta t} + B_o u_{t-\Delta t}\\
&\quad P_t^- = P_{t-\Delta t} + Q\\
&\quad B_o = [U_r, V_r, W_o],\ u_{t-\Delta t} = [\cos(2\pi f_o), \sin(2\pi f_o), f_o]^T\\
&\textit{correction:}\\
&\quad K_t = P_t^- H^T (H P_t^- H^T + R)^{-1}\\
&\quad \hat{\psi}_t = \hat{\psi}_t^- + K_t(\psi_t - H\hat{\psi}_t^-)\\
&\quad P_t = (I - K_t H) P_t^-,
\end{aligned} \tag{5.14}$$

where Q, R are the process and measurement-noise covariance matrices, $f_o \sim \mathcal{N}(0,1)$ represents the particles' random trajectories, and H is the model prediction with respect to measurements. Here, we use known parameters, such as water density and diffusion coefficients, for the calculation of flotation U_r, V_r and vertical W_o velocities. Table 5.1 shows the initial values for the oil spill model.

number of oil particles	$N_o = 100$
tracer volume	$V_0 = 1$ m^3
gravity acceleration	$g = 9.81$ m/s^2
saltwater density	$\rho_w = 1025$ kg/m^3
oil initial density	$\rho_0 = 980$ kg/m^3
water viscosity	$v_w = 0.893$ μm^2/s
wave energy	$\sigma = 36$ kWs/m^2
wave period	$\omega = 2\pi 0.1$ rad/s
coefficients	$k_1 = 0.57$, $k_2 = 0.725$, $K_w = 0.3$, $K_c = 1$

Table 5.1: Initial conditions for the oil model

Results

First, we wish to demonstrate the quality of adding the γ-agents' match-making locations. A three-phase procedure is depicted in Figure 5.4. On the right side, the agents' initial distribution is shown, where the agents are deployed randomly and not necessarily inside the oil spill. Next, the agents locate and monitor the oil spill's highest concentration during its movement (middle and left) as a result of simulated wind and current in each direction. Next, tracking the oil spill's surface is depicted in figure 5.5; (a) shows the flocking final result and (b) compares the behavior of agent i over time and along the x axis. It is readily apparent that while using flocking, the agent is able to hold its position on the oil surface; with formation, the behavior fluctuates more due to the contradiction between the level-surface-tracking task and the formation constraint.

5.2 Flocking and Formation Cooperative Control

Here we present a novel approach that combines these two fundamental techniques - flocking and formation. Motivated from the advantages in both techniques we propose the

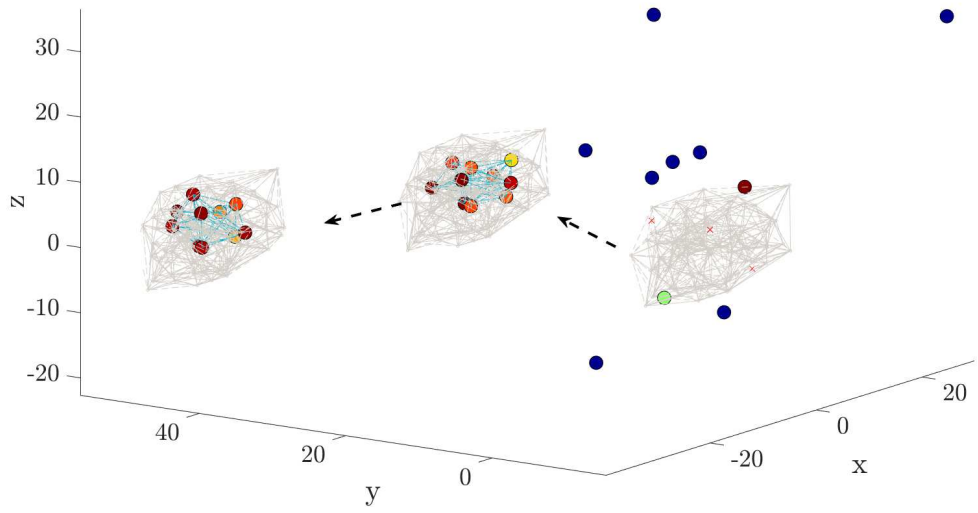

Figure 5.4. Agents using the gradient-free flocking protocol to locate and track a time-varying oil spill.

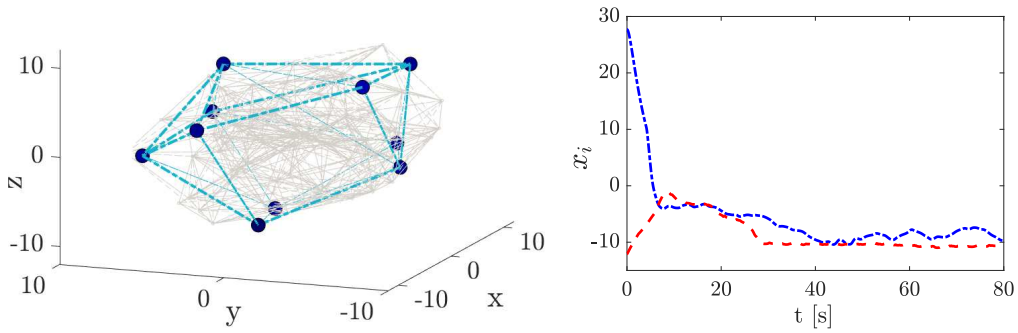

(a) (b)

Figure 5.5. (a) Oil spill level-surface tracking; (b) flocking (red,dashed) and formation (blue,dashed-dot) comparison of tracking the surface where the fluctuation in formation is noticeable

following: (i) two-level architecture with flocking for virtual-leaders, double integrator, as γ-*agents* at the top-level, and unicycle formations at the bottom level (each such formation representing a "combined sensor" measuring the average concentration in its range); (ii) demonstrating its benefits by application to a gradient-free source seeking strategy based on Glowworm Swarm Optimization. The two-level separation reduces the analysis and synthesis complexity of a unified law, which enables the use of complex agent models but

still benefits from flocking.

5.2.1 Definitions

First we need to establish several definitions to distinguish between the formation and flocking levels (notice that here i, j index describes an agent and m, n a virtual agent). Consider a MAS of N mobile, autonomous agents and let $G_1 = (\mathcal{V}_1, \mathcal{E}_1)$ be an undirected graph. Each agent is modeled by the unicycle model introduced in (3.36),

$$\dot{x}_i = v_i \cos(\theta_i),\ \dot{y}_i = v_i \sin(\theta_i),\ \dot{\theta}_i = \omega_i,$$

where, with respect to agent i, $q_i = [x_i, y_i]^T \in \mathbb{R}^2$. It is said that the set of neighbors with respect to agent i is

$$\mathcal{N}_i = \{j \in \mathcal{V}_1 : a_{ij} = 1, \forall j \in N\}. \tag{5.15}$$

The agents are arranged into groups of $|\mathcal{N}_i| + 1$, so the total number of groups is

$$N_l = \frac{N}{|\mathcal{N}_i| + 1}. \tag{5.16}$$

Let $G_2 = (\mathcal{V}_2, \mathcal{E}_2)$ be an undirected graph topology for a group of γ-*agents* ($|\mathcal{V}_2| = N_l$) and let $\mathcal{N}_l^n$ be the set of all agents corresponding to a γ-*agent* $n \in G_2$ located at their center.

$$\mathcal{N}_l^n = \{i \in N : J_{(i,n)} = 1, \forall n \in G_2\}, \tag{5.17}$$

where $J \in \mathbb{R}^{N \times N_l}$ assigns an agent to a γ-*agent*, $n \in G_2$, which corresponds to the equations of motion.

$$\begin{aligned} \dot{q}_n &= p_n \\ \dot{p}_n &= u_n, \end{aligned} \tag{5.18}$$

where $q_n, p_n, u_n \in \mathbb{R}^2$ (e.g., $q_n = [x_n, y_n]^T$), and the notation $q = [q_1^T, \ldots, q_{N_l}^T]^T$ and $p = [p_1^T, \ldots, p_{N_l}^T]^T \in \mathbb{R}^{2N_l}$ are the position and velocities of the whole network of agents stacked up. Now, the neighborhood set of agent n is

$$\mathcal{N}_n = \{m \in \mathcal{V}_2 : ||q_m - q_n|| \leq r_s\}, \tag{5.19}$$

where r_s is the possible radial sensing range between two agents from different groups. We let the adjacency matrix $\hat{A} = [a_{nm}] \in \mathbb{R}^{N_l \times N_l}$ representing the communication topology between the virtual leaders similar to a_{ij} with the corresponding $\hat{L}$. Figure 5.6 illustrates the hierarchy structure of the swarm.

The problem studied in this section is to achieve the following goal:

C1 As $t \to \infty$, the maximum ("source") located at q_s must lie inside the convex hull of the swarm center of mass - i.e. $q_s \in \text{convexhull}(q^*)$; this must satisfy

$$||q_m - q_n|| = d,\ \forall m \in \mathcal{N}_n,$$

where d is a desired inter-agent distance.

In the following we propose a distributed control law that achieves C1 under field assumptions A1 and A2 from chapter 4.

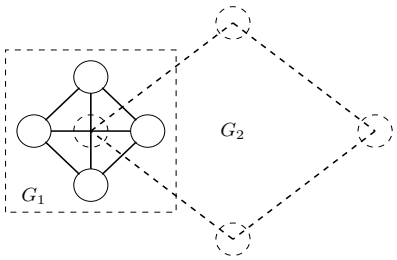

Figure 5.6. Hierarchical flocking/formation, where the γ-*agents* (dashed circle) located at the center of each group of agents (solid circles) and the topology between agents and γ-*agents* are drawn in solid and dashed lines, respectively.

5.2.2 Cooperative Flocking and Formation Technique

As introduced in Chapter 4, group convergence to a source location is achieved using the following control rule:

$$u_n = \sum_{m\in\mathcal{N}_n} \phi_n^m(q)\delta_{mn} + \sum_{m\in\mathcal{N}_n} a_{nm}(p_m - p_n) - cp_n + k\sum_{m\in\mathcal{N}_n}(\psi_m - \psi_n)\delta_{mn} \tag{5.20}$$

under the following definitions:

$$\begin{aligned}
\phi_n^m(q) =& \rho_h(q_{mn}/r_\alpha)\phi_s(q_{mn} - d_\alpha)\\
q_{mn} =& ||q_m - q_n||_\sigma\\
\delta_{mn} =& (q_m - q_n)/(1+\epsilon||z||_\sigma),\ d_\alpha = ||d||_\sigma,\ r_\alpha = ||r_s||_\sigma\\
c >& 0 : \text{ damping term,}
\end{aligned}$$

where each virtual leader measures the field's concentration according to

$$\psi_n = \frac{1}{|\mathcal{N}_i|+1}\sum_{i\in\mathcal{N}_l^n}\psi_i. \tag{5.21}$$

For achieving formation consensus followed by leader tracking in each subgroup, we propose the following. The control law applied on each agent $\varphi_i \in \mathbb{R}^2$ comprises a formation element and a navigational term tracking a γ-*agent* with respect to $i \in \mathcal{N}_l^n$ and is in the form of

$$\varphi_i = k_f\hat{L}_i(q_f - \hat{q}) + k_l(q_n - q_i), \tag{5.22}$$

where $q_f, \hat{q} \in \mathbb{R}^{2N}$ is the relative formation and position vectors where $\hat{q} = [q_1^T, \ldots, q_N^T]^T$, $\hat{L}_i \in \mathbb{R}^{2\times 2N}$ is the i-th rows $([\hat{L}_{xi}, \hat{L}_{yi}]^T)$ of the Laplacian matrix $\hat{L} = L \otimes I_2 \in \mathbb{R}^{2N\times 2N}$, and $k_f, k_l > 0$ are tuning parameters. We can decompose (5.22) into the x, y components

$$\begin{aligned}
\varphi_{xi} =& k_f L_i(x_f - x) + k_l(x_n - x_i)\\
\varphi_{yi} =& k_f L_i(y_f - y) + k_l(y_n - y_i)
\end{aligned} \tag{5.23}$$

where $L_i \in \mathbb{R}^{1\times N}$ is the i-th row of the Laplacian matrix L and $x, y, x_f, y_f \in \mathbb{R}^N$ (e.g. $x = [x_1, \ldots, x_N]^T$). Now we can construct the local controller $u_i = [v_i, \omega_i]^T$ that controls the linear and angular velocities of each agent with respect to (5.23) and determines the

desired location and orientation θ_{di}

$$\begin{aligned}\varphi_{\theta i} =&\theta_i - \theta_{di},\ \theta_{di} = \tan^{-1}(\frac{\varphi_{yi}}{\varphi_{xi}})\\ v_i =&k_v d_{vi}\cos(\varphi_{\theta i}),\ d_{vi} = \sqrt{\varphi_{xi}^2 + \varphi_{yi}^2}\\ \omega_i =&-k_\omega \varphi_{\theta i} + \dot{\theta}_{di}.\end{aligned} \tag{5.24}$$

γ-*Agent* Constraints

Since the γ-*agents* possess dynamics different from that of the physical agents, one needs to constrain the flocking convergence speed of the top level leader according to the agents' convergence rate. Following the proposed control law in (5.20), we add a continuous-adaptive *bump-function* with a dependency on φ_i where

$$\begin{aligned}u_{\mu_n} =&u_n \rho_h(\mu_n)\\ \mu_n =&\frac{1}{|\mathcal{N}_i|+1}\sum_{i\in\mathcal{N}_l^n} |\varphi_i|/\varphi_{\max}^n.\end{aligned} \tag{5.25}$$

where $\varphi_{\max}^n = \max_{i\in\mathcal{N}_l^n}\varphi_i$.
First we place a lemma showing that a group stays together following their leader.

Lemma 5.2. *Consider a group of N_l^n agents with dynamics (3.36) applying the control law (5.24). Then, the group track their γ-agent with a bounded steady-state error in formation.*

Proof. Since q_n depends on ψ_n and μ_n (see (5.21),(5.25)) then $||q_n - q_c|| \leq \epsilon$ where $q_c = \frac{1}{|\mathcal{N}_i|+1}\sum_{i\in\mathcal{N}_l^n} q_i$ is the group center of mass. Thus it follows that $||q_n - q_i|| \leq \varepsilon$ where $\varepsilon = \epsilon + ||q_c - q_i|| = \epsilon + q_{f,i}$. To reach formation consensus we use the following Lyapunov candidate function

$$V = \frac{1}{2}\sum_i(\varphi_{xi}^2 + \varphi_{yi}^2) + \frac{1}{2}\sum_i \varphi_{\theta i}^2$$

then

$$\dot{V} = -\sum_i \dot{x}_i\varphi_{xi} - \sum_i \dot{y}_i\varphi_{yi} - \sum_i \dot{\varphi}_{\theta i}\varphi_{\theta i}.$$

Without loss of generality, assume that $k_f, k_l = 1$. Now, by substituting $\theta_i = \varphi_{\theta i} + \theta_{di}$ and from (5.24) using $v_i = k_v d_{vi}\cos(\varphi_{\theta i})$ and $\cos(\varphi_{\theta i}) = \frac{\varphi_{xi}}{d_{vi}}$, $\sin(\theta_{di}) = \frac{\varphi_{yi}}{d_{vi}}$ we obtain

$$\begin{aligned}\dot{x}_i =&v_i\cos(\varphi_{\theta i} + \theta_{di}) = v_i[\cos(\varphi_{\theta i})\cos(\theta_{di}) - \sin(\varphi_{\theta i})\sin(\theta_{di})]\\ =&k_v d_{vi}\cos(\varphi_{\theta i})[\cos(\varphi_{\theta i})\frac{\varphi_{xi}}{d_{vi}} - \sin(\varphi_{\theta i})\frac{\varphi_{yi}}{d_{vi}}]\\ =&k_v\varphi_{xi}\cos^2(\varphi_{\theta i}) - k_v\cos(\varphi_{\theta i})\sin(\varphi_{\theta i})\varphi_{yi}\\ \dot{y}_i =&v_i\sin(\varphi_{\theta i} + \theta_{di}) = v_i[\sin(\varphi_{\theta i})\cos(\theta_{di}) + \cos(\varphi_{\theta i})\sin(\theta_{di})]\\ =&k_v d_{vi}\cos(\varphi_{\theta i})[\sin(\varphi_{\theta i})\frac{\varphi_{xi}}{d_{vi}} + \cos(\varphi_{\theta i})\frac{\varphi_{yi}}{d_{vi}}]\\ =&k_v\varphi_{yi}\cos^2(\varphi_{\theta i}) + k_v\cos(\varphi_{\theta i})\sin(\varphi_{\theta i})\varphi_{xi}\\ \dot{\varphi}_{\theta i} =&\varphi_{\theta i}(\dot{\theta}_i - \dot{\theta}_{di}) = -k_\omega\varphi_{\theta i}^2.\end{aligned}$$

Eventually $\dot{V}$ is in the form of

$$\dot{V} = -k_v\sum_i \cos^2(\varphi_{\theta i})(\varphi_{xi}^2 + \varphi_{yi}^2) - k_\omega\sum_i \varphi_{\theta i}^2,$$

hence, $\dot{V} \leq 0$ and $\dot{V} = 0$ iff $\varphi_{xi}, \varphi_{yi}, \varphi_{\theta i} = 0$.

□

Next, to achieve convergence to the source location in flocking (C1), we place the following proposition.

Proposition 5.3. *Consider a group of N agents, divided to small groups of N_l^n agents, and consider a group of N_l, γ-agents with dynamics (5.18) and the control law (5.25). Then, under the described assumptions, all γ-agents' trajectories asymptotically converge to the equilibrium $(q^*, 0)$ s.t. $q_s \in$ convexhull(q^*), where each is tracked by a group of N_l^n agents in formation.*

Proof. We first show that the weighted control law does not affect the *energy structure* of the agents' dynamics. Applying (5.25) on (5.20),

$$\begin{aligned}
u_{\mu_n} =& u_n \rho_h(\mu_n) = \sum_{m \in \mathcal{N}_n} \big[\phi_n^m \delta_{mn} + a_{nm}(p_m - p_n) - c p_n + (\psi_m - \psi_n)\delta_{mn}\big]\rho_h(\mu_n) \\
=& \sum_{m \in \mathcal{N}_n} \big[\phi_n^m \rho_h(\mu_n)\delta_{mn} + a_{nm}(p_m - p_n)\rho_h(\mu_n) - c\rho_h(\mu_n)p_n + (\psi_m - \psi_n)\rho_h(\mu_n)\delta_{mn}\big] \\
=& \sum_{m \in \mathcal{N}_n} \rho_h(q_{mn}/r_\alpha)\rho_h(\mu_n)\phi_s(q_{mn} - d_n^m)\delta_{mn} + \sum_{m \in \mathcal{N}_n} a_{nm}(p_m - p_n)\rho_h(\mu_n) \\
& - c\rho_h(\mu_n)p_n + \sum_{m \in \mathcal{N}_n} (\psi_m - \psi_n)\rho_h(\mu_n)\delta_{mn} \\
=& \sum_{m \in \mathcal{N}_n} \breve{\rho}_h \phi_s \delta_{mn} + \rho_h(\mu_n) \sum_{m \in \mathcal{N}_n} a_{nm}(p_m - p_n) - \breve{c} p_n + \breve{f}_\gamma(q) \\
=& -\nabla \breve{U}(q) - \hat{L}_2^w p_n - \breve{c} p_n + \breve{f}_\gamma(q)
\end{aligned}$$

where $\breve{U}(q)$ is a potential function and $\hat{L}_2^w = \hat{L}^w \otimes I_2$ and $\hat{L}^w$ is a weighted Laplacian matrix. This leads to the closed-loop collective dynamics

$$\begin{aligned}
\dot{q} &= p \\
\dot{p} &= -\nabla \breve{U}(q) - \hat{L}_2^w p_n - \breve{c} p_n + \breve{f}_\gamma(q).
\end{aligned}$$

The product with (2.13) produces weighted elements of the potential function $U(q)$, Laplacian matrix $\hat{L}$, damping constant c, and field climbing element $f_\gamma(q)$. This modification does not affect the energy structure of the agent's dynamics or the convergence analysis, only the convergence rate. Next, we organize the dynamics as

$$\begin{aligned}
\dot{q} =& p \\
\dot{p} =& -\nabla \breve{U}(q) - (\hat{L}_2(q) + c)p + \nabla \Psi(q) + (f_\gamma(q) - \nabla \Psi(q)) \\
=& -\nabla \tilde{\breve{U}}(q) - (\hat{L}_2(q) + c)p + e(q).
\end{aligned}$$

The last equation is similar to the proposed structural dynamics in (4.3) where the proof is in two parts; part A use La Salle's invariance principle showing that the Hamiltonian is a dissipative particle system; part B shows that the proposed protocol leads to a stable dynamics and finally convergence to the equilibrium $(q^*, 0)$. The steps are similar and thus omitted. Finally, from Lemma 5.2, each group of agents remain in formation and track their leader, which eventually leads to the source being located by the swarm.

□

5.2.3 Simulation Results

In all simulations and experiments, the blue lines connecting the agents represent the formation topology and the red lines represent the flocking connectivity between the γ-*agents*. The dashed black curves are the field's concentration levels, where a narrow circle corresponds to the higher concentration level.
A group of $N = 20$ non-holonomic agents performs the proposed extremum-seeking technique on a scalar field

$$\psi(z) = A_\psi[e^{-((z-q_s)^T H_1(z-q_s))} + e^{-((z-q_s)^T H_2(z-q_s))}],$$

where $H_1 = \text{diag}(\frac{1}{2\sigma_{x_1}^2}, \frac{1}{2\sigma_{y_1}^2}), H_2 = \text{diag}(\frac{1}{2\sigma_{x_2}^2}, \frac{1}{2\sigma_{y_2}^2})$, $\sigma_{x_1} = 10, \sigma_{y_1} = 50, \sigma_{x_2} = 80, \sigma_{y_2} = 30, A_\psi = 3$, and a maximum is located at $q_s = [40, 40]^T$ with a value of $\psi_{\max} = 6$. The agents are divided into a group of $|\mathcal{N}_i| + 1 = 4$ (i.e., $N_l = 5$ γ-*agents*) with an initial arbitrary location around $[0, 0]^T$. Figure 5.7 (a) presents the measured concentration level ψ_i over time. During the search procedure, the agents locate the field's maxima at $[30, 40]^T$ with an average value of $\text{Avg}_{\forall i}(\psi) = 5.85$, as expected. In addition, in (b), the errors of the control laws (5.22) and (5.25) are plotted over time. Owing to the use of the gradient-free technique as the navigation function, both inputs approach zero.

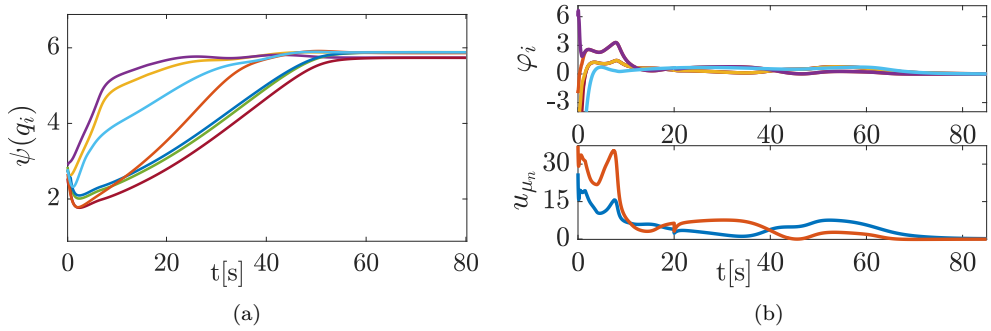

Figure 5.7. (a) Field concentration measurements over time. When agents locate the field's extremum they remain there as expected. (b) Agents (top) and γ-*agents* (bottom) errors decreasing behavior over time.

Chapter 6

Experimental Results

This chapter presents a number of experiments evaluating the proposed algorithms in the previous chapters under different conditions. The experiments are conducted under the *Robotarium* project by Georgia Institute of Technology [Pickem et al., 2017] using a swarm of mobile, two-wheeled robots called "GRITSBot" (Figure 6.1 (a)). The size of the GRITSBot size is $4 \times 4 \times 3$ cm. It can reach a maximum forward speed of approximately 10 $[\frac{\text{cen}}{\text{sec}}]$ and can turn at up to 1 $[\frac{\text{rot}}{\text{sec}}]$. A group of up to 20 mobile robots can be used in an

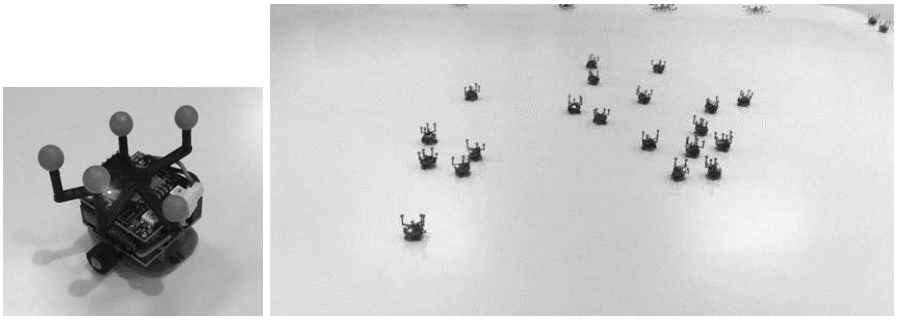

(a) (b)

Figure 6.1. (a) a GRITSBot agent and (b) the arena.

arena with a size of 1.6×1.0 m (Figure 6.1 (b)). A camera-based position technique is used to determine each agent's location, which also assists in creating virtual fields and obstacles projected on the arena table. Nevertheless, the agents' control remains distributed. In addition, the Robotarium implements barrier certificates to handle and prevent collisions between agents.

6.1 MESA

In Section 3.3, the algorithm for multiple extrema is presented. This technique involves elements of formation and gradient estimation, as well as nature-imitation techniques, such as GSO. In addition, the concept of a predefined matching location is introduced to connect agents in the search for neighbors or to repulse agents from occupied extrema. Two experiments with a group of 10 agents are conducted. The agents are required to form

two groups of 5 in a "plus" formation, where two extrema are posed (the field's different concentration levels are drawn in circles, where the source is located at the center). The difference between the experiments is the distance between those two extrema. Initially, in experiment 1 (Figure 6.2), the sources are located far from one another and the agents are deployed at the center of the connecting line between them. The agents are first assigned into two groups, which are then each attracted to a different extremum (the attraction level is the same) and finally rest in both. To challenge our algorithm, we next move the

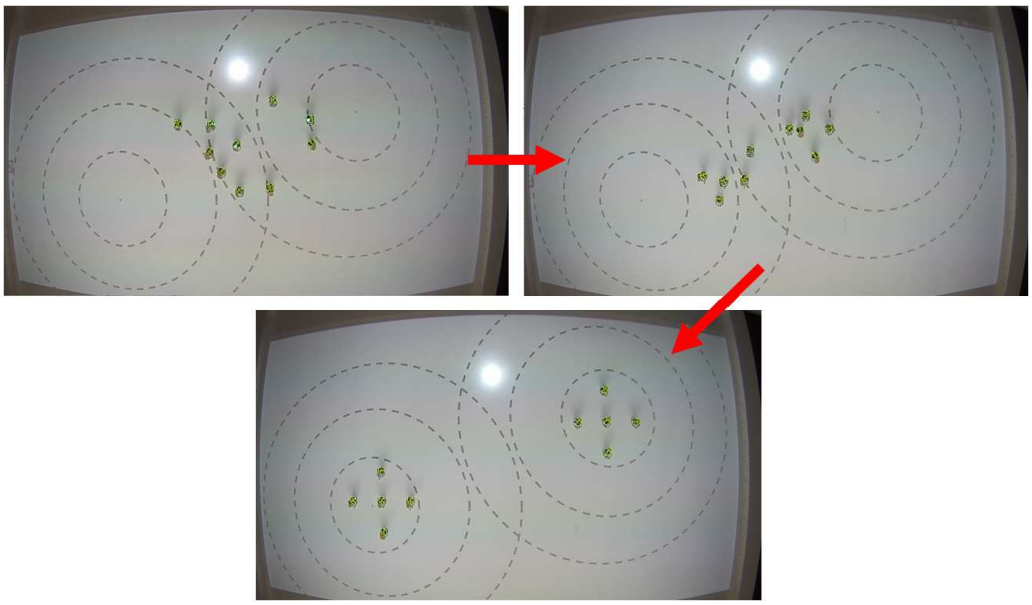

Figure 6.2. MESA 1 - field with 2 extrema located far apart.

two extrema closer, as shown in Figure 6.3. Now, all agents are attracted to the nearest extremum. This results in an over-populated source. Without MESA, the agents would have remained at this location, leaving one extremum unattended, and thus would have failed the task. The actual result is that one group takes over the detected source, and the rest are sent (using match-making locations) to search for the second, undiscovered source. Finally, both extrema are occupied with same number of agents (equal density), as requested.

6.2 Gradient-Free Method with Flocking

In Chapter 4, source seeking using a gradient free technique is developed. Here, as opposed to the previous section, the agents motion is dictated according the flocking rules which are added to a modification of the GSO rule. Agents are attracted to both source and neighbors, creating smooth movements using 2D consensus based on distance and velocity. The experimental results with $N = 8$ wheeled robots are presented in Figure 6.4 (Experiment 1) and Figure 6.6 (Experiment 2). The 2-D scalar field indicated by its level curves (dashed circles) with a maximum at its center in $q_s = [-0.5, 0.5]^T$. In the first experiment the agents navigate in a free environment from initially arbitrary locations to a swarm with flocking behavior searching for the extremum.
The agents' trajectories over time are depicted in (b), where the field's extremum location

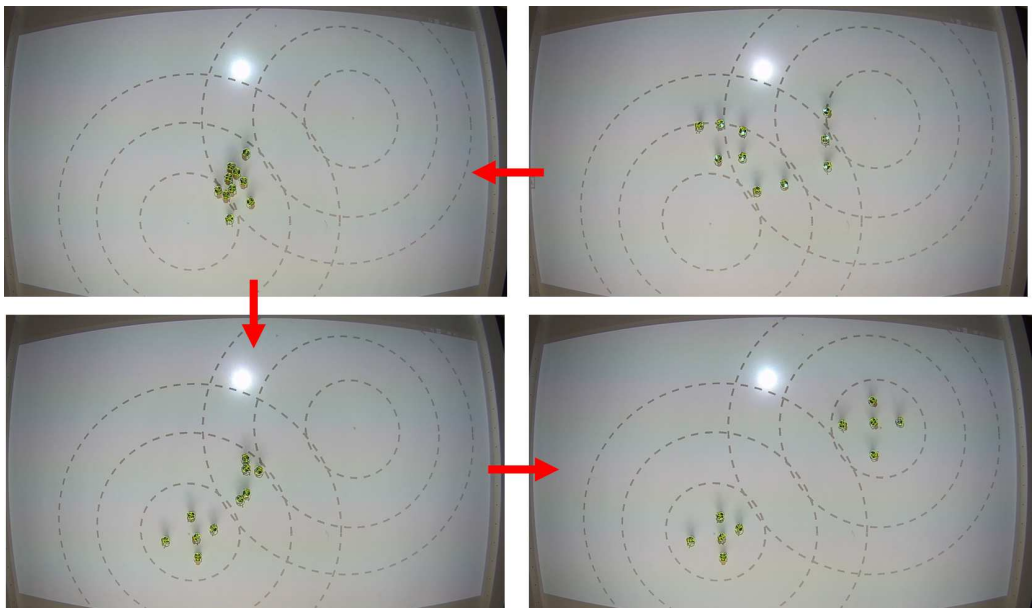

Figure 6.3. MESA 2 - field with 2 extrema located close together.

is indicated by dashed lines. One can observe that the agents' center of mass converges to the extremum (i.e., $q_c = q_s$).
To evaluate the performance, we compare our proposed technique with flocking and the gradient-estimation technique (3.4) computes the slope of field measurements between agents. The control law is then

$$u_{Fg_i} = k_\alpha u_i^\alpha + k_g \hat{g}_i.$$

An experimental comparison of the two is depicted in Figure 6.5. The interference between flocking and gradient estimation is observable compared with the smooth behavior of the proposed technique.

The second experiment is conducted in a constrained environment (Figure 6.6). First, the agents locate the source and construct a flocking structure. Subsequently, unknown obstacles (gray squares) appear and the field starts moving in the positive x direction. The agents keep tracking the field while avoiding obstacles during the whole movement until the field comes to a rest. The obstacle-avoidance technique is based on the method proposed in Section 3.2.

6.3 Cooperative Flocking and Formation

Here, we combined both the formation and flocking techniques to achieve the benefits of both, where, in the lower level, the wheeled robots achieve a triangular or diamond shape formation, providing better measures of the field's concentration, and at the higher level, virtual $\gamma-agents$ perform flocking, which prevents the different groups from diverging. Here, instead of having an unnecessary explicit formation between the different groups, all that is needed is to maintain cohesion and alignment. In Experiment 1 (Figure 6.7), a group of $N = 12$, 2-wheeled robots are preassigned to groups of $\Lambda = 4$ in a diamond

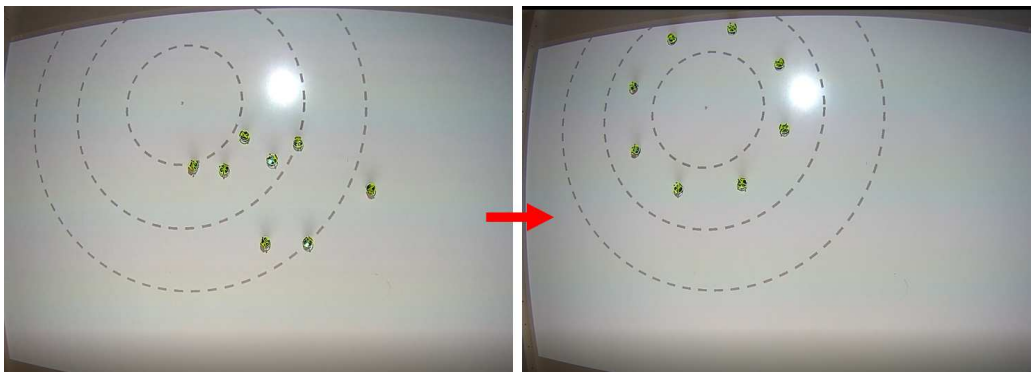

(a)

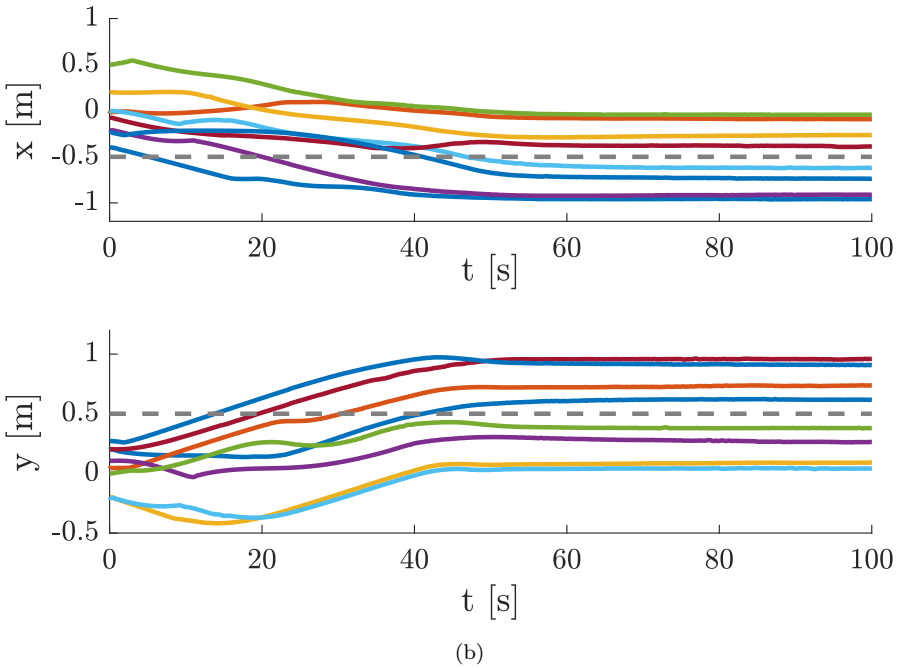

(b)

Figure 6.4. (a) (left) Robots' initial locations. (right) final location around the field's maximum. (b) x-y trajectory plot of 8 mobile robots locating an unknown extremum.

formation shape. The expected triangular shape of the γ-*agents* (N_l=3) is drawn with red lines. The agents start in arbitrary locations and, by using the proposed cooperative flocking and formation technique (CFFT), construct the three subgroups and monitor the field's maxima. The γ-*agents'* flocking behavior maintains the desired distance d (cohesion and separation), as well as velocity consensus (alignment), which enables smooth tracking behavior of the swarm.

In Experiment 2 (Figure 6.8 (a)), a group of $N = 15, \Lambda = 3$ agents with corresponding $N_l = 5$ γ-*agents* was created. Here, the agents construct the desired triangular formation shape with a pentagon flocking shape. The input (5.25) constrain the γ-*agents*' speed of convergence with the agents' consensus rate, which guarantees that the γ-*agents* do not

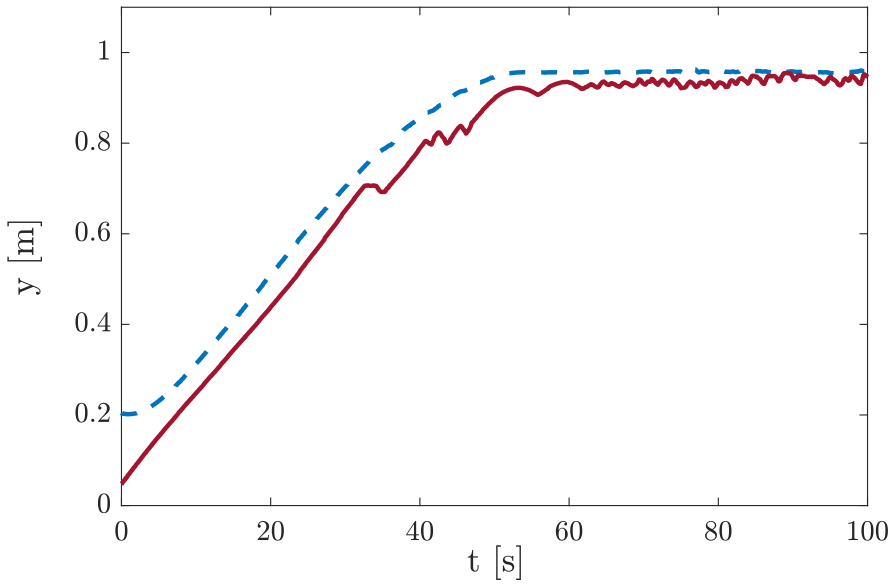

(a)

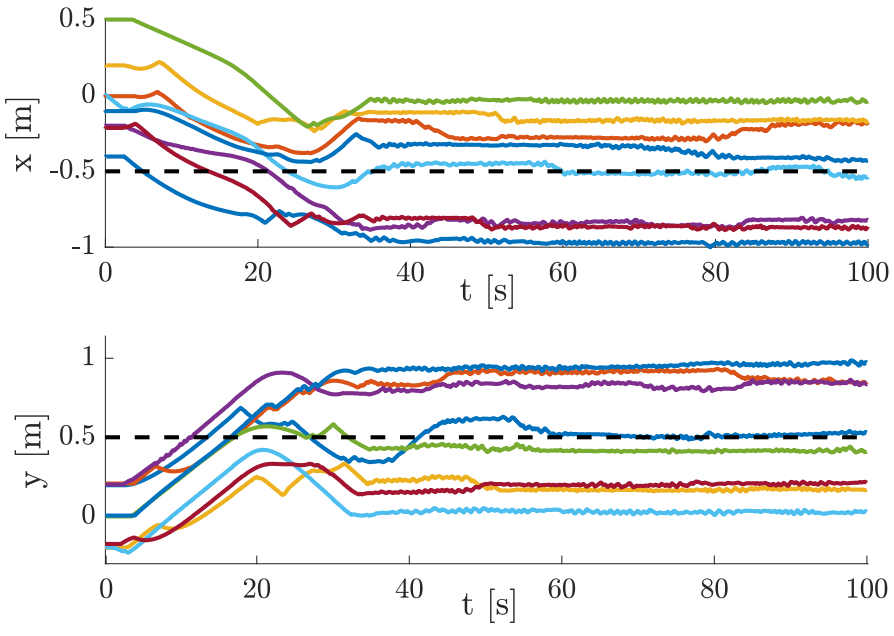

(b)

Figure 6.5. (a) Trajectory samples comparing the agents' behavior over time in two experiments; proposed algorithm (blue,dashed) and flocking+gradient (red,solid). (b) Complete x, y trajectories of gradient-based approach, where the perturbed behavior is easily noticeable.

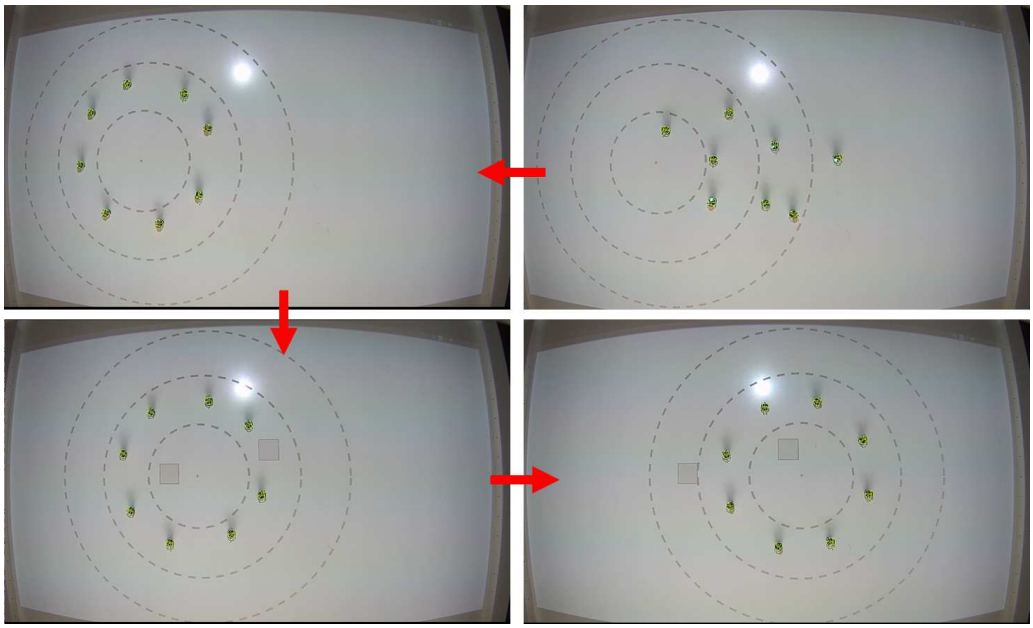

Figure 6.6. Experiment screenshots of the swarm behavior under different states: initial distribution, source located, and tracking the time-varying source while avoiding obstacles until the final position of the source is reached.

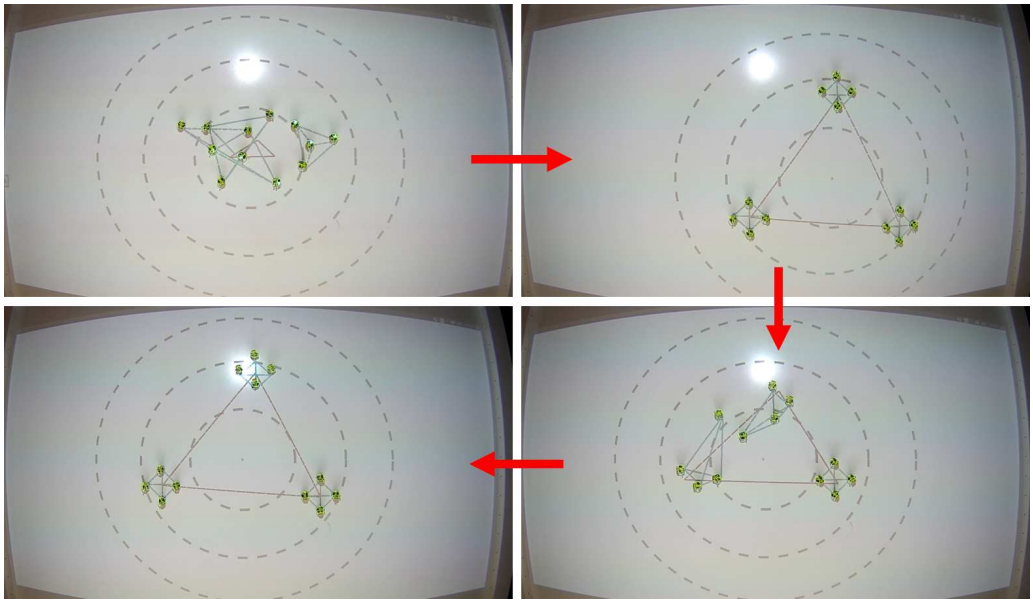

Figure 6.7. *Experiment 1* - A group of 12 agents divided into 3 subgroups of 4, each in a diamond formation structure, where the γ-*agents* construct a triangular shape according the the flocking rules.

diverge.
Figure 6.8 (b) plots the average error of the γ-*agents* throughout the experiment. The

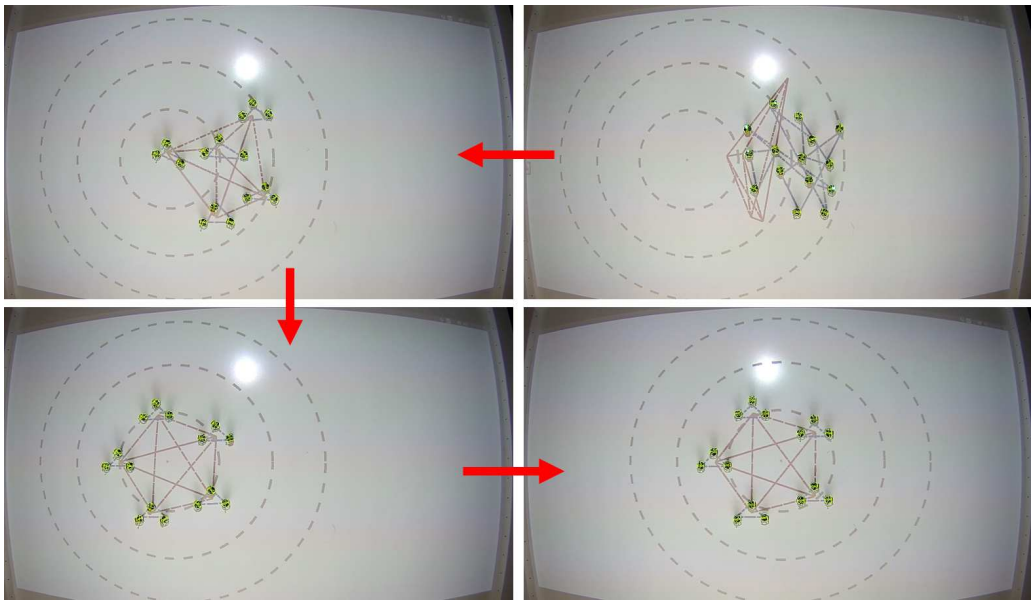

(a)

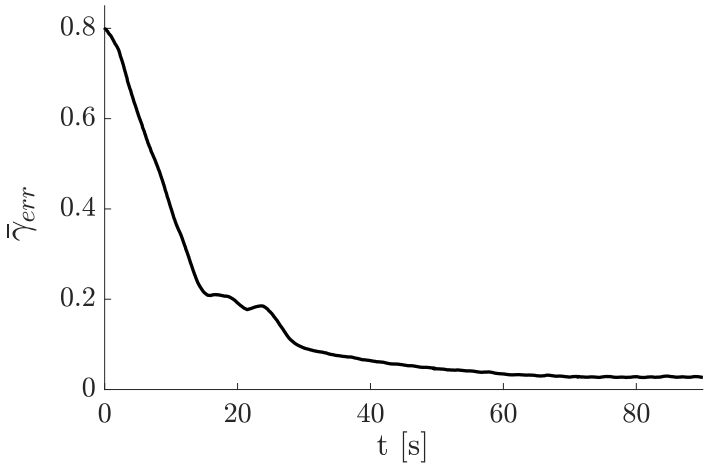

(b)

Figure 6.8. *Experiment 2* - (a) Subgroups of 3 agents in a triangular formation track γ-*agents* in a pentagon shape to seek the extremum. (b) γ-*agents* average error plot over time. The flocking error decreases to the minimum value where the swarm keeps monitoring the source location using the proposed CFFT.

error decreases until a relatively small steady-state value is reached, where the pentagon shape is achieved along with formation consensus by the agents. The dynamic constraint added in (5.25) is noticeable in the range of [15–25] sec., where the error decrease rate is slowed until all agents track their corresponding γ-*agent* in formation.

Chapter 7

Conclusions and Outlook

The present dissertation details the use of different distributed control schemes to navigate a group of identical agents through different tasks. Here, we focus on the task of source-seeking, where the agents are required, based on limited measurements, such as local concentration or neighbors' knowledge, to locate and monitor an unknown field's extremum. Presently, this challenge is important for applications to the unfortunately vast quantity of disasters, either natural or manmade. The use of autonomous mobile robots under conditions of high risk or limited accessibility is advantageous and, in some cases, unavoidable. Here, we have proposed and examined the differences between two common cooperative control techniques, formation and flocking, under different scenarios and agent models, such as single and double integrators and non-holonomic kinematics.

Tasks of locating an unknown source or tracking a certain level curve require a vector to be generated that points to the extremum location. Section 3.1 first introduces the distributed gradient-estimation process, where an agent generates a force pointing to the source by computing the slope between the different field measurements in its neighborhood. Then, to reach a consensus among a large group of agents, they are divided into different groups, and we use a hierarchy structure to reduce the calculation time and introduce a new technique for reaching a discrete consensus. Formation-based control is used to achieve a rigid structure for better estimation in the lower hierarchy. Nature is not a sterile environment, and agents therein can encounter obstacles or noise-corrupted measurements in both concentration and position. Thus, in Section 3.2, we extend the previous proposed approach to include an obstacle-avoidance technique with the use of the potential function. For noise robustness, the agents modify the formation structure with respect to the SNR. The assumption of a single extremum is unrealistic, where in practice, a substance has several extrema (points of interest), so in Section 3.3, we propose a novel complete solution to explore such a field. We define the *source density* characteristic to ensure that all extrema are properly explored. In addition, we assign match-making locations to generate groups of rejected or lone agents.

The second part of this thesis proposes a different approach to tackle the task at hand. Here, our approach is to mimic natural behavior. Flocking is a natural method to keep individuals together with respect to their relative distance and velocity. The latter allows us to relax the use of an explicit rigid formation and enables more flexible motion of the swarm. To avoid the process of gradient estimation, we use the concept of glowworms, where agents are attracted to others based on a modified cost function. The main contribution is the combination of the two requirements into one unified rule. The case of double-integrator agents is well introduced and synthesized in Section 4.1, and the

proposition of extension to a non-holonomic kinematic and dynamic model is elaborated in Section 4.2.

After introducing these two approaches, we try to evaluate and classify which is suitable for which kind of problem (Section 5.1). We use complex scenarios, such as a time-varying 3D sphere model and numeric representation of an oil spill. The comparison focuses on the convergence speed and tracking abilities for cases, such as a moving field and level surface monitoring. Our first conclusion is that both approaches have high performance and are suitable for most tasks. Nevertheless, by examining the details, one can find several differences. Formation involves a rigid structure, which required when dealing with noise-corrupted measurements in position or concentration. If it is necessary to modify the group in the explicit structure (for energy efficiency, for instance) or to form preassigned groups with respect to the agents, formation is the way. This field of research is investigated thoroughly, with synthesis and analysis results under varied kinematic and dynamic models. Therefore, if the task is well-defined with characteristics of convergence speed (λ_2) and known topology, formation control is the suitable solution. In flocking, on the other hand, the direct result of mimicking nature is fluid behavior. Without a priori knowledge or the need for an agent's neighborhood, the swarm maintains cohesive behavior by simply keeping a desired distance. Although the shape is not explicitly designed, in many cases, one can guess the α-lattice structure. This provides the swarm with robust abilities that enable it to react to changes more smoothly and to track any level-surface structure more efficiently. The flocking framework has been analyzed well for the double-integrator case, and the results for the kinematic and dynamic models are presented, but more work remains for different types of models and techniques (such as involving LPV design). From our observation in the simulation and experiments, flocking seems to be a promising technique, where, with small and simple control effort, one can provide varied solutions that guarantee that the agents remain together.

In addition, we propose a novel solution to converge all agents to the field area for any arbitrary initial location, which relaxes the strict assumptions. Next, we wish to benefit from both advantages. Therefore, in Section 5.2 we propose a cooperative approach. Again, a hierarchy structure is used, where in the lower level, agents reach formation consensus by tracking their center of mass (presented as a virtual agent), and in the higher level, the different groups maintain cohesion and field exploration by using flocking.

The last chapter of the dissertation provides several application examples using the Robotarium arena, where the agents are small two-wheeled mobile robots. We tested our different mission-control strategies for the case of a multiple-extrema field, gradient-free flocking, and a cooperative flocking and formation technique by generating the structures of motion of different virtual fields.

Remarks and Future Research Opportunities

The satisfactory results of both formation and flocking shall encourage further research in the field of source seeking.
The different field models (toxic cloud, oil spill, etc.) are normally not stationary, and require constant tracking in a time-varying environment. Although in this thesis, we presented our observation results on such a model, further analysis shall be conducted.
A heterogeneous group of agents would pose an interesting challenge, handling such complex tasks. For instance, having the ability to control and reach consensus among aerial and underwater vehicles may be a suitable solution for tracking a substance in the ocean. The shared information from both the air and sea can assist in better localization and

field monitoring. A cooperation of flocking and formation with different convergence ratios (fast and slow dynamics) may be a suitable approach.
An important aspect of more realistic scenario, is communication limitation. From time delays to package drops, the agents' main decision-making protocol is based on information sharing, where such problems may result in critical failures that must be handled properly. This is also applied for the agents' localization abilities, both for outdoors, where GPS accuracy is not satisfactory, and indoors, where GPS is not available and which requires different approaches, such as landmarks or distance-based determination.
In the author's opinion, flocking seems to be the most suitable solution. The flexible structure involves great advantages, such as robustness and adjustment. For example, once a non-smooth field is obtained with flocking, agents can adapt their position to cover the field's structure based only on the relative distance (in contrast to formation, which lacks this ability without prior knowledge of the structure). Thus, we encourage further research on the synthesis and analysis for a wide range of agent models under different problems and scenarios.

Appendix A

Aerial and Naval 3D Exploration

Here, we present an extension of the formation gradient-based approach (as introduced in Section 3.1) for exploring 3D field.

A.1 Cooperative 3D Source Seeking

First, we require the agents to obtain a given formation that facilitates gradient estimation. Whereas in the 2D case, the agents form a diamond shape in the plane for enhanced sensitivity against time-varying field changes, here, the desired shape is a *tetrahedron*, which has 4 triangular faces, 6 edges, and 4 vertices.
To achieve a desired formation, a relative formation-reference vector is provided by $q_f = [q_{f,1}^T, \dots, q_{N,f}^T]^T$. Then,

$$e_f = k_f L_p (q_f - q), \tag{A.1}$$

where k_f is a tuning parameter and $L_p = L \otimes I_3 \in \mathbb{R}^{3N \times 3N}$, so $e_f \in \mathbb{R}^{3N}$. The gradient is again computed using the slope of the field measurements between agents.

$$\hat{g}_i = (R_i^T R_i)^{-1} R_i^T b_i,$$

where $\hat{g} \in \mathbb{R}^{3N}$ and the inverse of $(R_i^T R_i)^{-1}$ exists iff R_i is full column rank, which requires $|\mathcal{N}_i| \geq 3$. Here, we consider a bounded Hessian $||\nabla^2 \psi(q_i)|| \leq \alpha$ and a formation structure where all reference distances are equal, $\bar{q}_f = ||q_j - q_i||$, so the estimation error is

$$\begin{aligned} e_{H,i} &= (R_i^T R_i)^{-1} R_i^T c_i \\ c_i &= [c_{i_1}, \dots, c_{i_{\mathcal{N}_i}}]^T,\ c_{i,j} = \frac{1}{2}(q_j - q_i)^T \nabla^2 \psi(q_i)(q_j - q_i) \end{aligned} \tag{A.2}$$

and bounded by

$$\begin{aligned} ||c_i|| &\leq \frac{1}{2}\sqrt{|\mathcal{N}_i|\alpha^2}||q_j - q_i||^2 \leq \frac{1}{2}\sqrt{|\mathcal{N}_i|}\alpha \bar{q}_f^2 \\ ||e_{H,i}|| &\leq ||(R_i^T R_i)^{-1} R_i^T||||c_i|| \leq \frac{1}{2}\sqrt{|\mathcal{N}_i|}\alpha \bar{q}_f^2 ||(R_i^T R_i)^{-1} R_i^T||. \end{aligned} \tag{A.3}$$

The gradient contribution to the control input is

$$e_g = k_g \cdot \hat{g}, \tag{A.4}$$

where k_g is a tuning parameter. The total input is a composition of the two:

$$e = e_f + e_g. \tag{A.5}$$

A.1.1 Simulation Results

The simulated scalar field is described as

$$\begin{aligned}
&\psi(q_i) = A_\psi(e^{-(q_i-q_m)^T H_1 (q_i-q_m)} + e^{-(q_i-q_m)^T H_2 (q_i-q_m)}) \\
&H_1 = \begin{bmatrix} \frac{1}{2\sigma_{x_1}^2} & 0 & 0 \\ 0 & \frac{1}{2\sigma_{y_1}^2} & 0 \\ 0 & 0 & \frac{1}{2\sigma_z^2} \end{bmatrix}, \; H_2 = \begin{bmatrix} \frac{1}{2\sigma_{x_2}^2} & 0 & 0 \\ 0 & \frac{1}{2\sigma_{y_2}^2} & 0 \\ 0 & 0 & \frac{1}{2\sigma_z^2} \end{bmatrix} \\
&q_m = [x_\psi^{\max}, y_\psi^{\max}, z_\psi^{\max}]^T
\end{aligned} \tag{A.6}$$

using the parameters $\sigma_{x_1} = 10, \sigma_{y_1} = 50, \sigma_{x_2} = 80, \sigma_{y_2} = 30, \sigma_z = 2, A_\psi = 3$. The maximum location is in $q_m = [40, 60, 0]^T$. Figure A.1 shows the simulation results for 4 AUV agents in a tetrahedron formation seeking the unknown source. To graphically display the concentration levels in $x - y - z$ coordinates, we plot $x - y$ cross scenarios of the field along the z axis. The source, in this case, is located at $z = 0$ (marked as green *) with a value of $\psi_{\max} = 17$. The agents start in $q(0) = [0, 0, -3]^T$ and climb toward

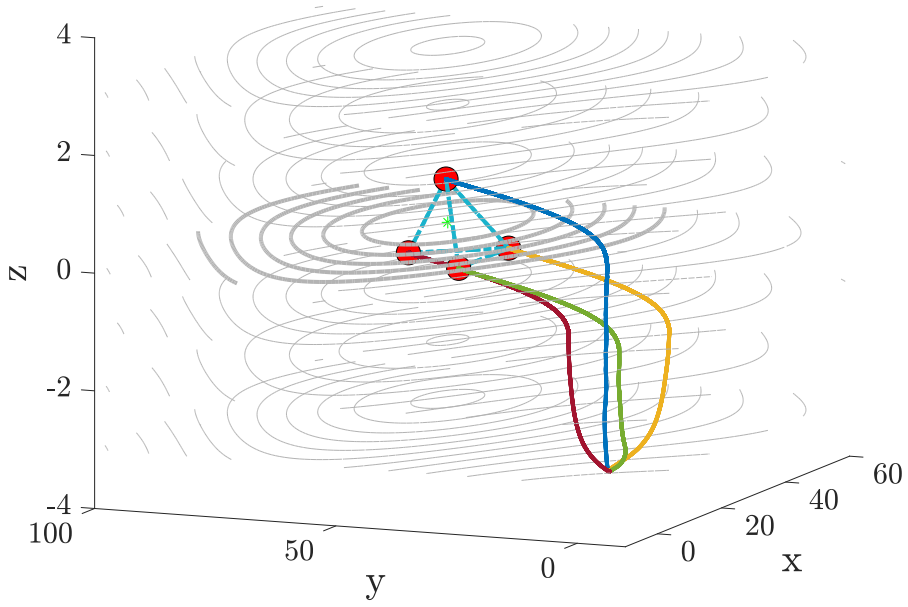

Figure A.1. 3D source seeking of a scalar field.

the source by using control law (A.5). Initially, because of the tetrahedron formation, the gradient has a significant z component and the agents ascend rapidly; subsequently, they move toward the maximum with similar linear velocities in all axes. Figure A.2 presents

the (a) formation and (b) gradient errors over time. The agents reach formation consensus after a short period of time and keep it during the rest of the simulation. The gradient errors' behavior is different among the three axes. It starts with a larger error in z, which causes the early ascending movement. Then, a peak is observed where the steepest change occurs; finally, all errors decrease to $e_g \leq 0.2$, $e_f = 0$.

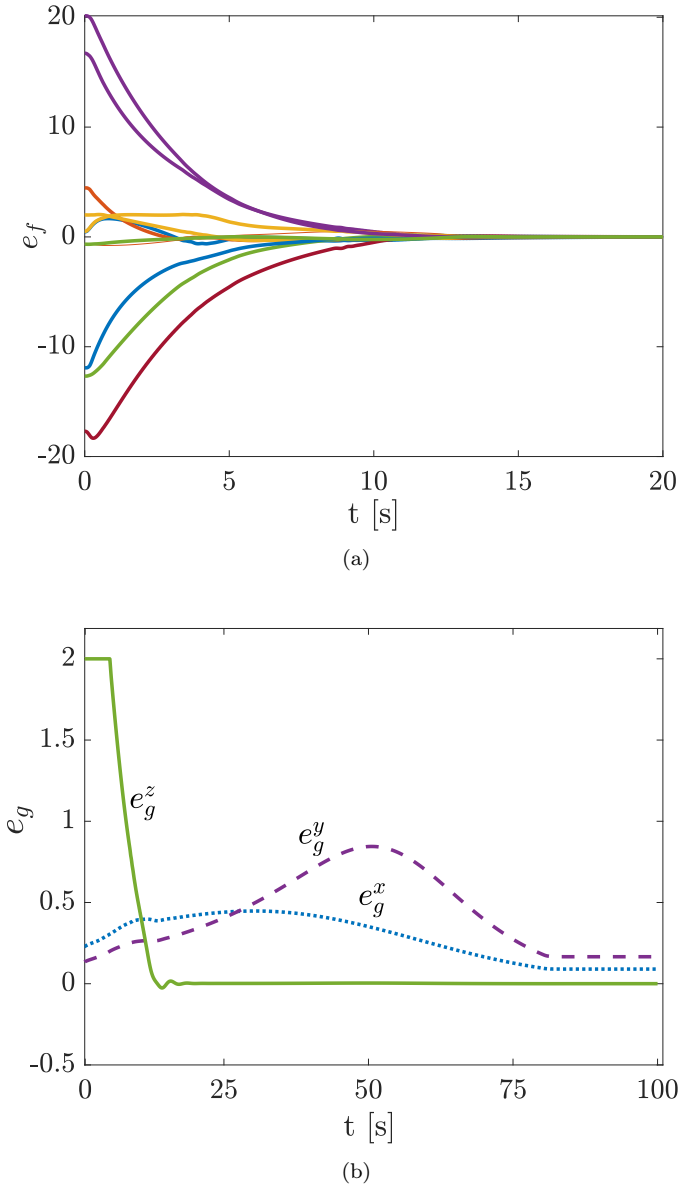

Figure A.2. (a) Formation error; (b) gradient error where: e_g^z (solid),e_g^y (dash), e_g^x (dot).

A.2 Oil Spill Exploration Algorithm

Here, we use the oil spill model introduced in Section 5.1.6. Similar to the algorithm proposed in MESA, our control law is based on formation, gradient estimation, and GSO, where

$$e = e_f + e_g + e_l. \tag{A.7}$$

It is shown in [Krishnanand and Ghose, 2009] that l_i increases/decreases monotonically and asymptotically converges to $l_i^* = (\frac{\zeta}{\rho})\psi(q_i)$. Therefore, the attraction movement proceeds until an equilibrium is reached, where

$$\lim_{t\to\infty} e_{l,i} = \lim_{t\to\infty} s \cdot \frac{q_{\hat{j}} - q_i}{||q_{\hat{j}} - qr_i||} \leq s||\bar{q}_f||, \tag{A.8}$$

so the tracking error is bounded.

A.2.1 Simulations

The oil spill tracking in time are plotted in Figure A.3 under different natural changes, such as the diffusion or wind and current velocities. First, we simulate a quasi-static oil spill; in other words, we assume that the current and wind effects on the oil spill are negligible and time-varying changes are affected by the diffusion and evaporation processes in the model. Then, we apply wind and current effects so that the oil model starts drifting in the $x - y$ plane. The agents were able to track the oil spill model under these different conditions and changes. Figure A.3 presents the different stages of the oil spill.

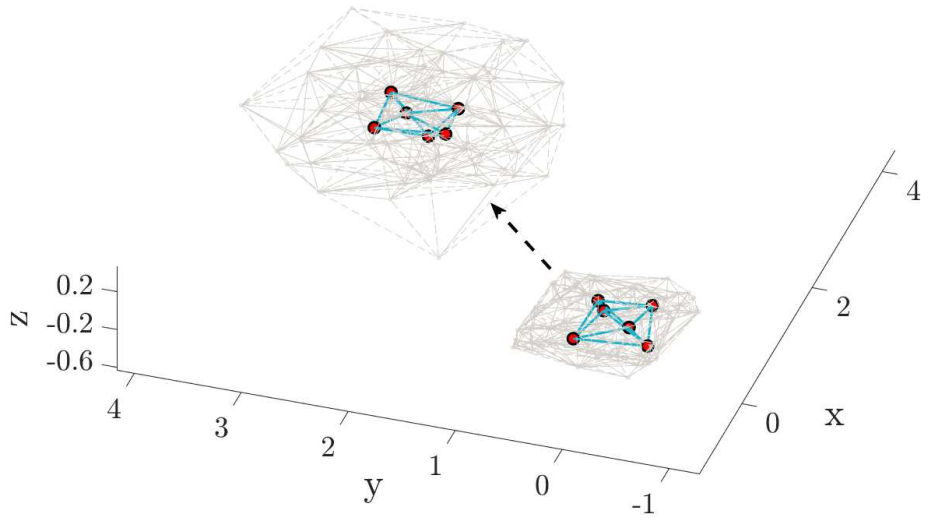

Figure A.3. Capture of oil spill simulation under internal and external interference.

Appendix B

Flocking Adaptive Potential Function

In Chapter 4, a gradient-free source-seeking algorithm with flocking is introduced. Here, we propose a different approach for the same problem. By using a time-varying potential function, one can adjust the relation between two neighbor agents based on their attractiveness and distance. This potential function embodies both the flocking alignment/separation rule and extremum seeking by imitating glowworms. The main contribution is that instead of having several elements added together (the common approach), here, the forces act together based on a single function.

Source-Seeking Navigational Protocol

Inspired by GSO, where, based on an objective function, agents with higher values attract others, we set ψ_i as the agent's level of attractiveness. This way, an agent with larger ψ_j pulls agents with lower ψ_i, which causes movement of the swarm in the extremum direction. The relation between two neighbor agents is described as

$$l_{ji} = \frac{d}{\psi_{\max}}(\psi_j - \psi_i), \tag{B.1}$$

where we assume that $\psi_{\max}$ is predictable or known. As explained, the concept is to modify the potential function in (2.20) to generate an action function that drives agents toward the source in flocking. In other words, we wish to define a stable equilibrium where both conditions (2.10) and $q_c \to q_s$ exist. To do so, we set a time-varying constraint with dependence not only on d but also on the relation of ψ_i and ψ_j,

$$d_i^j(q) = d_\alpha - l_{ji}(q). \tag{B.2}$$

Now, we can define a new set of constraints to produce the adaptive potential functions:

$$||q_j - q_i||_\sigma = d_i^j(q),\ \forall j \in \mathcal{N}_i. \tag{B.3}$$

A graphical interpretation is depicted in Figure B.1. For the case when $\psi_j = \psi_i$ (mid-solid curve), consensus is achieved (i.e., extremum located) and the repulsive/attractive relation between agents j and i is governed by the flocking protocol. When agent j is more attractive (located at a higher concentration level) than agent i, i.e., $\psi_j > \psi_i$ (left-dashed curve), then the attractive domain increases, as does the force driving agent i

toward agent j. The opposite case occurs when agent j is less attractive than agent i, i.e., $\psi_j < \psi_i$ (right-dot curve), and the repulsive area increases. This process proceeds until condition (B.3) holds; then, equilibrium is reached where $q_c = q_s$.

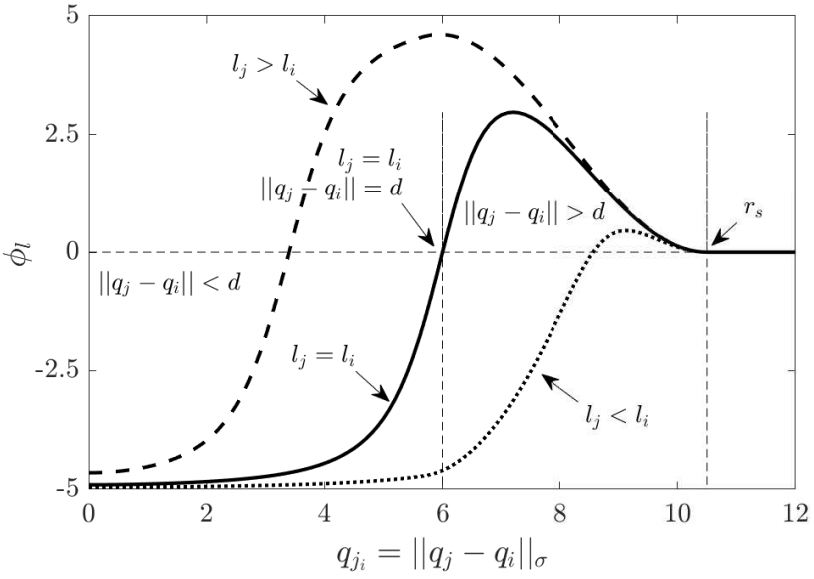

Figure B.1. $\phi_i^j(q)$ plot for different values of $\psi_j - \psi_i$, where values above zero indicate attractive forces and those below are repulsive (here, $r_s = 11, d = 6$).

The modified rule in (2.16) induces a smooth collective potential function

$$\begin{aligned} V =& \frac{1}{2}\sum_i \sum_{j\neq i} \phi_i^j(q) \\ \Phi_i^j(q) =& \int_{d_l}^{q_{ji}} \phi_i^j(s)ds = \int_{d_\alpha - l_{ji}(q)}^{q_{ji}} \phi_i^j(s)ds. \end{aligned} \tag{B.4}$$

The term $\phi_i^j \in \mathbb{R}^{2m} \to \mathbb{R}$ is the action function, where, by using (2.13) and (2.14), we receive a repulsive/attractive force driving agents toward the source

$$\phi_i^j(q) = \rho_h(q_{ji}/r_\alpha)\phi_s(q_{ji} - d_i^j), \tag{B.5}$$

where $r_\alpha = ||r_s||_\sigma$. The function ϕ_i^j in (B.5) embodies two of the Reynolds rules, cohesion and separation, when applying the attractive/repulsive force with respect to the term $||q_j - q_i||_\sigma - d_i^j$. To satisfy all three Reynolds rules, an additional element for reaching velocity consensus is added using a weighted a_{ij}:

$$a_{ij} = \rho_h(q_{ji}/r_\alpha). \tag{B.6}$$

Then, the alignment (velocity-matching) behavior is achieved by applying

$$u_i^p = a_{ij}(p_j - p_i). \tag{B.7}$$

Now, we can construct the complete protocol applied to an agent i. Let $n_{ij} = \sigma_\epsilon(q_j - q_i)$ be a vector along the line connecting q_i to q_j; then, for each agent i,

$$u_i = \sum_{j \in \mathcal{N}_i} \underbrace{\phi_i^j(q) n_{ij}}_{u_i^q} + \underbrace{a_{ij}(p_j - p_i)}_{u_i^p} - cp_i, \tag{B.8}$$

where cp_i with $c > 0$ is an additional damping term. The protocol in (B.8) combines the group objective with flocking behavior, which avoids the use of a noise-sensitive gradient-estimation process.

Observations

The simulation results are similar to the those presented in Chapter 4 where a smooth convergence behavior is observed. This encourage us to test the algorithm in a more realistic context. An experiment in complex environment is shown in Figure B.2, where agents show the ability to monitor an unknown source in the presence of an obstacle with flocking.

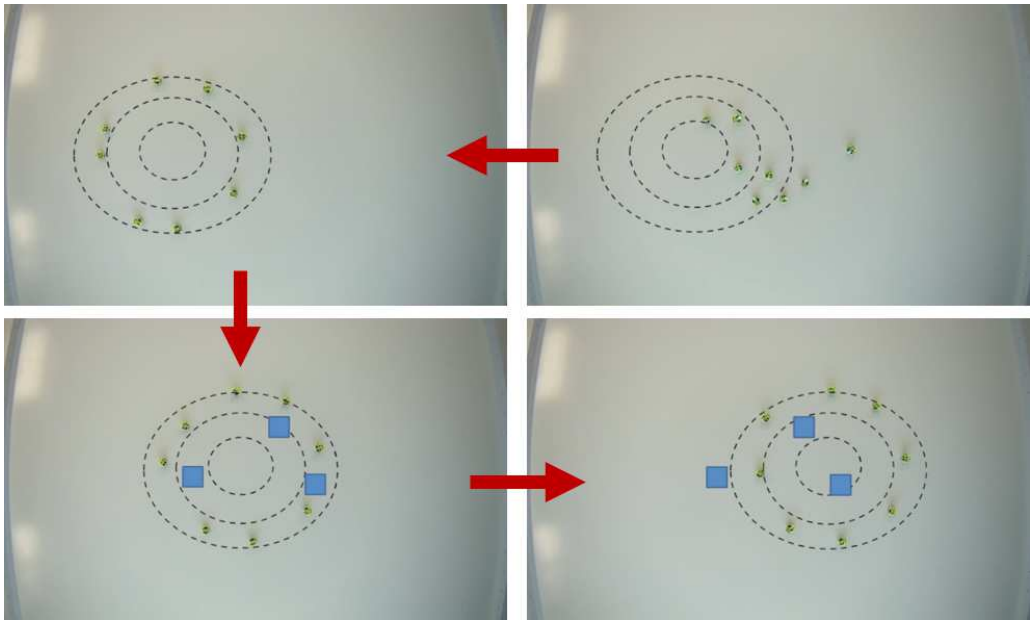

Figure B.2. Experiment screenshots of the swarm behavior under different states: initial distribution, source located, and tracking the time-varying field while avoiding obstacles.

Bibliography

[Ahmadi Barogh et al., 2015] Ahmadi Barogh, S., Rosero, E., and Werner, H. (2015). Formation control of non-holonomic agents with collision avoidance. In *American Control Conference*.

[Anderson et al., 2008] Anderson, B. D. O., Yu, C., Fidan, B., and Hendrickx, J. M. (2008). Rigid graph control architectures for autonomous formations. *IEEE Control Systems Magazine*, 28(6):48–63.

[Anderson et al., 2008] Anderson, B. D. O., Yu, C., Fidan, B., and Hendrickx, J. M. (2008). Rigid graph control architectures for autonomous formations. *IEEE Control Systems Magazine*, 28(6):48–63.

[Aragues et al., 2011] Aragues, R., Carlone, L., Calafiore, G., and Sagues, C. (2011). Multi-agent localization from noisy relative pose measurements. In *2011 IEEE International Conference on Robotics and Automation*, pages 364–369.

[Asimow and Roth, 1979] Asimow, L. and Roth, B. (1979). The rigidity of graphs, ii. *Journal of Mathematical Analysis and Applications*, 68(1):171 – 190.

[Awad et al., 2018] Awad, A., Chapman, A., Schoof, E., Narang-Siddarth, A., and Mesbahi, M. (2018). Time-scale separation in networks: State-dependent graphs and consensus tracking. *IEEE Transactions on Control of Network Systems*, pages 1–1.

[Barogh and Werner, 2016a] Barogh, S. A. and Werner, H. (2016a). Cascaded formation control using angle and distance between agents with orientation control (part 1). In *2016 UKACC 11th International Conference on Control*, pages 1–6.

[Barogh and Werner, 2016b] Barogh, S. A. and Werner, H. (2016b). Cascaded formation control using angle and distance between agents with orientation control (part 2). In *2016 UKACC 11th International Conference on Control*, pages 1–6.

[Barooah et al., 2010] Barooah, P., Russell, W. J., and Hespanha, J. a. P. (2010). Approximate distributed kalman filtering for cooperative multi-agent localization. In *Proceedings of the 6th IEEE International Conference on Distributed Computing in Sensor Systems*, DCOSS'10, pages 102–115, Berlin, Heidelberg. Springer-Verlag.

[Bartels and Werner, 2014] Bartels, M. and Werner, H. (2014). Cooperative and consensus-based approaches to formation control of autonomous vehicles. In *19th IFAC World Congress*.

[Brinon-Arranz et al., 2011] Brinon-Arranz, L., Seuret, A., and Canudas-de Wit, C. (2011). Collaborative estimation of gradient direction by a formation of auvs under

communication constraints: Decision and control and european control conference (cdc-ecc), 2011 50th ieee conference on. In *50th Conference on Decision and Control*.

[Casbeer et al., 2006] Casbeer, D. W., Kingston, D. B., Bear, R., McLain, T., Li, S., and Mehra, R. (2006). Cooperative forest fire surveillance using a team of small unmanned air vehicles. *International Journal of Systems Science*, 37(6):251–360.

[Chen et al., 2010] Chen, Z., Chu, T., and Zhang, J. (2010). Swarm splitting and multiple targets seeking in multi-agent dynamic systems. In *2010 49th IEEE Conference on Decision and Control (CDC)*, pages 4577–4582.

[Cochran and Krstic, 2009] Cochran, J. and Krstic, M. (2009). Nonholonomic source seeking with tuning of angular velocity. *IEEE Transactions on Automatic Control*, 54(4):717–731.

[Cochran et al., 2009] Cochran, J., Siranosian, A., Ghods, N., and Krstic, M. (2009). 3-d source seeking for underactuated vehicles without position measurement. *IEEE Transactions on Robotics*, 25(1):117–129.

[del Valle et al., 2008] del Valle, Y., Venayagamoorthy, G. K., Mohagheghi, S., Hernandez, J. C., and Harley, R. G. (2008). Particle swarm optimization: Basic concepts, variants and applications in power systems. *IEEE Transactions on Evolutionary Computation*, 12(2):171–195.

[Dimarogonas and Kyriakopoulos, 2005] Dimarogonas, D. V. and Kyriakopoulos, K. J. (2005). Formation control and collision avoidance for multi-agent systems and a connection between formation infeasibility and flocking behavior. In *44th Conference on Decision and Control*.

[Dimarogonas and Kyriakopoulos, 2006] Dimarogonas, D. V. and Kyriakopoulos, K. J. (2006). A connection between formation control and flocking behavior in nonholonomic multiagent systems. In *Proceedings 2006 IEEE International Conference on Robotics and Automation, 2006. ICRA 2006.*, pages 940–945.

[Dimarogonas and Kyriakopoulos, 2008] Dimarogonas, D. V. and Kyriakopoulos, K. J. (2008). A connection between formation infeasibility and velocity alignment in kinematic multi-agent systems. *Automatica*, 44(10):2648 – 2654.

[Dorigo et al., 2006] Dorigo, M., Birattari, M., and Stutzle, T. (2006). Ant colony optimization. *IEEE Computational Intelligence Magazine*, 1(4):28–39.

[Dorigo and Caro, 1999] Dorigo, M. and Caro, G. D. (1999). Ant colony optimization: a new meta-heuristic. In *Proceedings of the 1999 Congress on Evolutionary Computation-CEC99 (Cat. No. 99TH8406)*, volume 2, page 1477 Vol. 2.

[Fainekos et al., 2005] Fainekos, G. E., Kress-Gazit, H., and Pappas, G. J. (2005). Temporal logic motion planning for mobile robots. In *Proceedings of the 2005 IEEE International Conference on Robotics and Automation*, pages 2020–2025.

[Fax and Murray, 2004] Fax, J. A. and Murray, R. M. (2004). Information flow and cooperative control of vehicle formations. *IEEE Transactions on Automatic Control*, 49(9):1465–1476.

[Fiorelli et al., 2006] Fiorelli, E., Leonard, N. E., Bhatta, P., Paley, D. A., Bachmayer, R., and Fratantoni, D. M. (2006). Multi-auv control and adaptive sampling in monterey bay. *IEEE Journal of Oceanic Engineering*, 31(4):935–948.

[Gastin and Oddoux, 2001] Gastin, P. and Oddoux, D. (2001). *Fast LTL to Büchi Automata Translation*, pages 53–65. Springer Berlin Heidelberg, Berlin, Heidelberg.

[Glavaški et al., 2008] Glavaški, S., Williams, A., and Samad, T. (2008). Connectivity and convergence of formations. In Shamma, J. S., editor, *Cooperative control of distributed multi-agent systems*, pages 43–61. John Wiley & Sons.

[Gong et al., 2011] Gong, Q., Zhou, Y., and Luo, Q. (2011). Hybrid artificial glowworm swarm optimization algorithm for solving multi-dimensional knapsack problem. *Procedia Engineering*, 15:2880 – 2884. {CEIS} 2011.

[Gonzalez et al., 2015] Gonzalez, A. M., Hoffmann, C., and Werner, H. (2015). Lpv formation control for a class of non-holonomic agents with directed and switching communication topologies. In *2015 54th IEEE Conference on Decision and Control (CDC)*, pages 2792–2797.

[Gonzalez Cisneros, 2014] Gonzalez Cisneros, P. S. (2014). Implementation of an information flow filter on a swarm of quad-rotor helicopters using robust control techniques. Project work, Hamburg University of Technology, Hamburg, Germany.

[Guo et al., 2013] Guo, M., Johansson, K. H., and Dimarogonas, D. V. (2013). Revising motion planning under linear temporal logic specifications in partially known workspaces. In *Robotics and Automation (ICRA), 2013 IEEE International Conference on*, pages 5025–5032. IEEE.

[He and Huang, 2016] He, L. and Huang, S. (2016). Improved glowworm swarm optimization algorithm for multilevel color image thresholding problem. *Mathematical Problems in Engineering*, 2016.

[Hu, 2012] Hu, G. (2012). Robust consensus tracking of a class of second-order multi-agent dynamic systems. *Systems and Control Letters*, 61(1):134 – 142.

[Jadbabaie et al., 2003] Jadbabaie, A., Lin, J., and Morse, A. S. (2003). Coordination of groups of mobile autonomous agents using nearest neighbor rules. *IEEE Transactions on Automatic Control*, 48(6):988–1001.

[Kan et al., 2012] Kan, Z., Dani, A. P., Shea, J. M., and Dixon, W. E. (2012). Network connectivity preserving formation stabilization and obstacle avoidance via a decentralized controller. *IEEE Transactions on Automatic Control*, 57(7):1827–1832.

[Kantaros and Zavlanos, 2016] Kantaros, Y. and Zavlanos, M. M. (2016). A distributed ltl-based approach for intermittent communication in mobile robot networks. In *2016 American Control Conference (ACC)*, pages 5557–5562.

[Kennedy and Eberhart, 1995] Kennedy, J. and Eberhart, R. (1995). Particle swarm optimization. In *Neural Networks, 1995. Proceedings., IEEE International Conference on*, volume 4, pages 1942–1948 vol.4.

[Kingston et al., 2008] Kingston, D., Beard, R. W., and Holt, R. S. (2008). Decentralized perimeter surveillance using a team of uavs. *IEEE Transactions on Robotics*, 24(6):1394–1404.

[Kloetzer et al., 2011] Kloetzer, M., Ding, X. C., and Belta, C. (2011). Multi-robot deployment from LTL specifications with reduced communication. *CoRR*, abs/1108.3240.

[Kress-Gazit et al., 2009] Kress-Gazit, H., Fainekos, G. E., and Pappas, G. J. (2009). Temporal-logic-based reactive mission and motion planning. *IEEE Transactions on Robotics*, 25(6):1370–1381.

[Krishnanand and Ghose, 2009] Krishnanand, K. N. and Ghose, D. (2009). Glowworm swarm optimization for simultaneous capture of multiple local optima of multimodal functions. *Swarm Intelligence*, 3(2):87–124.

[LaSalle, 1960] LaSalle, J. (1960). Some extensions of liapunov's second method. *IRE Transactions on Circuit Theory*, 7(4):520–527.

[Leitao et al., 2012] Leitao, P., Barbosa, J., and Trentesaux, D. (2012). Bio-inspired multi-agent systems for reconfigurable manufacturing systems. *Engineering Applications of Artificial Intelligence*, 25(5):934 – 944.

[Li et al., 2013] Li, H., Peng, J., Liu, W., Wang, J., Liu, J., and Huang, Z. (2013). Flocking control for multi-agent systems with communication optimization. In *2013 American Control Conference*, pages 2056–2061.

[Li et al., 2014] Li, S., Kong, R., and Guo, Y. (2014). Cooperative distributed source seeking by multiple robots: Algorithms and experiments. *IEEE/ASME Transactions on Mechatronics*, 19(6):1810–1820.

[Li and Zhang, 2009] Li, T. and Zhang, J.-F. (2009). Mean square average-consensus under measurement noises and fixed topologies: Necessary and sufficient conditions. *Automatica*, 45(8):1929 – 1936.

[Liao et al., 2011] Liao, W.-H., Kao, Y., and Li, Y.-S. (2011). A sensor deployment approach using glowworm swarm optimization algorithm in wireless sensor networks. *Expert Systems with Applications*, 38(10):12180 – 12188.

[Lin et al., 2014] Lin, J., You, K., and Song, S. (2014). Velocity regulation in 3d nonholonomic source seeking. In *Proceeding of the 11th World Congress on Intelligent Control and Automation*, pages 1112–1117.

[Liu and Krstic, 2010] Liu, S.-J. and Krstic, M. (2010). Stochastic nonholonomic source seeking. In *2010 49th IEEE Conference on Decision and Control (CDC)*, pages 6985–6990.

[Loizou and Kyriakopoulos, 2004] Loizou, S. G. and Kyriakopoulos, K. J. (2004). Automatic synthesis of multi-agent motion tasks based on ltl specifications. In *2004 43rd IEEE Conference on Decision and Control (CDC) (IEEE Cat. No.04CH37601)*, volume 1, pages 153–158 Vol.1.

[Lončar et al., 2012] Lončar, G., Leder, N., and Paladin, M. (2012). Numerical modelling of an oil spill in the northern adriatic. *Oceanologia*, 54(2):143 – 173.

[Lu et al., 2010] Lu, Y., Guo, Y., and Dong, Z. (2010). Multiagent flocking with formation in a constrained environment. *Journal of Control Theory and Applications*, 8(2):151–159.

[Matveev et al., 2014] Matveev, A. S., Hoy, M. C., and Savkin, A. V. (2014). 3d environmental extremum seeking navigation of a nonholonomic mobile robot. *Automatica*, 50(7):1802 – 1815.

[Mesbahi and Egerstedt, 2010] Mesbahi, M. and Egerstedt, M. (2010). *Graph Theoretic Methods in Multiagent Networks*. Princeton University Press, Princeton and Oxford.

[Ni and Cheng, 2010] Ni, W. and Cheng, D. (2010). Leader-following consensus of multi-agent systems under fixed and switching topologies. *Systems & Control Letters*, 59(3-4):209–217.

[Ogren et al., 2004] Ogren, P., Fiorelli, E., and Leonard, N. E. (2004). Cooperative control of mobile sensor networks:adaptive gradient climbing in a distributed environment. *IEEE Transactions on Automatic Control*, 49(8):1292–1302.

[Oh and Ahn, 2014] Oh, K.-K. and Ahn, H.-S. (2014). Distance-based undirected formations of single-integrator and double-integrator modeled agents in n-dimensional space. *International Journal of Robust and Nonlinear Control*, 24:1809–1820.

[Oh et al., 2015] Oh, K.-K., Park, M.-C., and Ahn, H.-S. (2015). A survey of multi-agent formation control. *Automatica*, 53:424 – 440.

[Olfati-Saber, 2005] Olfati-Saber, R. (2005). Distributed kalman filter with embedded consensus filters. In *Proceedings of the 44th IEEE Conference on Decision and Control*, pages 8179–8184.

[Olfati-Saber, 2006] Olfati-Saber, R. (2006). Flocking for multi-agent dynamic systems: algorithms and theory. *IEEE Transactions on Automatic Control*, 51(3):401–420.

[Olfati-Saber and Murray, 2002] Olfati-Saber, R. and Murray, R. M. (10-13 Dec. 2002). Graph rigidity and distributed formation stabilization of multi-vehicle systems. In *IEEE Conference on Decision and Control*, pages 2965–2971.

[Olfati-Saber and Murray, 2004] Olfati-Saber, R. and Murray, R. M. (2004). Consensus problems in networks of agents with switching topology and time-delays. *IEEE Transactions on Automatic Control*, 49(9):1520–1533.

[Olfati-Saber and Shamma, 2005] Olfati-Saber, R. and Shamma, J. S. (2005). Consensus filters for sensor networks and distributed sensor fusion. In *Proceedings of the 44th IEEE Conference on Decision and Control*, pages 6698–6703.

[Paliotta et al., 2015] Paliotta, C., Belleter, D. J., and Pettersen, K. Y. (2015). Adaptive source seeking with leader-follower formation control. *IFAC-PapersOnLine*, 48(16):285–290.

[Papusha et al., 2016] Papusha, I., Fu, J., Topcu, U., and Murray, R. M. (2016). Automata theory meets approximate dynamic programming: Optimal control with temporal logic constraints. In *2016 IEEE 55th Conference on Decision and Control (CDC)*, pages 434–440.

[Pickem et al., 2017] Pickem, D., Glotfelter, P., Wang, L., Mote, M., Ames, A., Feron, E., and Egerstedt, M. (2017). The robotarium: A remotely accessible swarm robotics research testbed. In *2017 IEEE International Conference on Robotics and Automation (ICRA)*, pages 1699–1706.

[Pilz, 2013] Pilz, U. (2013). *Cooperative Control of Multi-Agent Systems with Application to Quad-Rotor Helicopters*. PhD thesis, Hamburg University of Technology, Hamburg, Germany.

[Pilz et al., 2011] Pilz, U., Popov, A., and Werner, H. (2011). An information flow filter approach to cooperative vehicle control. In *18th World Congress*, pages 7432–7437.

[Pilz et al., 2012] Pilz, U., Popov, A., and Werner, H. (2012). An information flow filter approach to cooperative vehicle control and its application to formation flight of quadrotor helicopters. *Asian Journal of Control*.

[Rahmani, 2014] Rahmani, S. (2014). *Level curve tracking for formation control*. PhD thesis, Hamburg University of Technology.

[Ren and Atkins, 2007] Ren, W. and Atkins, E. (2007). Distributed multi-vehicle coordinated control via local information exchange. In *Special Issue: Communicating-Agent Networks*, volume 17, pages 1002–1033.

[Ren et al., 2007] Ren, W., Moore, K., and Chen, Y. (2007). High-order and model reference consensus algorithms in cooperative control of multivehicle systems. *Journal of Dynamic Systems Measurement and Control-transactions of The Asme*, 129:678–688.

[Rosero and Werner, 2014a] Rosero, E. and Werner, H. (2014a). Cooperative source seeking via gradient estimation and formation control (part 1). In *UKACC International Conference on Control*.

[Rosero and Werner, 2014b] Rosero, E. and Werner, H. (2014b). Modified distributed consensus filter for sensor networks. In *2014 European Control Conference (ECC)*, pages 892–895.

[Saber and Murray, 2003] Saber, R. O. and Murray, R. M. (2003). Flocking with obstacle avoidance: cooperation with limited communication in mobile networks. In *42nd IEEE International Conference on Decision and Control (IEEE Cat. No.03CH37475)*, volume 2, pages 2022–2028 Vol.2.

[Said and Fumin, 2018] Said, A.-A. and Fumin, Z. (2018). A distributed level curve tracking control law for multi-agent systems. In *2018 IEEE 57th Conference on Decision and Control (CDC)*.

[Sepulchre et al., 2007] Sepulchre, R., Paley, D. A., and Leonard, N. E. (2007). Stabilization of planar collective motion: All-to-all communication. *IEEE Transactions on Automatic Control*, 52(5):811–824.

[Stanković and Stipanović, 2010] Stanković, M. S. and Stipanović, D. M. (2010). Extremum seeking under stochastic noise and applications to mobile sensors. *Automatica*, 46(8):1243–1251.

[Stringari et al., 2013] Stringari, C. E., Marques, W. C., Eidt, R. T., and Mello, L. F. (2013). Modeling an oil spill along the southern brazilian shelf: Forcing characterization and its influence on the oil fate. *International Journal of Geosciences*, 4:397 – 407.

[Sun and Anderson, 2015] Sun, Z. and Anderson, B. D. O. (2015). Rigid formation control with prescribed orientation. In *2015 IEEE International Symposium on Intelligent Control (ISIC)*, pages 639–645.

[Sydney and Paley, 2014] Sydney, N. and Paley, D. A. (2014). Multivehicle coverage control for a nonstationary spatiotemporal field. *Automatica*, 50(5):1381 – 1390.

[Tanner et al., 2005] Tanner, H. G., Jadbabaie, A., and Pappas, G. J. (2005). *Flocking in Teams of Nonholonomic Agents*, pages 229–239. Springer Berlin Heidelberg, Berlin, Heidelberg.

[Turgeman and Werner, 2017] Turgeman, A. and Werner, H. (2017). Mission control - combined solutions for source seeking and level curve tracking in a time-varying field. In *2017 American Control Conference (ACC)*, pages 4268–4273.

[Verginis and Dimarogonas, 2018a] Verginis, C. K. and Dimarogonas, D. V. (2018a). Mode switching decentralized multi-agent coordination under local temporal logic tasks. *CoRR*, abs/1803.08288.

[Verginis and Dimarogonas, 2018b] Verginis, C. K. and Dimarogonas, D. V. (2018b). Motion and cooperative transportation planning for multi-agent systems under temporal logic formulas. *CoRR*, abs/1803.01579.

[Vásárhelyi et al., 2014] Vásárhelyi, G., Virágh, C., Somorjai, G., Tarcai, N., Szörényi, T., Nepusz, T., and Vicsek, T. (2014). Outdoor flocking and formation flight with autonomous aerial robots. In *2014 IEEE/RSJ International Conference on Intelligent Robots and Systems*, pages 3866–3873.

[Wang and Xin, 2011] Wang, J. and Xin, M. (2011). Multi-agent consensus algorithm with obstacle avoidance via optimal control approach. In *American Control Conference*.

[Wen et al., 2012] Wen, G., Duan, Z., and Chen, G. (2012). Distributed consensus of multi-agent systems with general linear node dynamics through intermittent communications. In *2012 24th Chinese Control and Decision Conference (CCDC)*, pages 1–5.

[Wolper, 2002] Wolper, P. (2002). Constructing automata from temporal logic formulas: A tutorial. In Brinksma, E., Hermanns, H., and Katoen, J.-P., editors, *Lectures on Formal Methods and Performance Analysis*, pages 261–277. Springer-Verlag New York, Inc., New York, NY, USA.

[Wu et al., 2012] Wu, B., Qian, C., Ni, W., and Fan, S. (2012). The improvement of glowworm swarm optimization for continuous optimization problems. *Expert Systems with Applications*, 39(7):6335 – 6342.

[Xiang and Lee, 2008] Xiang, W. and Lee, H. (2008). Ant colony intelligence in multi-agent dynamic manufacturing scheduling. *Engineering Applications of Artificial Intelligence*, 21(1):73 – 85.

[Xiao and Wang, 2008] Xiao, F. and Wang, L. (2008). Asynchronous consensus in continuous-time multi-agent systems with switching topology and time-varying delays. *IEEE Transactions on Automatic Control*, 53(8):1804–1816.

[Yan et al., 2011] Yan, J., Guan, X.-P., Luo, X.-Y., and Tan, F.-X. (2011). Target tracking and obstacle avoidance for multi-agent networks with input constraints. *International Journal of Automation and Computing*.

[Young et al., 2010] Young, G. F., Scardovi, L., and Leonard, N. E. (2010). Robustness of noisy consensus dynamics with directed communication. In *Proceedings of the 2010 American Control Conference*, pages 6312–6317.

[Zhang and Cowlagi, 2016] Zhang, Z. and Cowlagi, R. V. (2016). Motion-planning with global temporal logic specifications for multiple nonholonomic robotic vehicles. In *2016 American Control Conference (ACC)*, pages 7098–7103.

[Zhao et al., 2005] Zhao, B., Guo, C. X., and Cao, Y. J. (2005). A multiagent-based particle swarm optimization approach for optimal reactive power dispatch. *IEEE Transactions on Power Systems*, 20(2):1070–1078.

[Zou et al., 2015] Zou, R., Kalivarapu, V., Winer, E., Oliver, J., and Bhattacharya, S. (2015). Particle swarm optimization-based source seeking. *IEEE Transactions on Automation Science and Engineering*, 12(3):865–875.